SAHC

Characterization of the response of quasi-periodic masonry: Geometrical investigation, homogenization and structural application

Yhosimi Washington Esquivel Fernández

Portugal | 2012

ADVANCED MASTERS IN STRUCTURAL ANALYSIS
OF MONUMENTS AND HISTORICAL CONSTRUCTIONS

Master's Thesis

Yhosimi Washington Esquivel Fernández

Characterization of the response of quasi-periodic masonry: Geometrical investigation, homogenization and structural application.

University of Minho

Czech Technical University in Prague

Education and Culture

Erasmus Mundus



ADVANCED MASTERS IN STRUCTURAL ANALYSIS
OF MONUMENTS AND HISTORICAL CONSTRUCTIONS

Master's Thesis

Yhosimi Washington Esquivel Fernández

Characterization of the response of quasi-periodic masonry: Geometrical investigation, homogenization and structural application.

This Masters Course has been funded with support from the European Commission. This publication reflects the views only of the author, and the Commission cannot be held responsible for any use which may be made of the information contained therein.

Portugal | 2012

DECLARATION

Name: Yhosimi Washington Esquivel Fernández

Email: yesquivel@pucp.pe

Title of the Msc Dissertation: Characterization of the response of quasi-periodic masonry: Geometrical investigation, homogenization and structural application.

Supervisor(s): Professor Doctor Paulo José Brandão Barbosa Lourenço, Professor Doctor Gabriele Milani

Year: 2012

I hereby declare that all information in this document has been obtained and presented in accordance with academic rules and ethical conduct. I also declare that, as required by these rules and conduct, I have fully cited and referenced all material and results that are not original to this work.

I hereby declare that the MSc Consortium responsible for the Advanced Masters in Structural Analysis of Monuments and Historical Constructions is allowed to store and make available electronically the present MSc Dissertation.

University: University of Minho

Date: July-2012

Signature:

_____

To my family

ACKNOWLEDGEMENTS

I would like to express my sincere gratitude to Professor Paulo Lourenço, my supervisor, for the continuous support for his patience, motivation, enthusiasm and guidance, during the preparation of this thesis.

I also wish to thank Professor Gabriele Milani for his friendship, encouragement, enthusiasm; for explaining and his help with the algorithm, used to carry out this thesis without his support it would have been complicated the developed of the thesis.

My sincere thanks to Consortium for granting to me with the scholarship.

Thanks to CVUT in Prague for being good host, thanks for welcoming us and supporting our educational, professional development.

I owe my deepest gratitude to all my classmates, my friends for their accompaniment and friendship along of whole my stay in Europe.

I cannot find words to express my gratitude to my parents and my brother who always supported me during all this time. Thanks for everything that you did for me.

ABSTRACT

In many countries, historical buildings were built with masonry walls constituted by random assemblages of blocks and stones of variable dimensions, being this feature an issue for studying these structures since they display a non-linear behavior. The analysis of historic masonry structures requires often complex and expensive computational tools that in many cases are difficult to handle, given this condition of large variability of masonry. The present thesis attempts to show a strategy to face up the problematic of the characterization of the response of rubble masonry. First the objectives and motivation of the study are presented, followed by a brief state of the art regarding homogenization techniques and approaches in elastic and inelastic range, discussing the advantages and disadvantages of both approaches. Then, the characterization of the masonry and statistical analysis of the dimensions of the stone units from the walls of Guimarães castle are carried out. This is followed by the homogenized limit analysis of representative volume elements (RVEs) from the Alcaçova wall in the Guimarães castle in order to obtain its in-plane an out-of-plane failure surfaces at different orientations of a load and increasing compressive loads considering, respectively, the case of masonry with weak and strong mortar independently. Afterwards, the limit analysis was carried out in two numerical models of Alcaçova wall, being the first one built with a heterogeneous material and the second one with a homogeneous material that was obtained by means of homogenized the limit analysis of representative volume elements. The purpose is to determinate the reliability of results, limit load and failure mechanism, from the homogenized model, compared to the heterogeneous model. Finally, the conclusions of the study are presented.

RESUMO

Em muitos países, os edifícios históricos foram construídos com paredes de alvenaria constituída por conjuntos aleatórios de blocos e pedras de dimensões variáveis, sendo esta característica relevante para estudar estas estruturas uma vez que as mesmas exibem um comportamento não-linear. A análise de estruturas históricas de alvenaria exige muitas vezes ferramentas computacionais complexas e caras que em muitos casos, são difíceis de aplicar, dada esta característica de grande variabilidade da alvenaria. A presente tese procura mostrar uma estratégia para enfrentar a problemática da caracterização da resposta de alvenaria irregular. Em primeiro lugar os objetivos e motivação do estudo são apresentados, seguido por um breve estado da arte sobre técnicas de homogeneização e abordagens em regime elástico e inelástico, discutindo as vantagens e desvantagens de ambas as abordagens. Em seguida, a caracterização da alvenaria e análise estatística das dimensões das unidades de pedra das paredes de Guimarães castelo são realizadas. Depois uma análise limite com homogeneização de elementos de volume representativos (RVEs) a partir da parede Alcáçova no castelo Guimarães, Portugal, é realizada a fim de obter superfícies no plane e fora do plano de rotura em diferentes orientações de uma carga, aumentando a pré-compressão vertical e considerando, respetivamente, o caso de alvenaria com argamassa fraca e forte de forma independente. Posteriormente, a análise limite foi realizado em dois modelos numéricos da parede da Alcáçova, sendo o primeiro construído com um material heterogéneo e um segundo com um material homogéneo que foi obtido por meio de homogeneização de elementos de volume representativos. O objetivo é discutir a fiabilidade dos resultados, do fator de carga e dos mecanismos de rotura, a partir do modelo homogeneizado e em comparação com o modelo heterogéneo. Finalmente, apresentam-se as conclusões do estudo.

RESUMEN

En muchos países, los edificios históricos fueron construidos con muros de mampostería constituida por conjuntos de bloques al azar y piedras de dimensiones variables, siendo esta característica un problema para el estudio de estas estructuras, ya que presentan un comportamiento no lineal. El análisis de las estructuras de mampostería histórica requiere de herramientas computacionales a menudo complejas y costosas que en muchos casos son difíciles de manejar, teniendo en cuenta esta condición de la gran variabilidad de la mampostería. La presente tesis presenta una estrategia para enfrentar la problemática de la caracterización de la respuesta de la mampostería. En primer lugar los objetivos y la motivación del estudio se presentan, seguido de un breve estado del arte sobre las técnicas de homogeneización y enfoques en el rango elástico e inelástico, comentando las ventajas y desventajas de ambos enfoques. Despues, la caracterización de la mampostería y el análisis estadístico de las dimensiones de las unidades de piedra de las paredes de Guimarães castillo se llevan a cabo. Seguido por el análisis límite homogeneizado de elementos de volumen representativo (RVE) de la pared de la Alcáçova que pertenece al Guimarães con el fin de obtener la superficie de falla en el plano y la superficie de falla fuera del plano considerando diferentes orientaciones de carga y una carga incremental de compresión respectivamente, en el caso de mampostería con mortero de débil y fuerte de forma se consideran por separado uno de otro. Posteriormente, el análisis límite se llevó a cabo en dos modelos numéricos de Alcáçova pared, siendo el primero construido con un material heterogéneo y la segundo con un material homogéneo que se obtuvo por medio del análisis límite homogeneizado de los elementos de volumen representativos. El propósito es determinar la fiabilidad de los resultados, carga limite y mecanismos de falla, a partir del modelo homogéneo, en comparación con el modelo heterogéneo. Por último, las conclusiones del estudio se presentan.

CONTENTS

FIGURES

1. INTRODUCTION

1.1 Motivation

“The historic monuments of generations of people remain to the present day as living witnesses of their age-old traditions. People are becoming more and more conscious of the unity of human values and regard ancient monuments as a common heritage. The common responsibility to safeguard them for future generations is recognized. It is our duty to hand them on in the full richness of their authenticity” [1].

The masonry is a common material in many historical buildings around the world, have survived many seismic events throughout their existence but this fact does not mean historical buildings are out of danger. Nowadays, there are the knowledge and powerful analysis tools that allow to model and calculate the behavior of complex structures under different solicitations. However, the structural analysis of historical masonry buildings remains a challenge due to factors such as: The low tensile strength with quasi-brittle failure, which involves non-linear behavior from load currents small; the heterogeneity present in these constructions; the shear failure is not associated, due to the difference between the dilatancy angle and the internal friction angle; joints commonly represent planes of weakness; anisotropy. These factors increase the computational cost and complicate the numerical models. In recent years, and in several countries, interest in preserving the historical buildings and in finding efficient numerical models, has led to different research groups to develop a significant number numerical model for historical masonry buildings, from very simple to complex ones, which are able to simulate the behavior of the material under different type of loads. The choice depends on the degree of accuracy, sought in the analysis for each case particular.

1.2 General objectives

This thesis concerns the characterization of the response of quasi-periodic masonry by means of a geometrical study and a statistical analysis of stone units, homogenization of masonry and structural implementation.

1.3 Specific objectives

To carry out, the geometrical investigation of stones units from Guimarães castle to obtain statistical parameters and distribution of the height and length of the stones units, with the aim of determine the adequate size of the representative volume elements.

To perform, the homogenized limit analysis of representative volume elements (RVEs) to obtain their in-plane failure surfaces and out-of-plane failure surfaces.

To carry out the limit analysis of the Alcaçova wall and to compare the limit load and failure mechanisms from the homogeneous model and from the heterogeneous model, in order to check the reliability of the homogenous model.

2. STATE OF THE ART ON HOMOGENIZATION TECHNIQUES

Abstract

This chapter presents the state of the art on homogenization techniques for the study of masonry. First, a description of the homogenization process is presented, followed by a review of the approaches for homogenization of masonry in elastic range and inelastic range, discussing the advantages and disadvantages of both approaches.

2.1 Introduction: Modeling possibilities for masonry structures

Composite materials are made by two or more different constituent bonded by an interface. There are composite materials of natural and artificial origin. Moreover composites can be considered heterogeneous, such as masonry (composed of stones or bricks in a matrix of mortar), laminated wood, cracked media and porous media, or homogenous, such as metals and concrete, for which aggregates and matrix can be more or less recognizable. In the case of masonry a random or structured distribution of their components controls the behavior. This problem is faced up by a numerical representation what can focus on the micro-modeling of its components (units and mortar) of macro-modeling as a composite [2]. According to the level of accuracy and complexity to be achieved, it is possible to choose the following modeling strategies (Figure 1): In detailed micro-modeling, units and mortar are represented by continuum elements while the unit-mortar interface is represented by discontinuum elements; in simplified micro-modeling, units are expanded and represented by continuum elements whereas the behavior of the mortar joints and unit-mortar interface are lumped in discontinuum elements; in macro-modeling units, mortar and unit-mortar interface are lumped together in a continuum element

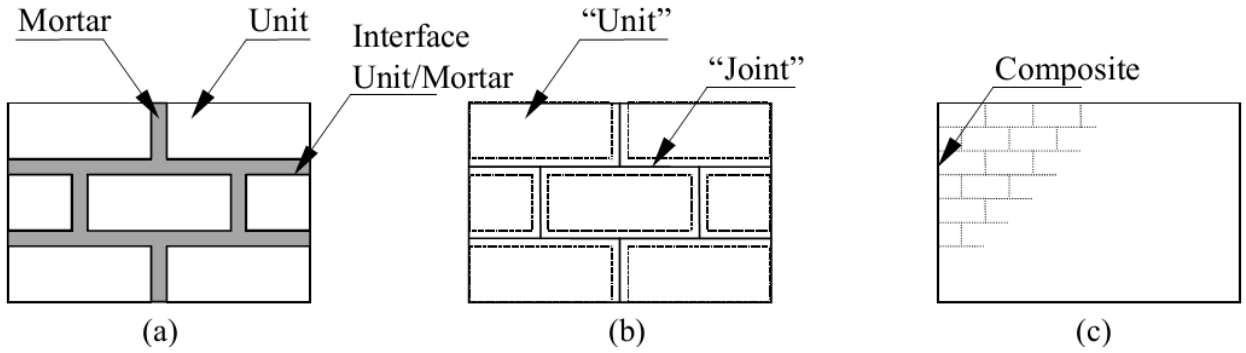

Figure 1. Modeling strategies for masonry structures: (a) Detailed micro-modeling. (b) Simplified micro-modeling. (c) Macro-modeling.

2.2 Homogenization process

The homogenization process consists of choosing a Representative Volume Element Y (RVE) from the microscopic structure which considers the effect that the microscopic structure causes on the macroscopic behavior [3]. Ergo, an entire wall can be represented by the repetition of a RVE (or basic cell) which is composed by unit, bed joint, head joint and cross joint. Therefore, two scales are considered, microscopic scale (y) which is small enough to represent the microstructures of masonry and macroscopic scale (X)

which is larger enough to represent the behavior of the composite structure (Figure 2).

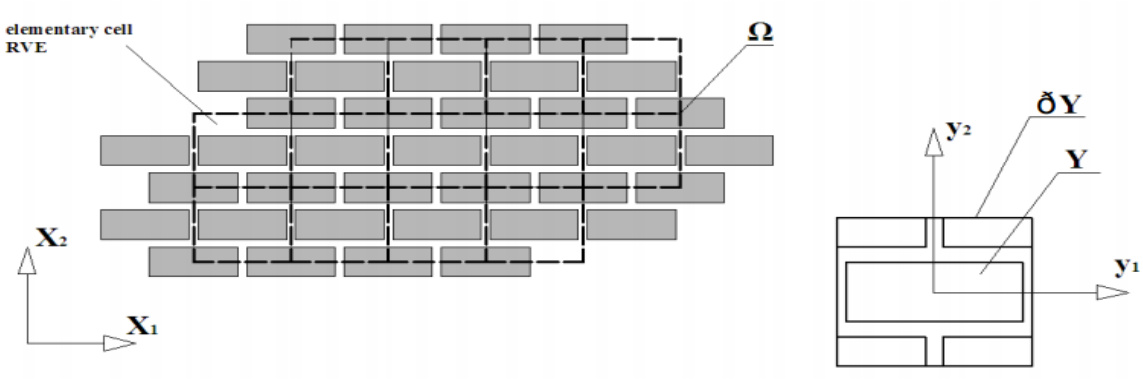

Figure 2. Basic cell for masonry and homogenization process: Macroscale "X" and microscale "y".

The overall effective properties of the composite can be determined introducing averaged quantities that represent the macroscopic stress (Σ) and strain tensors (E) [4] [5] [6], which are available from the study of the RVE and can be written as follows:

$$\boldsymbol{E} =< \varepsilon >= \frac{1}{V}\int_{Y} \varepsilon(\mathbf{u})\, dY \qquad \boldsymbol{\Sigma} =< \boldsymbol{\sigma} >= \frac{1}{V}\int_{Y} \sigma \; dY \tag{2.1}$$

Where:

V = Volume of the elementary cell

σ= Local stress tensor

ε= Local strain tensor

<*>= Averaging operator

Periodicity conditions are imposed on the stress field σ and the displacement field u, given by:

$$\begin{cases} \mathbf{u} = \mathbf{E}\mathbf{y} + \mathbf{u}^{per} & \mathbf{u}^{per} \text{ on } \partial Y \\ \boldsymbol{\sigma}\mathbf{n} & \text{anti-periodic on } \partial Y \end{cases} \tag{2.2}$$

where:

u is the total displacement field, **y** is la relative position between two points on the boundary of the representative volume element "Y", $\mathbf{u}^{per}$ stands for a periodic displacement field, $\sigma\mathbf{n}$ represent the micro-stress vector.

In the equation 2.3 shows the strength domains S^m, S^b and S^{hom} that were considered by Lourenco and Milani [6], [7]. Here, S^m is the strength domain of the mortar, S^b is the strength domain of the units and S^{hom} is the strength domain of the homogenized macroscopic material. Also, [8] has shown that the S^{hom} domain of the equivalent medium is defined in the space of the macroscopic stresses as follows [9]:

$$S^{\hom} = \left\{ \sum \middle| \left\{ \begin{array}{rl} \sum = <\boldsymbol{\sigma}> = \dfrac{1}{A}\displaystyle\int_Y \boldsymbol{\sigma} dY & (a) \\ div\boldsymbol{\sigma} = \mathbf{0} & (b) \\ [\![\boldsymbol{\sigma}]\!]\mathbf{n}^{\text{int}} = \mathbf{0} & (c) \\ \boldsymbol{\sigma}\mathbf{n} \quad \text{anti - periodic} \quad \text{on} \quad \partial Y & (d) \\ \boldsymbol{\sigma}(\mathbf{y}) \in S^m \quad \forall \mathbf{y} \in Y^m \;;\; \boldsymbol{\sigma}(\mathbf{y}) \in S^b \quad \forall \mathbf{y} \in Y^b & (e) \end{array} \right. \right\} \tag{2.3}$$

Here, [[σ]] is the jump of micro-stresses across any discontinuity surface of normal n^{int}. Conditions (a) and (d) are derived from periodicity, condition (b) imposes the micro-equilibrium, condition (c) establishes the equilibrium condition throughout the entire RVE (it is necessary to define boundary conditions of RVE in the composite) and condition (e) represents the yield criteria for the components (brick and mortar). It is important to say that for defining boundary conditions of RVE in the composite, uniform micro-strains on ∂Y are assumed. A dual kinematic definition of S^{hom}, also due to Suquet [6], can be derived through the support function $\pi^{hom}(D)$ as follows:

$$S^{\hom} = \left\{ \sum \middle| \left\{ \begin{array}{l} \sum : \mathbf{D} \le \pi^{\hom}(\mathbf{D}) \quad \forall \mathbf{D} \in R^6 \\ \pi^{\hom}(\mathbf{D}) = \inf\limits_{\mathbf{v}} \left\{ P(\mathbf{v}) \,|\, \mathbf{D} = \dfrac{1}{2\Gamma} \displaystyle\int_{\partial Y = \Gamma} (\mathbf{v} \otimes \mathbf{n} + \mathbf{n} \otimes \mathbf{v}) dS \right\} \\ P(\mathbf{v}) = \displaystyle\int_Y \pi(\mathbf{d}) dY + \int_S \pi([[\mathbf{v}]]; \mathbf{n}) dS \end{array} \right. \right\} \tag{2.4}$$

- v=Dy + v^{per} is the microscopic velocity field
- v^{per} is a periodic velocity field
- d and D are respectively, the microscopic and macroscopic strain rate fields
- S is any discontinuity surface of v in Y, n is the normal to S
- π ([[v]],n)= 1/2 ([[v]] ⊗ n + n ⊗[[v]])
-π (d)=max{σ:d; σ∈S(y)}

It is worth noting that, using the kinematic definition given by equation (2.4), it is possible to explicitly determine the homogenized strength domain of masonry in the space of the macroscopic stresses assuming infinitely resistant units and joints interfaces with Mohr-Coulomb failure criterion [10]. Alternatively, from the set of equations (2.3), S^{hom} can be statically obtained, solving the following optimization problem for every direction of the vector n_Σ:

$$\begin{cases} \max\{\hat{\lambda}\} \\ \text{such that} \begin{cases} \hat{\lambda}\mathbf{n}_\Sigma = \hat{\lambda}[\alpha_{11} \quad \alpha_{22} \quad \alpha_{12}]^T = \dfrac{1}{Y}\displaystyle\int_Y \boldsymbol{\sigma} dY \\ \boldsymbol{\sigma}\mathbf{n} \quad \text{anti-periodic} \quad \text{on} \quad \partial Y \\ div\boldsymbol{\sigma} = \mathbf{0} \\ \boldsymbol{\sigma}(\mathbf{y}) \in S^i(\mathbf{y}) = \begin{cases} S^b \text{ if } \mathrm{y} \in \text{blocks} \\ S^m \text{ if } \mathrm{y} \in \text{mortar} \end{cases} \end{cases} \end{cases} \tag{2.5}$$

where:

- $n_\Sigma = [\alpha_{11} \ \alpha_{22} \ \alpha_{12}]^T$ is a vector in the macroscopic stress space Σ_{12} Σ_{22} Σ_{11}.
- λn_Σ represents a macroscopic stress state on S^{hom} belonging to a straight line from the origin of direction n_Σ.

2.3 Approaches for homogenization

This section addresses briefly the most well-known approaches for obtaining a homogeneous material, in the elastic range and inelastic range. In each case, the approaches adopt different assumptions and simplifications according to the level of accuracy, complexity and computational cost of the numerical model to be achieved.

2.3.1 Approaches for homogenization of masonry in elastic range

a) Two-step approaches

These approaches were presented by Pande [11] who proposed a model in which a two-step stacked system with alternative isotropic layers was considered. For the first step, a single row of masonry units and vertical mortar joints were taken into consideration, and then homogenized as a layered system. For the second step, a layered system material was further homogenized with horizontal joints to obtain the final material (Figure 3). This way, a very simple mechanical system constituted by elastic springs was

obtained. Two step approaches are characterized by: Underestimation of the horizontal stiffness of the homogenized material; No information about the texture (running bond, stack bond, Flemish bond, etc.). For nonlinear analysis, the model entails errors as it is not able to take into account the regular offset of vertical mortar joints belonging to two consecutive layered unit courses. Then, a different homogenized material will be obtained if the steps of homogenization are reversed.

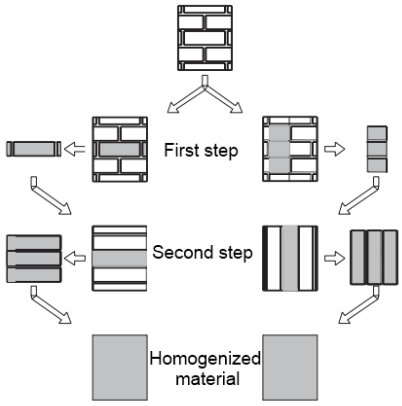

Figure 3. Two-step homogenization [11]: Horizontal homogenization first and vertical homogenization first.

b) Reduction of joints to interfaces

From the fact that masonry units are often stiffer than mortar and joints have a smaller thickness than the size of the masonry units, Felice [12] and Cecchi and Sab [13] presented an approach which consisted on the reduction of joints to interfaces (Figure 4). These studies resulted in the definition of the homogenized masonry constitutive function by means of the introduction of several parameters: ε called scale parameter which tended to zero (Figure 5a), which represents the ratio between the size of the cell and the dimension of the overall panel; ξ=Em/Eb where Em is the Young's modulus of the mortar and Eb is the Young's modulus of the masonry unit; φ=e/a where "e" is the thickness of the joints and "a" is the size of the characteristic module.

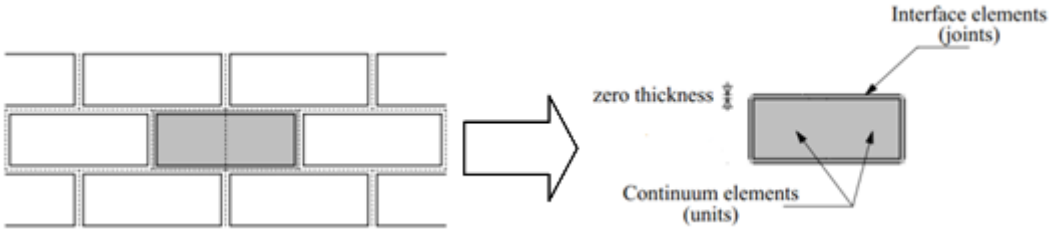

Figure 4. Elementary cell considering zero thickness of mortar joints

Then, when φ tends to zero the joint becomes an interface although if ξ tend to zero the mortar becomes infinitely deformable with respect to the unit. In order to solve that problem of infinite deformations, Felice [12] and Cecchi and Sab [13] proposed to represent the joints by elastic springs, hence the Poisson effect of is neglected. Also, de Felice [12] assumed rigid masonry units. Cecchi and Sab [13], using mathematical software, discretized the elementary cell by means of a coarse triangular mesh, considering deformable masonry units and finite thickness of the joints (Figure 5b). In this way these authors were able to find ‘‘quasi-analytical’’ formulas.

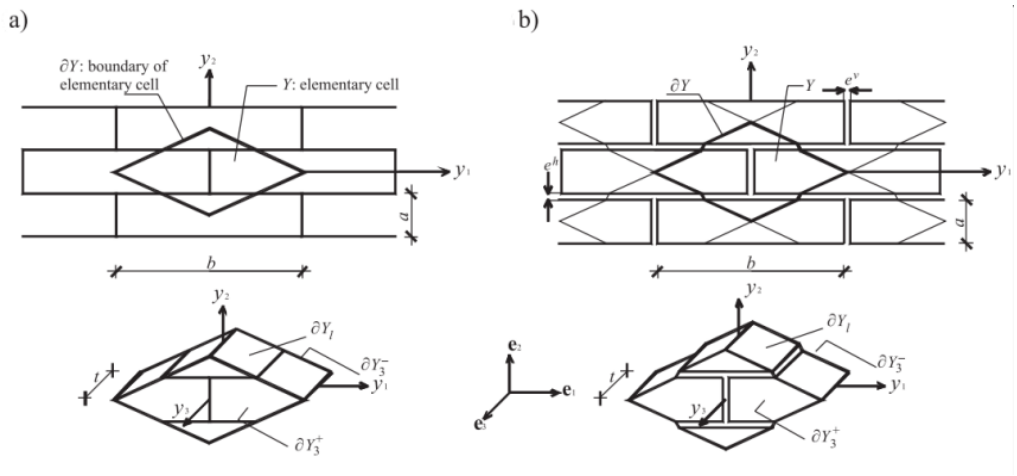

Figure 5. a) Elementary cell considering zero thickness of mortar joints and triangular discretization, b) Elementary cell considering finite thickness of mortar joints and triangular discretization

The disadvantages of this approach are: The reduction of joints to interfaces, which may strongly reduce the accuracy of the results in the presence of thick mortar joints and ratios tending to zero[14]. The introduction of elastic masonry units leads to only “quasi-analytical’’ formulas for the homogenization problem but increases the computational cost. The influence of joint thickness is lost when the simplifications assumed. Compared with FE approaches in the case of nonlinear analysis, the errors in the result can be no negligible.

c) Finite element procedures

In this approach, all the features of units and mortar joints (thickness), perfect continuity between units and mortar are considered in the evaluation of the homogenized modulus. It is important to indicate that some engineering approaches do not consider all the features of units and mortar joints [15]; [16]. Nevertheless, the important limitation of this approach is that the computational cost of a FE procedure is much higher than macroscopic approaches, which is particularly demanding for nonlinear analysis

2.3.2 Approaches for homogenization of masonry in inelastic range

For the non-linear analysis of masonry the most well-known approaches are briefly detailed next.

a) Engineered approaches

An engineered approach can be based on a two-step homogenization, which, in order to use be for nonlinear analysis, must include a plasticity model[17], a damage model [18], a cracking model [19]. Furthermore, micromechanical homogenization approaches must consider additional internal deformation mechanisms, which have been derived namely by van der Pluijm [20], Lopez et al. [15], and Zucchini and Lourenco [16]. According to the observations by Luciano and Sacco [21]; Gambarotta and Lagomarsino [22]; Calderini and Lagomarsino [23], masonry failure occurs with damage of mortar joints. Then, masonry failure could be present as result of a combination of bed and head joints failures (Figure 6). It is important to stress some limitations of these approaches: In each joints, uniform stress and strain states are assumed, which is only an approximation.

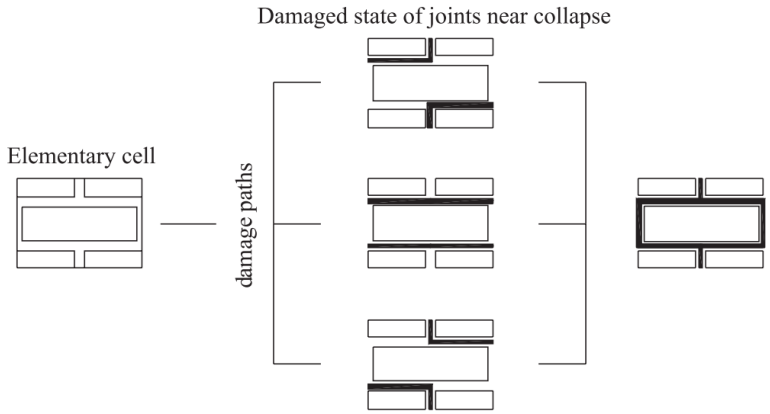

Figure 6. Nonlinear approach with joints failure, damaged state of joint near collapse

b) Limit analysis approaches

Limit analysis approaches [24], [7] are based on the assumption of a perfectly plastic behavior with an associated flow rule for the constituent materials. In this framework, Suquet [6] proved that both static and kinematic approaches can be used to obtain an upper- or lower-bound estimation of the homogenized failure surface of a periodic arrangement of rigid plastic materials. De Buhan and de Felice [10] were the first ones to apply the kinematic theorem of limit analysis in the masonry homogenization, assuming that joints are reduced to interfaces with a classic Mohr-Coulomb failure criterion and masonry units are infinitely resistant. Milani [7] adopted a static approach in which compressive failure, the thickness of the joints and unit crushing were considered.

These approaches have the following advantages: The computational cost of the limit analysis approach can compete with macroscopic approaches, while providing reliable information about failure. They can also be implemented in FE limit analysis codes for collapse analysis. Some of the limitations of these approaches are worth noting: Limit analysis is not able to give information about displacements when collapse produces. IMasonry behavior is also quasi-brittle and the assumption that the ductility of masonry is infinite is only an approximation.

c) Finite element nonlinear approaches

This approach considers a nonlinear damage model, proposed by Pegon and Anthoine [5] and Massart [25] for the constituent materials. In the microscopic step, for each Gauss point, the stress–strain relation is obtained by solving the homogenization problem at a cell level. Then, in the macroscopic step, the structural nonlinear problem is solved using the Gauss points information collected in the microscopic phase. The advantages of these approaches are: Even under complex combination of loads the inelastic masonry behavior can be reproduce well. For panels of small dimension, the computational costs of these approaches at a cell level is not so high and provides results with enough accuracy when compared with experimental tests, as shown by Massart [26]. Nevertheless, these approaches also have limitations, as the computational cost for analysis complex structures or whole 3D building is very high.

3. GUIMARÃES CASTLE: BRIEF REVIEW AND GEOMETRICAL CHARACTERIZATION OF THE MASONRY UNITS

Abstract

In this chapter, a geometrical characterization of the masonry unit from the wall Guimarães castle is carried out. First, review of historical aspects and descriptions of Guimarães castle are presented, followed by a characterization of the masonry and statistical analysis. Finally, the history of interventions is presented.

3.1 Historical aspects

The name of Portugal was not recognized in the Iberia nation until before the 10th century, before the widow of the Count of Tui, a Galician lady called the Countess Mumadona Dias, crossed all Minho region and settled in Vimaranes. Mumadona established her ownership in order to accomplish the Count of Tui wishes in his will, as he wanted to settle a monastery in his lands. Then, it was around this monastery that small early villages started to settle [27].

At that time, the Muslims invasions were repeated frequently. Due to the severity of attacks of the Muslims against the Lords of Leon, Mumadona decided that it was not enough to build a monastery with a firm foundation and solid walls to protect the monks and people. She ordered to build a castle, where religious and secular could be protected when the Muslim armies passed by. For the construction of the defensive structure, the Countess chose a hill called Monte Latito (Mount Latito). The castle was overlooking the place where the monastery was built. On this hill, the first walls of the castle were raised [27].

In the 11th century, Count D. Henrique and his wife D. Teresa, settled in Guimarães, remodeling and expanding the castle. Here was born D. Afonso Henriques, who, in 1128, fought the battle of Saint Mamede against the troops of his mother and Galician Count Fernão Peres de Trava, who tried to seize the government of the Portucalense County. D. Afonso Henriques gained independence and became the first king of Portugal.

Later, between 12th and 14th centuries, the castle of Guimarães suffered more changes. During the reign of D. Afonso III (1248-1279) the castle started to improve its defenses. This improvement was continued by his son D. Dinis and finished by D. Fernando in the 15th and 16th centuries. In this period, Portugal was looking for new frontiers across the seas and the old castle became the residence for the mayor. Years later, the castle was abandoned, and suffered damages caused by time and by the subsequent changes of use from a prison to military headquarters, and there was even a proposal for its demolition [28] The current condition is shown in Figure 7a.

3.2 Description

The plan view of the castle is pentagonal (Figure 7b). The castle is also surrounded by eight square towers, which delimit the main square, while in the center of the castle is settled the Tower of Menagem (main tower). The current version of the castle has Romanesque origin; it has a French model [29], with the geometric shield-shaped, with small central chamber and difficult access. It has many Gothic features

and it has been modified since the end of the thirteen century and in the next century, for example the tower of Menagem and the walls of the Alcáçova were enlarged, probably built on top of existing buildings.

Figure 7. a) Panoramic View of Guimarães Castle, b) Plan view of Guimarães Castle.

3.3 Characterization of the masonry and statistical analysis

The masonry of the castle is made using granite stone ashlars in the external leaves. The masonry features horizontal courses and is relatively regular, despite the fact that the height of the courses is not constant and that the length of the units is rather variable (Figure 8a). In order to represent this feature, a statistical description considering mean, standard deviation, coefficient of variation and probability distribution of the size of the stone units from four walls to will be calculated. The statistical study starts with a visit to Guimarães castle where photograph of its walls were taken, in order to register the geometry of each stone, a scale ruler of 15 cm was placed on the walls while photographs were taken (Figure 8b).

Figure 8. a) Random patterns with horizontal alignment in Guimarães castle b)Scale ruler on the wall

For the sake of simplicity the four walls that were chosen to this study will be called in hereafter Wall1, Wall2, Tower wall and Alcaçova wall will be located as it can be seen in the Figure 9.

Then the statistical analysis was carried out as follows: the first statistical analysis is done for each wall independently and thereafter all walls are analyzed together in order to consider the castle as a whole. It is important to note that for starting the statistical analysis the variables and the population must to be defined whereby the length (l) and height (h) of stone units have been considered as variables and the numbers of stone units considered in each sample of walls are the following: Wall1 has 110 units; Wall2 has 110 units; the Tower wall has 110 units and Alcaçova wall has 308 units.

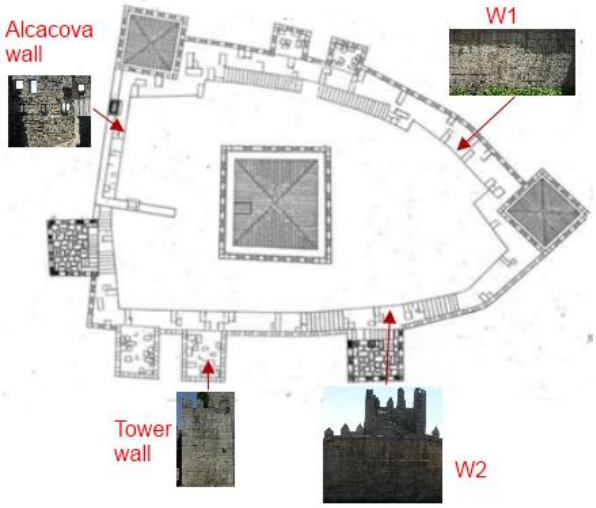

Figure 9. Location of the Wall1, Wall2, Tower wall and Alcaçova wall

The results from the statistical analysis of Wall1, Wall2, Tower wall, Alcaçova wall and the entire sample walls are presented below:

In Wall1 (Figure 10), the mean values of the length and height of the stones are 75.8 cm and 38.9 cm respectively; the standard deviation values for the length and height of the stones are 25.6 cm (coefficient of variation CoV of 34%) and 7.94 cm (CoV of 20%) respectively. The length of stones is typically about 67.5 cm. Unit lengths between 60 cm and 75 cm have the largest frequency with 30 out of 110 stones. The smallest lengths are about 37.5cm and the largest length is about 172.5 cm, which is atypical with frequency of only one stone. The histogram is slightly skewed to the right. The height of stones is typically about 40 cm. Heights between 36 cm and 44 cm have the largest frequency with 42 out 110 stones. The smallest height is about 18cm and the largest height is about 40 cm. There are atypical heights of 22 cm with a frequency of 2 stones. The best fit for probabilistic distributions for both variables is the 3-parameters lognormal (Figure 11), been a general skew distribution in which the logarithm of any linear function of the variables is normally distributed

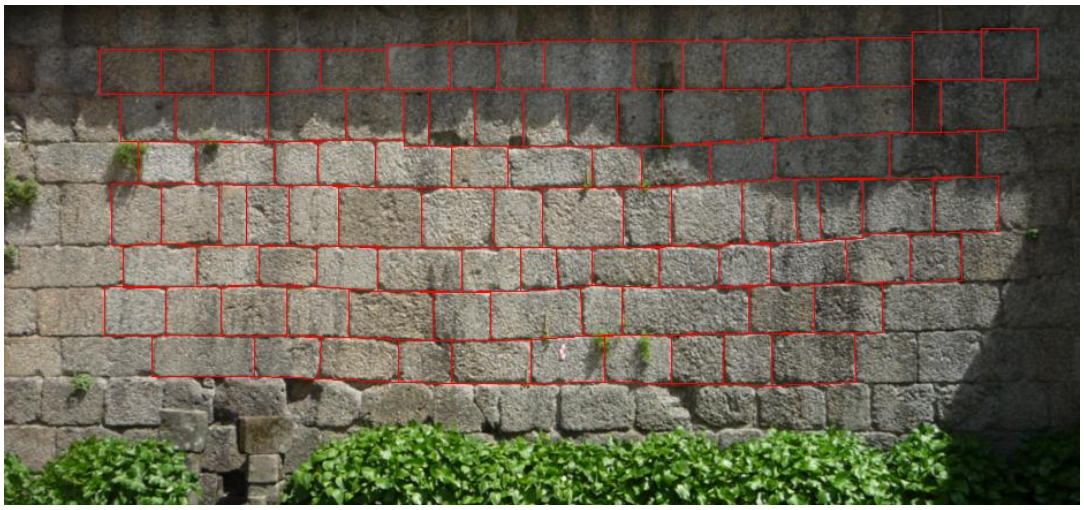

Figure 10 Identification of the stones inside the Wall1

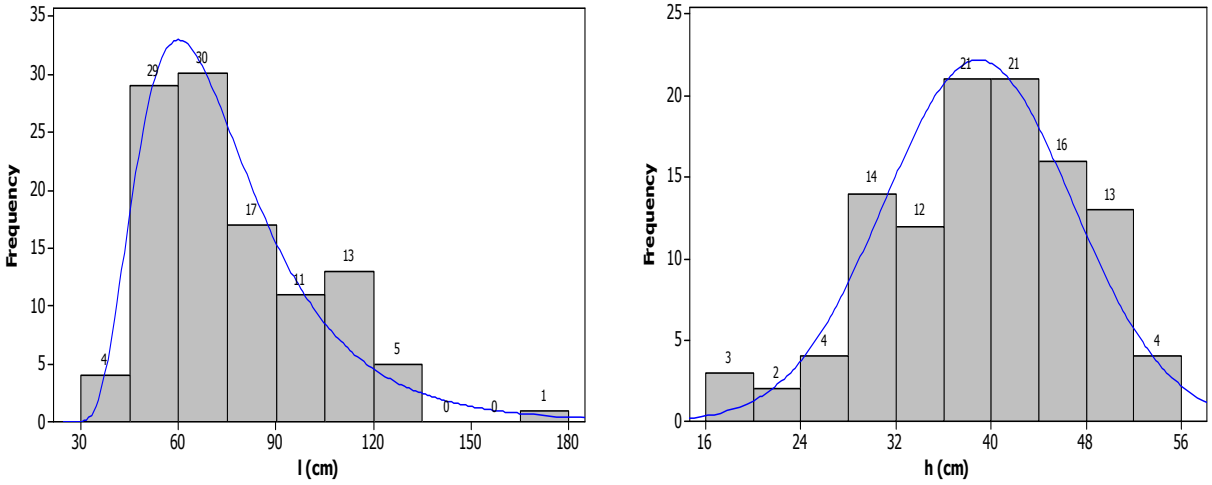

Figure 11. Distribution of length (l) and the height (h) of the stones in the Wall 1

In Wall2 (Figure 12), the mean values of the length and height of the stones are 69.7 cm and 43.8cm, respectively; the standard deviation values the length and heights of the stones are 18.9 cm (CoV of 27%) and 8.17 cm (CoV of 19%) respectively. The length of stones is typically about 65 cm. Lengths between 60 cm and 70 cm have the largest frequency with 30 out of 110 stones. The smallest lengths are about 45cm and the largest length is about 135 cm. There is atypical length of 125 cm with a frequency of 1 stone. The histogram is slightly skewed to the right. The height of stones typically is about 40 cm. Heights between 38 cm and 40 cm have the largest frequency with 27 out 110 stones. Also there is a second group of stones with a frequency of 24 stones, with lengths between 44 and 46cm. The smallest height is

about 24cm and the largest is about 60 cm. The best fit probabilistic distribution for both variables is the 3-parameters lognormal (Figure 13).

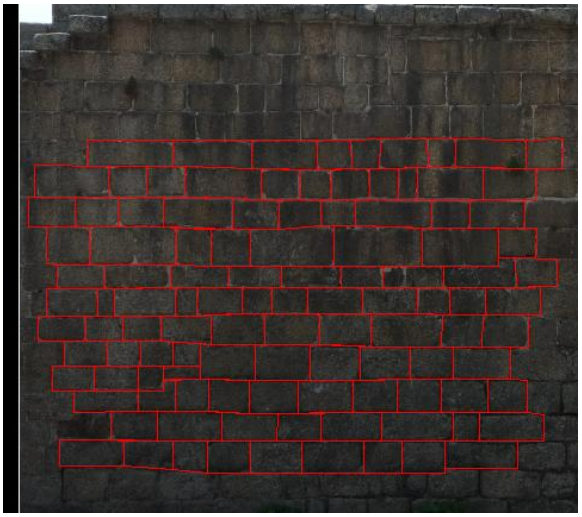

Figure 12. Identification of the stones inside the Wall2

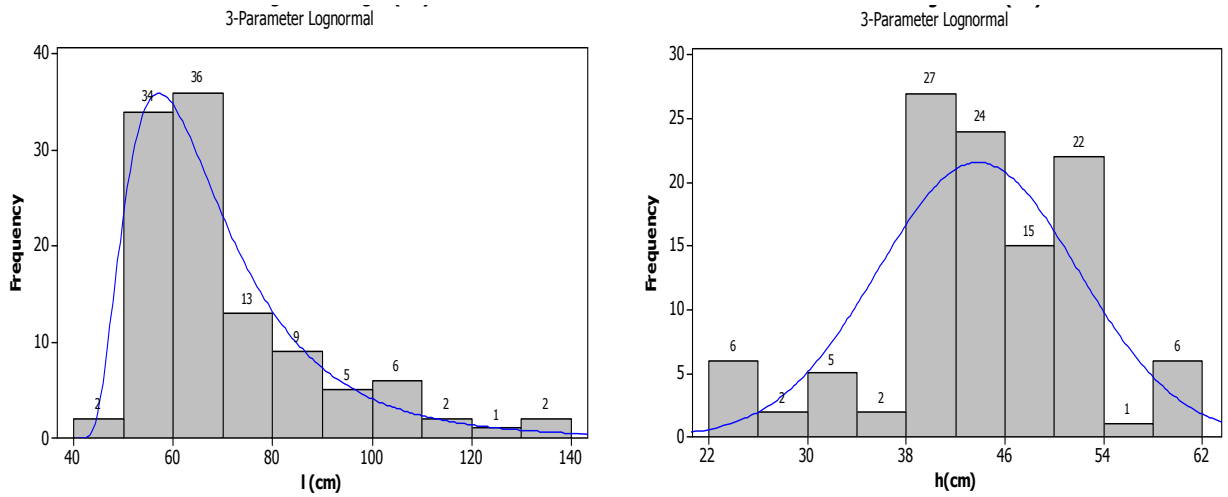

Figure 13. Distribution of length (l) and the height (h) of the stones in the Wall 2

In the Tower wall (Figure 14), the mean values of the length and height of the stones are 85.2 cm and 45.7 cm, respectively; the standard deviation values the length and heights of the stones are 31.63 and 7.57 respectively. The length of stones (b) typically is about 62.5 cm. Lengths between 55 cm and 70 cm have frequency of 37 stones. The smallest lengths are about 47.5 cm and the largest is about 182.5 cm which is atypical with frequency of 2 stone. The histogram is slightly skewed to the right. The height of stones (h) typically is about 49.5 cm. Heights between 47 cm and 52 cm are quite frequent. The smallest

heights are about 14.5 cm and the largest is about 59.5 cm which is frequency of 1 stone. The histogram is slightly skewed to the left. The probabilistic distribution for both variables is 3-parameters lognormal (Figure 15).

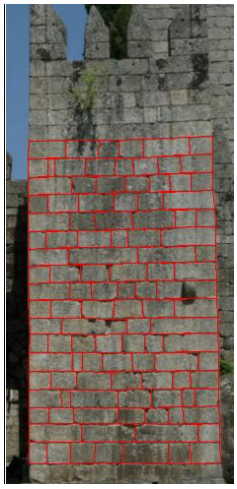

Figure 14. Identification of the stones inside the Tower wall

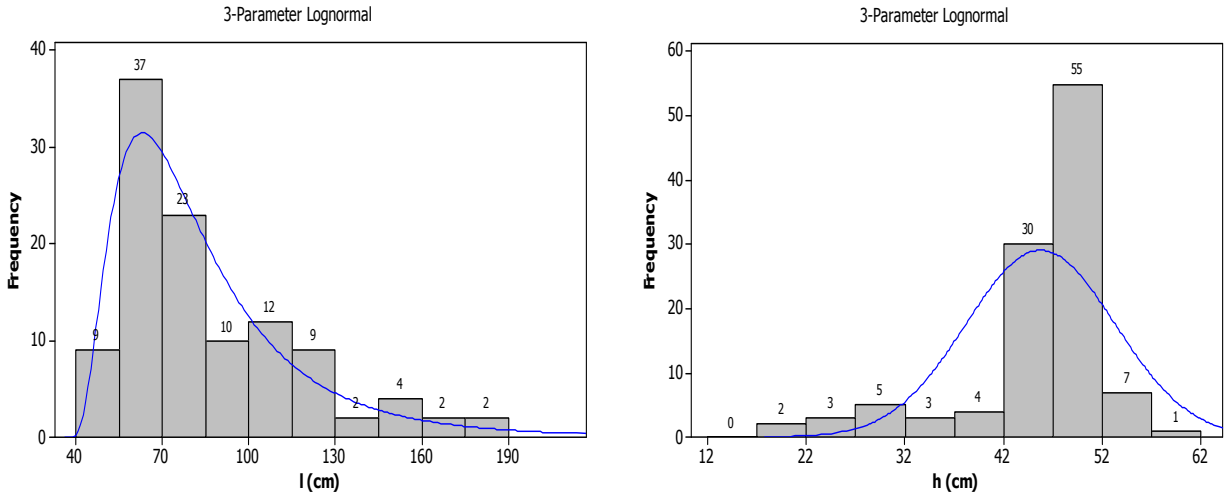

Figure 15. Distribution of length (l) and the height (h) of the stones in the Wall 1

In Alcaçova wall (Figure 16), the mean values of the length and height of the stones are 59.8 cm and 33.5 cm, respectively; the standard deviation values the length and heights of the stones are 26.35 cm and 7.62cm respectively. The length of stones (b) typically is about 45 cm. Lengths between 40 cm and 50 cm have frequency of 77 stones. The smallest lengths are about 25 cm and the largest is about 210 cm which is atypical with frequency of only 1 stone. The histogram is slightly skewed to the right. The height of

stones (h) typically is about 39 cm. Heights between 38 cm and 40 cm are quite frequent. Also there is a second group of stones with frequency of 50 whose lengths are between 26 and 28cm. The smallest heights are about 15 cm and the largest is about 62 cm which is atypical with frequency of 1 stone. The probabilistic distribution for both variables is 3-parameters lognormal. (Figure 17),

Figure 16. Identification of the stones inside the Alcaçova wall

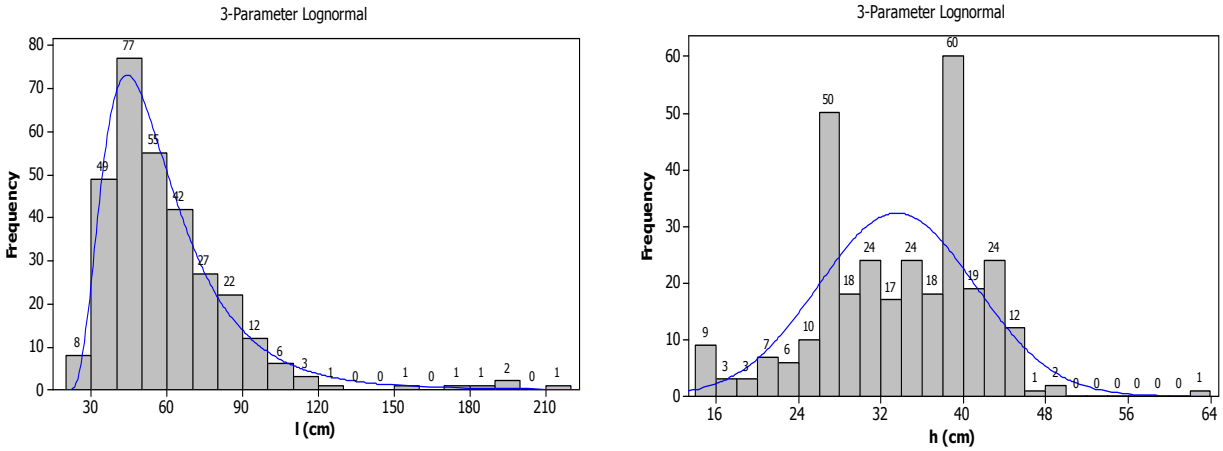

Figure 17. Distribution of length (l) and the height (h) of the stones in the Alcaçova wall

When all samples are considered together, the mean values of the length and height of the stones are 68.6 cm and 38.4, respectively; the standard deviation values the length and height of the stones are 27.8 cm (CoV of 40%) and 9.26 cm (CoV of 24%) respectively. The length of stones is typically about 55 cm. Lengths between 50 cm and 60 cm have the largest frequency (133 out 639 stones). Also there is a

second group of stones with a large frequency (125 out 639 stones), with lengths between 60 and 70cm. The smallest lengths are about 25 cm and the largest is about 210 cm, being both atypical. The histogram is slightly skewed to the right. The height of stones is about typically 39 cm. Heights between 38 cm and 40 cm are quite frequent. The smallest heights are about 13 cm and the largest is about 62 cm, which are both very atypical. The probabilistic distribution for both variables is the 3-parameters lognormal (Figure 18).

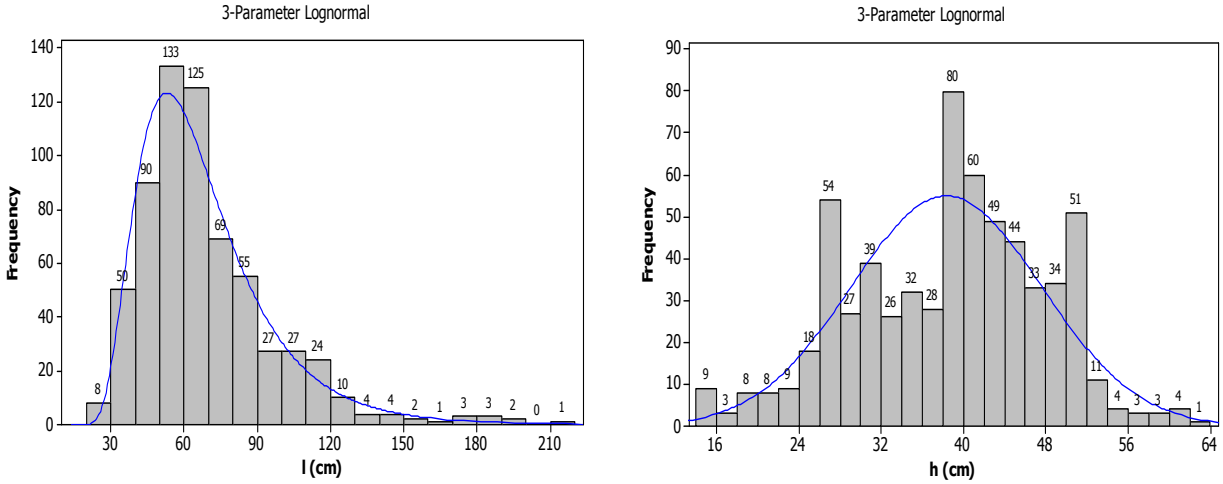

Figure 18. Distribution of length (l) and the height (h) of the stones in the all samples together

In the Table 1, it can see a summary of the more significant parameters that were by the statistical analysis

Sample	Mean Length (l)	Mean Height (h)	h/l
Wall1	75.79	38.94	0.51
Wall2	69.67	43.81	0.63
Tower wall	85.23	45.73	0.54
Alcaçova wall	59.81	33.55	0.56
All samples	68.65	38.35	0.56

Table 1. Statistical parameters of wall samples from Guimarães castle

From the statistical analysis is worth to note the following points:

- There is a large variation between the mean value of the stone length and height in the four walls selected for sampling (60 to 80 cm in length and 34 to 46 m in height). The ratio between the maximum and minimum value found is similar to both quantities (about 75%).

- The stone geometrical ratio is rather important for the quality of the masonry bond. The value of h/b for the average geometrical dimensions is about 56% (1:1.8). Only in Wall2, a slightly different h/b ratio is found, equal to 63% (1:1.6).
- The scatter found in the length is always much larger than the scatter found in the height, being the scatter in the full sample not so much different from the scatter in the individual samples.
- Wall 2 is the sample with lowest scatter and the Alcaçova is the sample with the largest scatter, despite that fact that the Alcaçova sample is three times larger than Wall 2.
- The difference between averaging the total sample, weighted by the number of samples or weighted equally is only moderate, with about 5% change in the dimensions.
- The probabilistic distribution for the length is clearly skewed, requiring a lognormal distribution. The probabilistic distribution for the height is relatively symmetric, meaning that a normal distribution can be used.

3.4 History of interventions

The geometrical study carried out will be used to assess the safety of the Alcaçova wall, identified recently as the part of the castle presenting the largest structural vulnerability. For this purpose, the past, recent and planned interventions are briefly revised next.

3.4.1 Past interventions

The Castle of Guimarães is of military architecture, Romanesque and Gothic, but the currently building is the result of many interventions since the second half of the thirteenth century. According to Fonte [30] with the arrival of D. Henrique, the Castle suffered a series of changes, including the expansion of its area, the addition of the Tower of Menagem, the addition of the battlements and loopholes, the opening of two gates and the construction of the Alcazaba Condal (housing two floors) in the northern part.

Later on, D. Afonso III built the fence around the "Vila do Castelo" and D. Dinis and D. João I built the two towers flanking the entry doors. Along time, the use of the castle changed, from prison, military barracks, and finally the monument. The Capuchin friars were responsible for the disappearance of the Hall of the Castle (ruins of the citadel), because the stones were used to build a convent. Also the south part was severely damaged due to stones removed to pave the streets of Guimarães. For building the house of the guard, the battlements of the Tower of Menagem were cut down on three sides.

By 1937, the original floors from the tower of Menagem had been replaced by others located at different levels than the originals. The old cover of roof was slated and supported by a timber truss poorly built and of poor quality. The part of the castle in worse condition of conservation was located on North area, specifically in the area of the Alcáçova. The south wall (angular part) was consolidated, together with the reconstruction of all timber floors, timber stairs and timber roof of the Menagem tower. In 1958, the bridge which connects the tower and the walls was installed. In 1971, stairs and floors of the north tower were reconstructed [31], [32]. The demolition of several masonry walls recently been built in the main square was made, as these walls covered up the foundations of the ancient citadel, whose plan is now clearly defined. Finally, the works also included consolidation of the walls of the Alcáçova, which were in ruin, and partial reconstruction of the chimney.

3.4.2 Recent Intervention

Between 2008 and 2009, interventions were conducted by Direcção de Serviços dos Bens Culturais da Direcção Regional de Cultura do Norte (DRCN) to consolidate the foundations and stabilization of the wall of the north west Tower due to damage such as openings in the walls. The wall of the Alcáçova was partly consolidated and conservations works were made at the entrance door of the Castle. In the Alcáçova, the chimney of the North wall was strengthened using a set of metal plates in its interior, together with the placement of a capping mortar on top of the wall of the Alcáçova in order to prevent water ingress.

3.4.3 Planned Intervention

As previously mentioned, the Guimarães city has several cultural and historic spaces of reference at a local and national level in Portugal, being Guimarães castle, one of icons of the Portuguese history and the independency of the country, home of the first King in 12th century. It is national monument since 1910 and forms part of a World Heritage Site; given the historical importance of the castle, over the years Guimarães castle been subjected to several interventions to conserve it. Then in 2008, TecMinho, a private non-profit association and sponsored by the University of Minho and the Association of Municipalities of Vale do Ave, at the request of the ICM (Instituto dos Museus e da Conservação) executed a set of non-destructive test to the Castle of Guimarães , carried out by the FEUP (Faculdade de Engenharia da Universidade do Porto) in 2008 to assess whether the anomalies in the Castle might create structural problems that jeopardizes the integrity of the building or not.

Non-destructive tests were carried out on the wooden roofs of the north tower, the south tower and the Menagem tower. In the wooden roofs of the towers, the tests were performed using a hygrometer, with

pylodin and resistographer, while Alcaçova wall was carried out an inspection, using a baroscopic camera and sonic and dynamic tests (Figure 19). Visual inspection with the baroscopic camera allowed to verify that Alcaçova wall is built with granite stones and composed of two leaves and rubble infill. Each leaf is has a thickness between 30 and 40 cm equipped granite, while the infill is composed gravel and rubble, with the existence of voids. Through this inspection was also possible to identify several layers of mortar and water within of the walls. The sonic tests allow to verify as it was said before, the existence of voids within the wall that, been an alternative to solve this problem to consolidate the wall by means of the technique of injection of grout. Finally, the dynamic test has verified that the structure has a slightly high natural frequency as a consequence of some locking in the wall, providing by adjacent buildings.

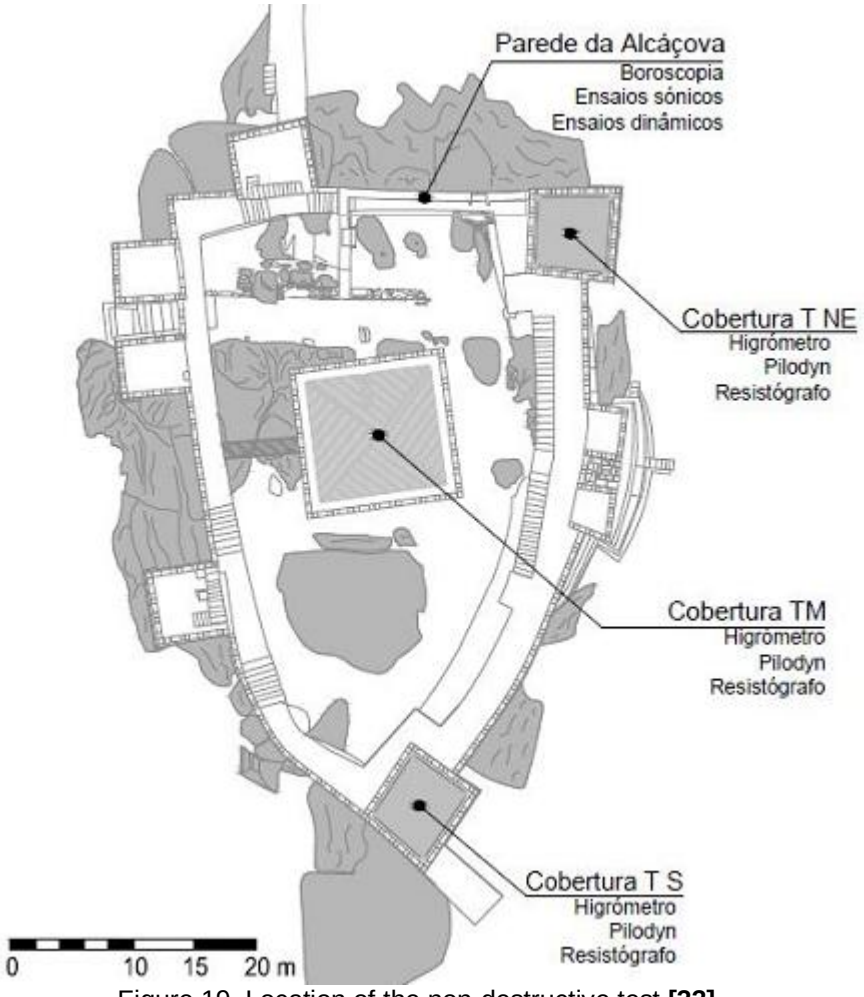

Figure 19. Location of the non-destructive test **[33]**

At the present, due to the event Guimarães 2012 European Capital of Culture, a set of actions at the level of conservation, accessibility and communication have been raised, allowing the castle to be in proper

condition to receive thousands of visitors, One of these actions is a project of intervention about one of the walls of the castle that is located in the north part and known as Alcáçova (Figure 9) in where it is planning to use injections of grout in the joint of the wall whereby, this thesis will be focused in particularly in Alcáçova, being one of its main characteristics the quasi periodic arrangement of the stones, this characteristic become a issue from the point of view of the structural analysis due to the difficulties for obtaining proper and efficient numerical models capable to predict its behavior under out-of-plane loads such as earthquakes loads. In the next chapter, samples (representative volume elements) will be taken from the wall in order to estimate the masonry properties.

4. HOMOGENIZED LIMIT ANALYSIS OF REPRESENTATIVE VOLUME ELEMENTS

Abstract

This chapter presents homogenized the limit analysis of nine representative volume element (RVE) samples from the Alcaçova wall in the Guimarães castle, Portugal. The RVEs are analyzed under in-plane load in order to obtained the in-plane surface failure at different orientations of a load with respect to the bed joint, considering masonry with weak and strong mortar joint independently .Also, the RVEs are analyzed under out-of-plane load in order to obtained the out-of-plane surface failure at increasing compressive loads; again considering masonry with weak and strong mortar independently. The result allows subsequent implementation of the obtained failure surfaces in the study of the full masonry wall.

4.1 Introduction

Limit analysis has been extensively used in the study of masonry structures [7] because it requires only a low number of material parameters and provides inputs such as failure mechanisms, limit multipliers of loads, at least on critical sections and the stress distribution at collapse. The aim of the studies carried out here through limit analysis is to determinate the in-plane and out-of-plane homogenized failure surfaces of randomly assembled stone masonry for different representative volume elements (RVE), from observations in different walls of Guimarães castle. For this purpose homogeneous models composed by random assemblage of stones with variable dimensions, with lognormal distributions of height and width, are considered, assuming that joints are reduced to interfaces. Two different possibilities for the joints are analyzed using different sizes of cell level (RVE) in order to obtain the masonry failure surfaces: the first case consists in masonry with weak mortar and the second case is masonry with strong mortar, being representative of masonry adequately bonded for example using lime based grout. In-plane failure surfaces are described by horizontal strength (σ_h) and vertical strength (σ_v). Out-of-plane failure surfaces are described by horizontal bending moment (M11), vertical bending moment (M22) and torsional moment, or torsion, (M12).

4.2 Numerical Models

4.2.1 Geometry of the representative volume elements (RVEs)

The finite element model which represents the RVE is built using samples of walls from Guimarães castle, more precisely from the Alcaçova wall, which has approximately a length of 14.30 m and a height of 6.90 m. The wall is built using two eternal leaves with an average thickness of 400mm each and separated by an infill. The wall was built with 308 stones irregularly disposed, but maintaining the horizontal alignment of the bed joints (coursed masonry). It was decided to consider three RVEs of different size: the first size, called 3x3, has dimensions three times the mean width and the mean height of stone; the second size, called 4x4, is four times the mean width and the mean height of stone; and the third size, called 5x5, is fifth times the mean width and the mean height of stone. The mean widths and mean heights of stone were calculated by the process explained in the chapter 3. For each size of RVE, three different samples located randomly on the wall are taken into account (Figure 20 and Table 1). Also, three artificial RVEs were built using mean size stones and periodic arrangement in order to compare the failure surfaces between the RVEs with quasi periodic arrangement and the RVEs with periodic arrangement using average geometry. A linearized Lourenço and Rots [34] failure criterion is adopted for joints reduced to interfaces and a classic Mohr-Coulomb failure criterion is used for brick interfaces [10] as it was done by Lourenço and Rots[34], Milani et al. [7] and Sutcliffe et al.[35]. In their analyses, all authors

reduce the joints to interfaces and adopt a frictional-type failure behavior for mortar. A non-linear cap model is chosen in [34], whereas a linear approximation of the cap, is adopted in[35], with the aim of studying the problem in the framework of linear programming.

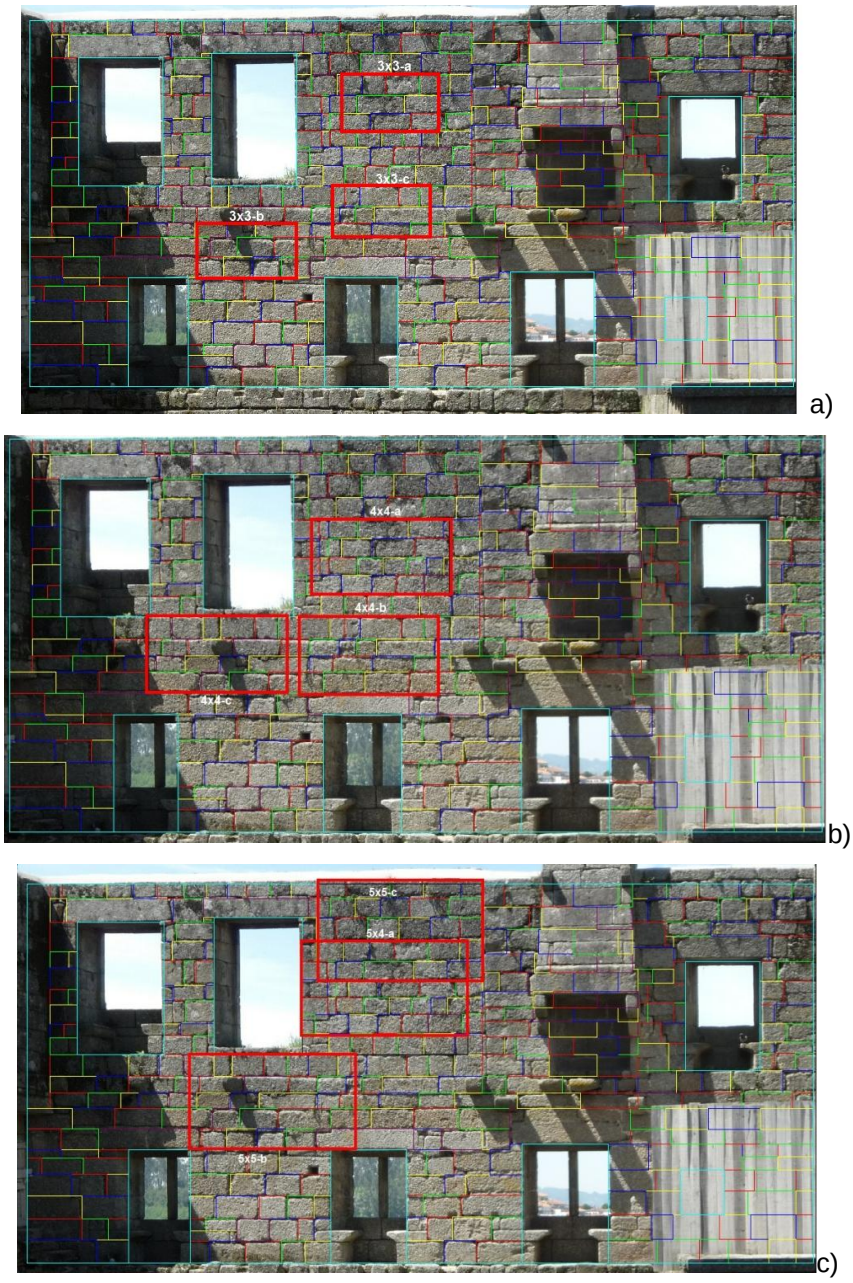

Figure 20 Location of representative volume elements a) 3x3 RVE. b) 4x4 RVE c) 5x5 RVE

	Width (cm)	Height (cm)
Mean Stone	59.81	33.55
3x3	179.43	100.65
4x4.	239.24	134.2
5x5	299.05	167.75

Table 1 Geometry of the representative volume element

4.2.2 Construction of the numerical models for representative volume elements (RVEs)

For the preparation of the models, first of all using finite element software and adopting a micro-modeling approach, nine representative volume element were taken from Alcaçova wall as it was described previously (three for each average dimensions). The finite element mesh is built dividing each stone of the wall using triangular continuum elements and reducing the joints to zero thickness interfaces. 3x3-a RVE has 96 triangular elements and 64 nodes; 3x3-b RVE has 59 triangular elements and 41 nodes; 3x3-c RVE has 69 triangular elements and 47 nodes; 4x4-a RVE has 341 triangular elements and 198 nodes, 4x4-b RVE has 97 triangular elements and 63 nodes; 4x4-c RVE has 64 triangular elements and 101 nodes; 5x5-a RVE has 201 triangular elements and 353 nodes, 5x5-b RVE has 91 triangular elements and 148 nodes, 5x5-c RVE has 84 triangular elements and 137 nodes. An artificial RVE with a periodic arrangement of stones is also prepared for each geometry (See Table 2). It is important to notice that each representative volume element is built of different elements which correspond to stones (each color represents a different stone) so that the algorithm can recognize whether the interface lying between two elements belong to the brick or mortar (Figure 21-Figure 24). Also it is necessary to define two different elements which represent rigid elements for the boundary conditions. It is worth to say that, in the generation of the RVE models, simplifications with respect to the real conditions of the stones such as the existing cracking, deterioration or other damage.

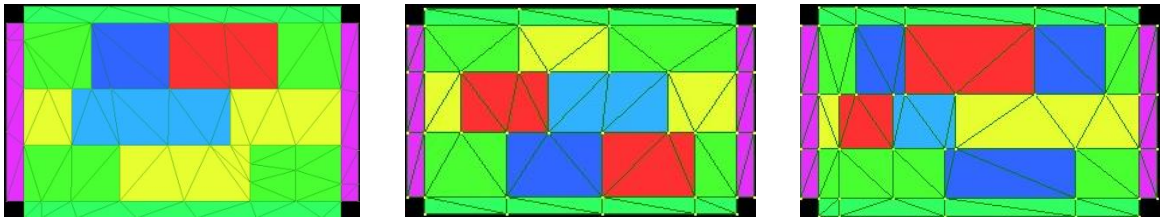

3x3-a 3x3-b 3x3-c

Figure 21. 3x3 RVE numerical models, taken from Alcaçova wall with a triangular mesh

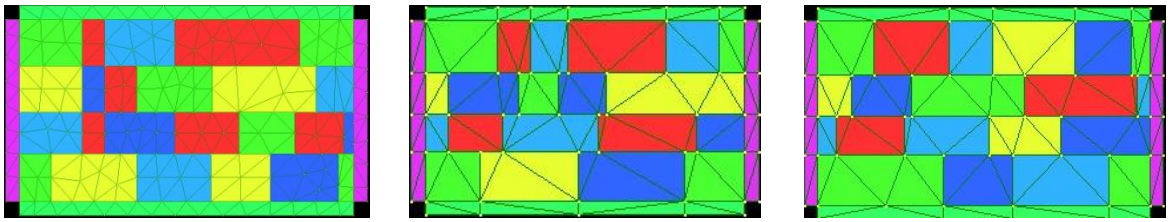

4x4-a 4x4-b 4x4-c

Figure 22. 4x4 RVE numerical models, taken from Alcaçova wall with a triangular mesh

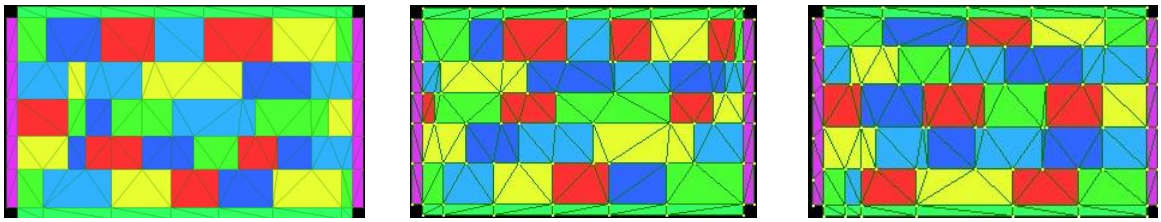

5x5-a 5x5-b 5x5-c

Figure 23. 5x5 RVE numerical model, taken from Alcaçova wall with a triangular mesh

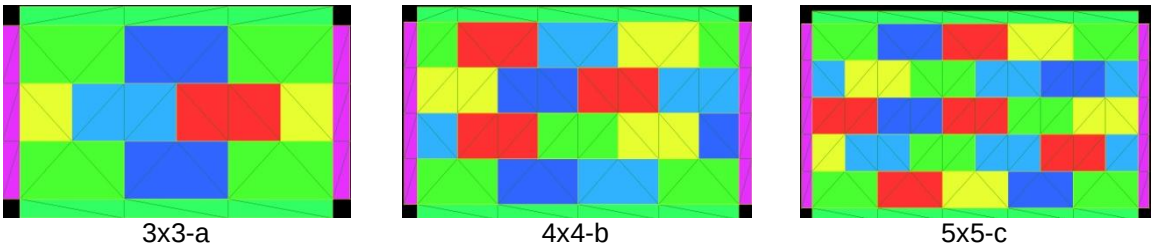

3x3-a 4x4-b 5x5-c

Figure 24. Artificial RVE numerical model, taken from Alcaçova wall with a triangular mesh and periodic arrangement

RVE	Number of nodes	Number of elements
3x3-a	64	96
3x3-b	41	59
3x3-c	47	69
3x3-periodic	38	54
4x4-a	198	341
4x4-b	63	97
4x4-c	64	101
4x4-periodic	59	91
5x5-a	201	353
5x5-b	91	148
5x5-c	84	137
5x5-periodic	80	130

Table 2. Number of nodes and number of triangular elements of the representative volume elements (RVE)

4.3 In-plane homogenized failure surfaces

4.3.1 Formulation to obtain in-plane homogenized failure surfaces

The in-plane homogenized failure surfaces (σ_v – σ_h) are obtained keeping ϑ angle fixed. This angle is formed between the bed joint and the macroscopic horizontal action (σ_{hh}) and changing ψ angle which is defined by ψ=tan-1 σ_{vv}/σ_{hh}, where σ_{vv} is the macroscopic vertical action. Then, the unit vector can be expressed by the objective functions in terms of ϑ and ψ in (Equation 4.1). Using objective functions, it is possible to solve this problem and to obtain the load multiplier and failure surface [36].[35] [7]

$$\Sigma_{1,1} = \frac{1}{2}(\cos(\psi)(1+\cos(2\vartheta)) + \sin(\psi)(1-\cos(2\vartheta)))$$
$$\Sigma_{1,2} = \frac{1}{2}(\cos(\psi)(1-\cos(2\vartheta)) + \sin(\psi)(1+\cos(2\vartheta)))$$
$$\Sigma_{1,3} = \frac{1}{2}(\cos(\psi)\cos(2\vartheta) - \sin(\psi)\cos(2\vartheta))\tan(2\vartheta) \qquad 4.1$$

Here Σ1,1; Σ1,2; and Σ1,3 represent compression, tension, and shear respectively. Three different ϑ angles are considered ϑ=0°, ϑ=22.5° and ϑ=45° (Figure 25) in analogy to Page [37] experimental result. For each RVE and in each orientation ϑ, 32 values with steps of 11.25º have been calculated. The 32 points were connected by a line in order to draw failure surfaces. Nevertheless, it will show up an optimization problem, given by Equation (4.2) and it is non-linear. When S^i stands for the failure surface of the component (block or mortar) belonging to the i^{th} sub-domain. The optimization problem is solved by using an algorithm code, developed in [36]

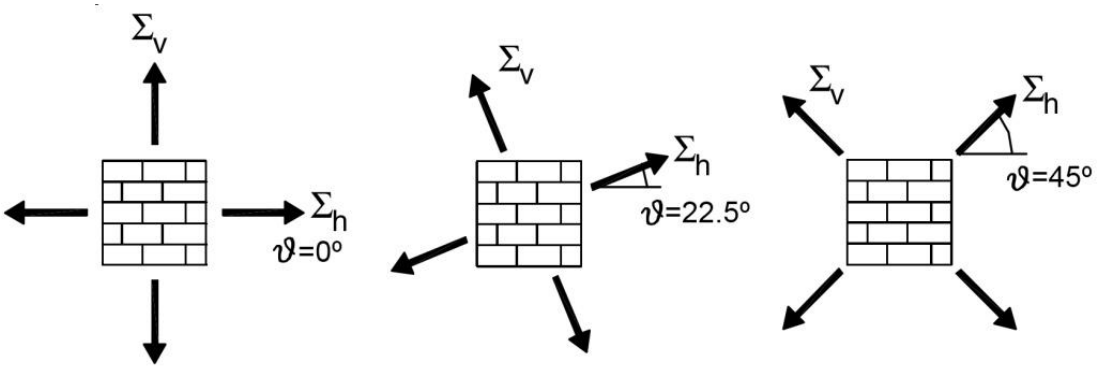

Figure 25. ϑ angle: orientations of the external load with respect to the bed joint **[38]**

In order to use linear programming algorithms, each of the non-linear inequalities of Equation (4.2), that generally is non-linear [39], can be approximated by a set of linear inequalities (as proposed in the past, for instance, by Anderheggen and Knopfel [40] or Maier [41]), replacing the yield surfaces with inscribed hyper-polyhedrons. Finally, the convergence of the solution obtained should be checked by progressively increasing the number of planes of the approximation [42].[9]

$$\begin{cases} \max\left\{\hat{\lambda}\right\} \\ \text{such that} \begin{cases} \hat{\lambda}\mathrm{n}_{\Sigma} = \dfrac{1}{Y}\sum_{k}\int_{Y}\widetilde{\mathrm{X}}^{(\mathrm{k})}(\mathrm{y})\widetilde{\mathrm{S}}dY \\ \mathrm{y}^{\mathrm{j}} \equiv \text{nodal point} \\ \widetilde{\sigma}^{\mathrm{j}} = \widetilde{\mathrm{X}}^{(\mathrm{k})}\left(\mathrm{y}^{\mathrm{j}}\right)\widetilde{\mathrm{S}} \\ \widetilde{\sigma}^{\mathrm{j}} \in S^{i} \quad j = 1,\ldots,rq \\ k = 1,\ldots,4k^{\max} \end{cases} \end{cases} \tag{4.2}$$

An iterative procedure is used in this thesis to solve the optimization problem as it is more efficient. The main idea of iterative procedure is: in the starting step, a coarse linear approximation of the non-linear failure surfaces of the components is adopted (Figure 26) [43]. The application of the simplex method in the optimization at the ith step leads to an optimal solution in a corner of the domain. From the iterative ith solution point, a new tangent plane is added in P', (Figure 26b), then (i+1)th optimization procedure is restarted. The iterations continue until a fixed error tolerance between the ith and (i+1)th solution is reached [44].

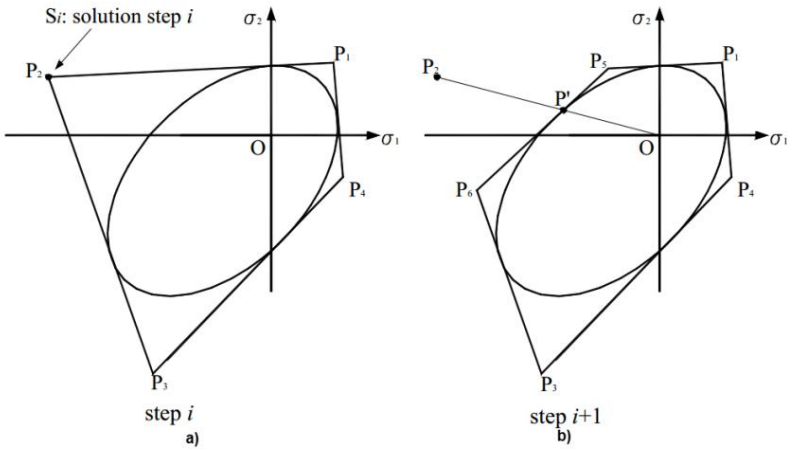

Figure 26 Iterative procedure utilized in the optimization problem. a) Step i. b) Step i+1 **[44]**

The goal of the iterative procedure is to give an approximation of the yield surface by a circumscribed polyhedron which represents an approximated solution of the optimization problem [45]. Then, in order to solve the optimization problem, equation 4.1 is added to equation 4.2 as follow:

$$\begin{cases} \max\{\hat{\lambda}\} \\ \text{such that} \begin{cases} \hat{\lambda}\mathbf{n}_{\Sigma} = \frac{1}{Y}\sum_{k} \int_{Y} \widetilde{\mathbf{X}}^{(k)}(\mathbf{y})\widetilde{\mathbf{S}}\,\mathrm{d}Y \\ \mathbf{y}^{j} \equiv \text{nodal point} \\ \tilde{\boldsymbol{\sigma}}^{j} = \widetilde{\mathbf{X}}^{(k)}(\mathbf{y}^{j})\widetilde{\mathbf{S}} \\ \tilde{\boldsymbol{\sigma}}^{j} \in S^{k} \quad j = 1,\ldots,rq \quad k = 1,\ldots,4k^{\max} \\ n_{\Sigma,1} = \frac{1}{2}(\cos(\psi)(1+\cos(2\vartheta)) \\ \qquad +\sin(\psi)(1-\cos(2\vartheta))) \\ n_{\Sigma,2} = \frac{1}{2}(\cos(\psi)(1-\cos(2\vartheta)) \\ \qquad +\sin(\psi)(1+\cos(2\vartheta))) \\ n_{\Sigma,3} = \frac{1}{2}(\cos(\psi)\cos(2\vartheta) \\ \qquad -\sin(\psi)\cos(2\vartheta))\tan(2\vartheta) \end{cases} \end{cases} \qquad 4.3$$

Where the direction of the load $[\Sigma 11\ \Sigma 22\ \Sigma 12]^{T}$ depends on the orientation ϑ of the principal directions with respect to the bed joints (Figure 25). Once the limit multiplier values from each step at the end of each simulation are obtained, those values shall be expressed on the principal axes (Equation 4.4), using Mohr circle theory. This process must be performed for each value of ϑ (0º, 22.5º and 45º). [7]

$$\begin{cases} \textit{for } \cos(\psi) < \sin(\psi) & \begin{cases} \Sigma_{V} = \dfrac{\Sigma_{x}+\Sigma_{y}}{2} + \sqrt{\left(\dfrac{\Sigma_{x}-\Sigma_{y}}{2}\right)^{2} + \Sigma_{xy}^{2}} \\ \Sigma_{H} = \dfrac{\Sigma_{x}+\Sigma_{y}}{2} - \sqrt{\left(\dfrac{\Sigma_{x}-\Sigma_{y}}{2}\right)^{2} + \Sigma_{xy}^{2}} \end{cases} \\ \textit{otherwise} & \begin{cases} \Sigma_{V} = \dfrac{\Sigma_{x}+\Sigma_{y}}{2} - \sqrt{\left(\dfrac{\Sigma_{x}-\Sigma_{y}}{2}\right)^{2} + \Sigma_{xy}^{2}} \\ \Sigma_{H} = \dfrac{\Sigma_{x}+\Sigma_{y}}{2} + \sqrt{\left(\dfrac{\Sigma_{x}-\Sigma_{y}}{2}\right)^{2} + \Sigma_{xy}^{2}} \end{cases} \end{cases} \qquad 4.4$$

4.3.2 Algorithm for obtaining in-plane homogenized failure surfaces

In order to obtain homogenized failure surfaces the properties of the components of the masonry must be defined. For masonry with weak mortar, the compressive strength of masonry is assumed equal to 12MPa and the ultimate tensile strength of joints is assumed equal to 0.05 MPa. The compressive strength of

stones is assumed equal to 89.5 MPa and their ultimate tensile strength is equal to 0.93 MPa [46]. For masonry with strong mortar, only the ultimate tensile strength of masonry is changed, assuming a value equal to 0.3 MPa. For the joints a linearized failure criterion [34] is adopted (Figure 27).

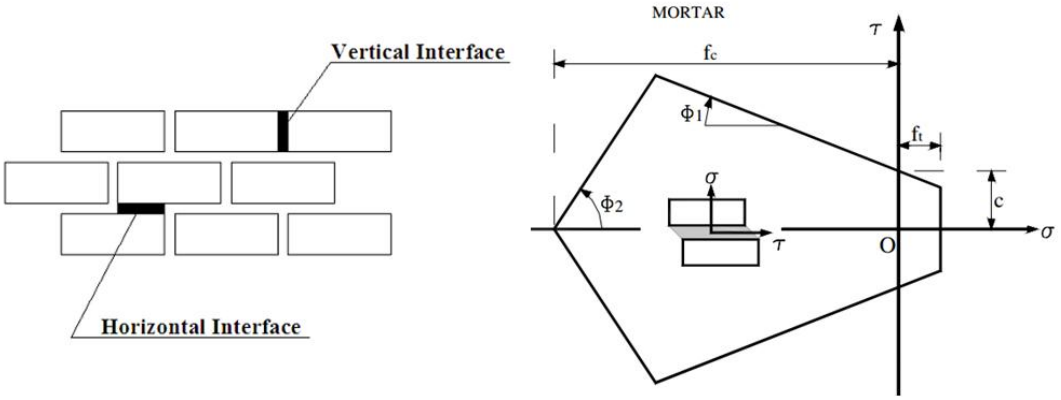

a) b)

Figure 27.a) Joints reduce to interfaces b) Interface failure surface adopted for mortar and stone joints[34]

For the definition of the mesh, it is necessary to build two matrices, one called matrix A that stores all the information with respect to the nodes, placing in the first column the node number and placing in the second, third and fourth columns the coordinate of the nodes.

```
A=[ Node     1    0.0000000000000E+0    6.8359677109180E+0    0.0000000000000E+0
    Node     2    9.0121424342482E-1    6.8359677109178E+0    0.0000000000000E+0
    Node     3    2.4753998749829E+0    6.8359677109178E+0    0.0000000000000E+0
    Node     4    3.3943980190097E+0    6.8359677109180E+0    0.0000000000000E+0

    Node   124    1.0557570428470E+1    0.0000000000000E+0    0.0000000000000E+0
    Node   125    1.2357570428470E+1    0.0000000000000E+0    0.0000000000000E+0
    Node   126    1.4157570428470E+1    0.0000000000000E+0    0.0000000000000E+0
    Node   127    1.4400000000000E+1    0.0000000000000E+0    0.0000000000000E+0   ];
```

Figure 28 Example of Matrix A with nodes data

The topology of elements is stored in Matrix B (Figure 29) and its consecutive columns contain the following information: element type, element number, digit 1, material code, and node numbers.

```
B=[Tri3      1      1      1      1     12      2
   Tri3      2      1      1      1     16     12
   Tri3      3      1      1     12     16     17
   Tri3      4      1      1      3      2     12

   Tri3    170      1      3    125    113    114
   Tri3    171      1      3    125    126    113
   Tri3    172      1      3    113    126    115
   Tri3    173      1      3    126    127    115 ];
```

Figure 29 Example of Matrix B with elements data

The boundary conditions on displacement are stored in matrix bc_u (Figure 30) where from the first to the fourth columns there are the nodes coordinates which will be fixed, and the fifth and six columns store the values of initial velocities, which are assumed as zero here, and the seventh column stores the directions in which velocity is fixed. Here, the number 1 represents velocity in direction X and the number 2 represents the velocity Y. These boundary conditions allow e.g. performing calculations for tension and compression, as well as for shear with tension or shear with compression.

```
bc_u=[      x1          y1          x2          y2
1.130376e+0 9.102325e-1 1.078531e+0 7.400169e-1 0 0 1
1.130376e+0 9.102325e-1 1.078531e+0 7.400169e-1 0 0 2
```

a)

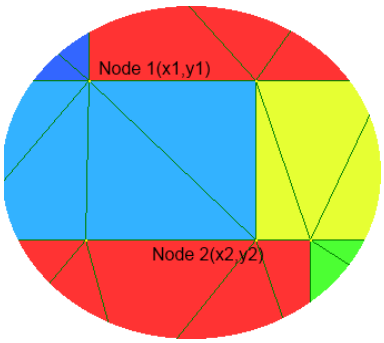

b)

Figure 30 a) Boundary conditions in the matrix bc_u b) Fixed boundary conditions in triangular element of RVE

The next step is to define the objective function which is stored in the matrix called ob, where it is possible to set the direction of the load according to the ϑ angle, see Figure 31. In the present work the loading angle of the representative volume element ϑ takes values of 0º, 22.5º and 45º, which are provided to the algorithm successively and provide different failure surfaces. The number of points for which the failure surfaces will be drawn is defined according the ψ angle. Defining properly this objective function is important because it not only provides failure surfaces but also provides multiplier limit loads.

```
ob=[
     0     0     0     H     -alfa     -alfa     1     0
     0     0     L     0     -beta     -beta     2     0
     L     0     L     H      alfa      alfa     1     0
     0     H     L     H      beta      beta     2     0

     0     0     0     H     -gamm     -gamm     2     0
     0     0     L     0     -gamm     -gamm     1     0
     L     0     L     H      gamm      gamm     2     0
     0     H     L     H      gamm      gamm     1     0
```

$$alfa = \frac{1}{2}\left(\cos(\psi)(1+\cos(2\vartheta)) + \sin(\psi)(1-\cos(2\vartheta))\right)$$

$$beta = \frac{1}{2}\left(\cos(\psi)(1-\cos(2\vartheta)) + \sin(\psi)(1+\cos(2\vartheta))\right)$$

$$gamm = \frac{1}{2}\left(\cos(\psi)\cos(2\vartheta) - \sin(\psi)\cos(2\vartheta)\right)\tan(2\vartheta)$$

Figure 31 Objective functions to solve the homogenization problem

4.3.3 Results of the analysis of the representative volume elements for in-plane loads

Figure 32 shows a typical in-plane homogenized failure surfaces for RVEs of masonry with weak mortar at different orientations of the load with respect to the bed joint. The RVEs exhibit the usual anisotropic behavior of masonry and are different for each orientation of the load (ϑ=0º, ϑ=22.5º and ϑ=45º). In the case that the load are applied parallel to the bed joints (ϑ=0º), the failure surface shows the compressive strength of masonry, equal to 12 MPa.

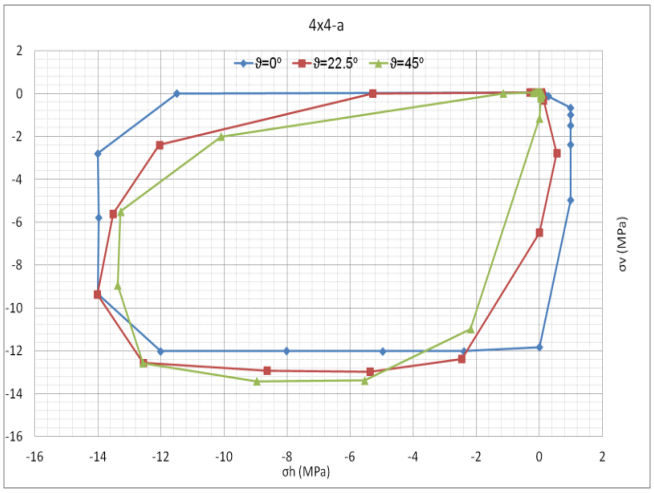

Figure 32 Typical in-plane homogenized failure surfaces for 4x4 RVE of masonry with weak mortar at different orientations of the load with respect to the bed joint

When the orientation of the load is ϑ=22.5º and ϑ= 45º, the failure surfaces shape change with respect to the failure surface ϑ=0º, showing higher values in compression strength. Figure 33 shows a typical in-plane homogenized failure surfaces for RVEs of masonry with strong mortar at different orientations of the load with respect to the bed joint. These failure surfaces, as shown in the previous cases, have a clear

anisotropic behavior (The failure surfaces of all the RVEs can be seen in the ANNEX Figure 63-Figure 68).

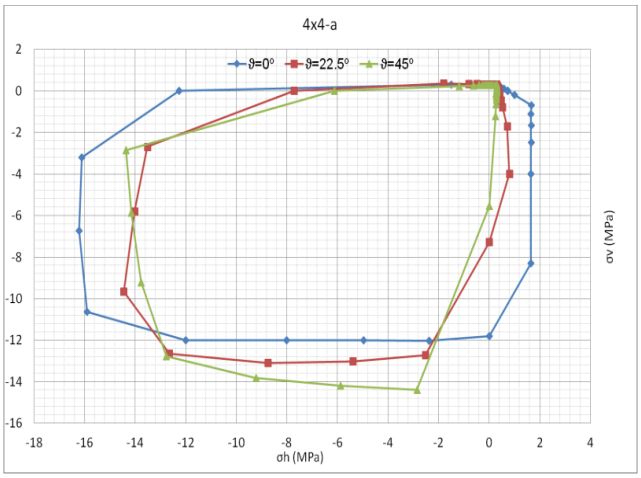

Figure 33 In-plane homogenized failure surfaces for 4x4 RVE of masonry with strong mortar at different orientations of the load with respect to the bed joint

Figure 34, masonry with weak mortar, and Figure 35, masonry with strong mortar, show a comparison between in-plane homogenized failure surfaces obtained from RVEs of the same size and artificial RVEs with periodic arrangement for masonry at different orientations of the load with respect to the bed joint. As it can be seen if failure surfaces obtained from RVEs of the same size are compared, their failure surfaces are similar, while more deviation is found for the artificial RVE, with significant differences in horizontal strength. Furthermore, in both cases, with weak and strong mortar, the continuous alignment of the bed joint means that there is no variation of the vertical strength (σ_h). Therefore, the representative volume element tends to fail along the preferential plane of weakness formed by the bed joint (The failure surfaces of all the RVEs can be seen in the ANNEX Figure 69-Figure 74)

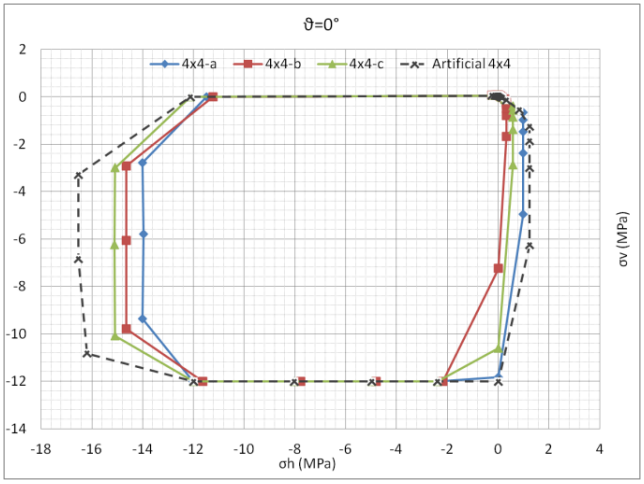

Figure 34. Comparison between in-plane homogenized failure surfaces obtained from 4x4 RVEs and artificial 4x4 RVE for masonry with weak mortar masonry at different orientations of the load

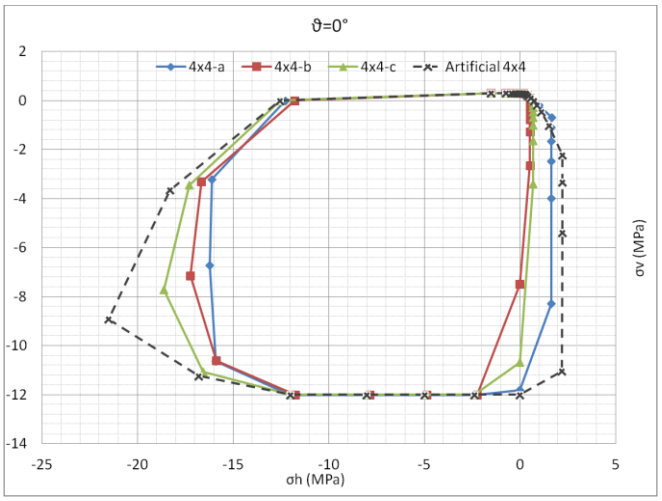

Figure 35. Comparison between in-of-plane homogenized failure surfaces obtained from 4x4 RVEs and artificial 4x4 RVE for masonry with strong mortar at different orientations of the load

Figure 36a - Figure 38a, masonry with weak mortar, and Figure 36b-Figure 38b, masonry with strong mortar, show a comparison between the mean values of in-plane homogenized failure surfaces at different orientations of the load with respect to the bed joint for each size of RVEs. All failure surfaces provide similar average results, with the exception of the 3x3 mean failure surface at ϑ=0° that is not in agreement with the other surfaces, because 3x3 RVEs (see Figure 23) have better interlocking of stones. The failure surfaces of all the RVEs can be seen in the ANNEX Figure 75-Figure 77. These preliminary results seem to indicate that the average of 3 masonry samples, with minimum size of 3x3, provides a reasonable estimate of the true failure surface.

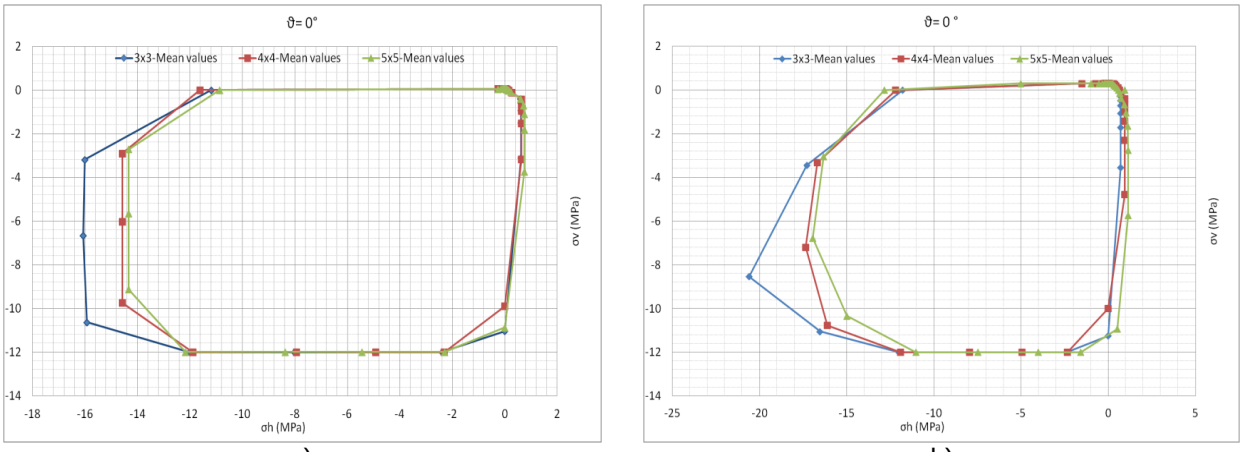

Figure 36. Comparison between the mean values of in-plane homogenized failure surfaces for each size of RVEs at the load to ϑ=0º a) RVE with weak mortar and b) RVE with strong mortar

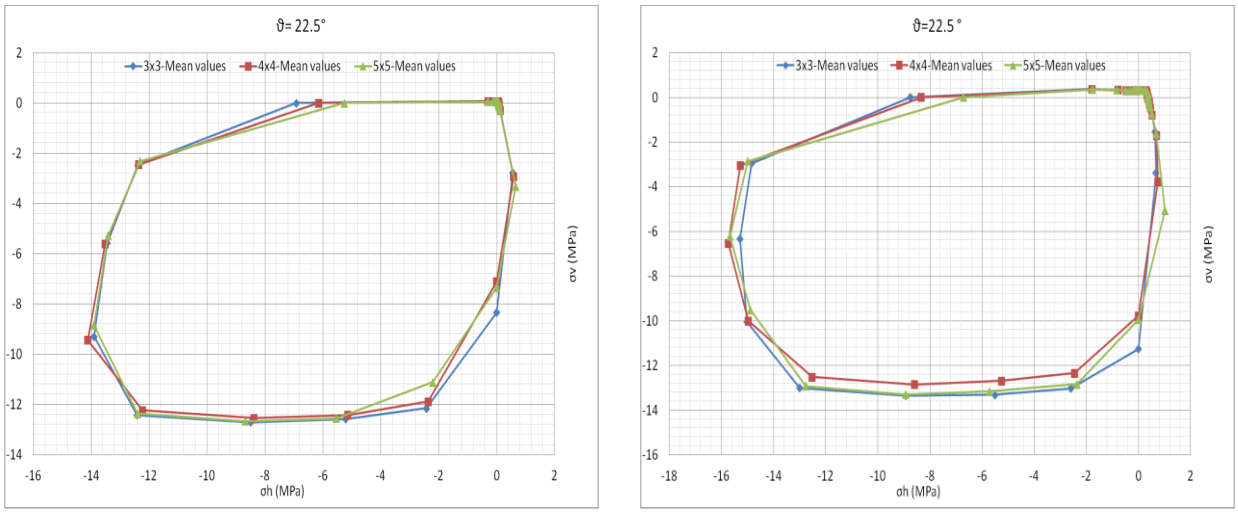

Figure 37. Comparison between the mean values of in-plane homogenized failure surfaces for each size of RVEs at the load to ϑ=22.5º a) RVE with weak mortar and b) strong mortar

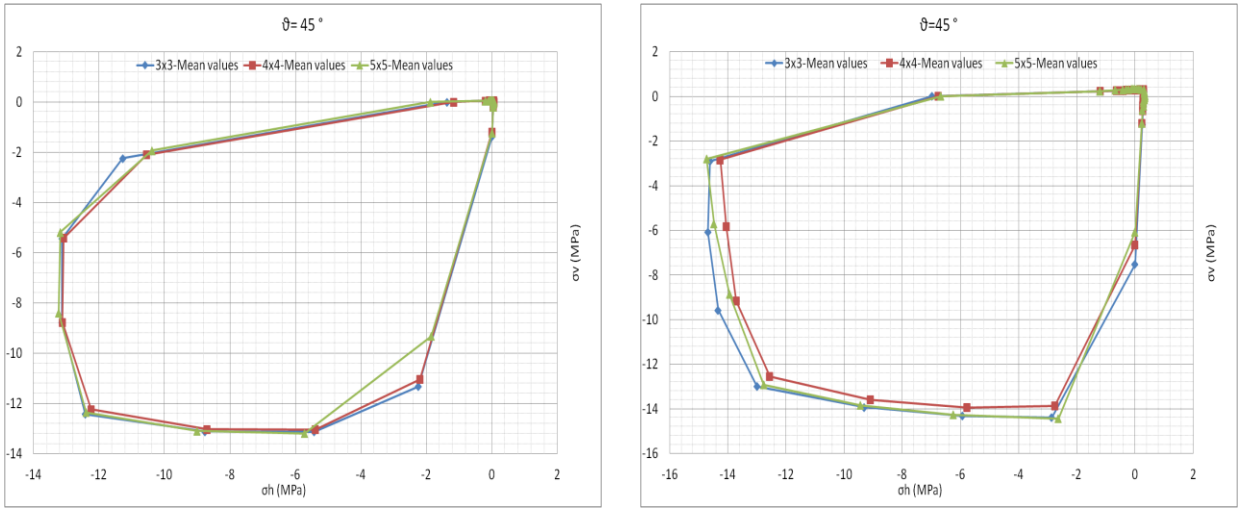

Figure 38. Comparison between the mean values of in-plane homogenized failure surfaces for each size of RVEs at the load to ϑ=45º a) RVE with weak mortar b) RVE with strong mortar

4.3.4 Qualitative comparison between in-plane failure modes of the representative volume element and experimental in-plane failure modes obtained by Dhanasekar

The failure modes obtained from representative volume element are depicted in Figure 39-Figure 41 and are compared with the failure modes obtained experimentally by Dhanasekar [47], as there is no

experimental data related with failure surfaces in the Alcaçova wall. It is worth saying that the comparisons are only qualitative, in terms of failure modes. Figure 39 allows to verify the similarities between the experimental and representative volume element failure patterns at orientations of the load equal to ϑ=0º for masonry with weak and strong mortar. A staircase crack in the 4x4 representative volume element if found independently of the quality of the mortar. It is noted that dilatancy [48] is present in the numerical model, even if it is believed that the influence in the global behavior is very low (the upper boundary is allowed to move up, meaning that an artificial confining stress built up does not occur). Figure 40 and Figure 41 show the same comparison for an orientations of the load equal to ϑ=22.5º and ϑ=45º, where it is observed that the diagonal crack is also well captured by the model, even if a perfect similarity to the experimental tests from Dhanasekar are not possible, as the non-periodic arrangement of the units of the masonry in the experimental stage influence in the cracking patterns. The failure modes of all the RVEs can be seen in the ANNEX Figure 63-Figure 68.

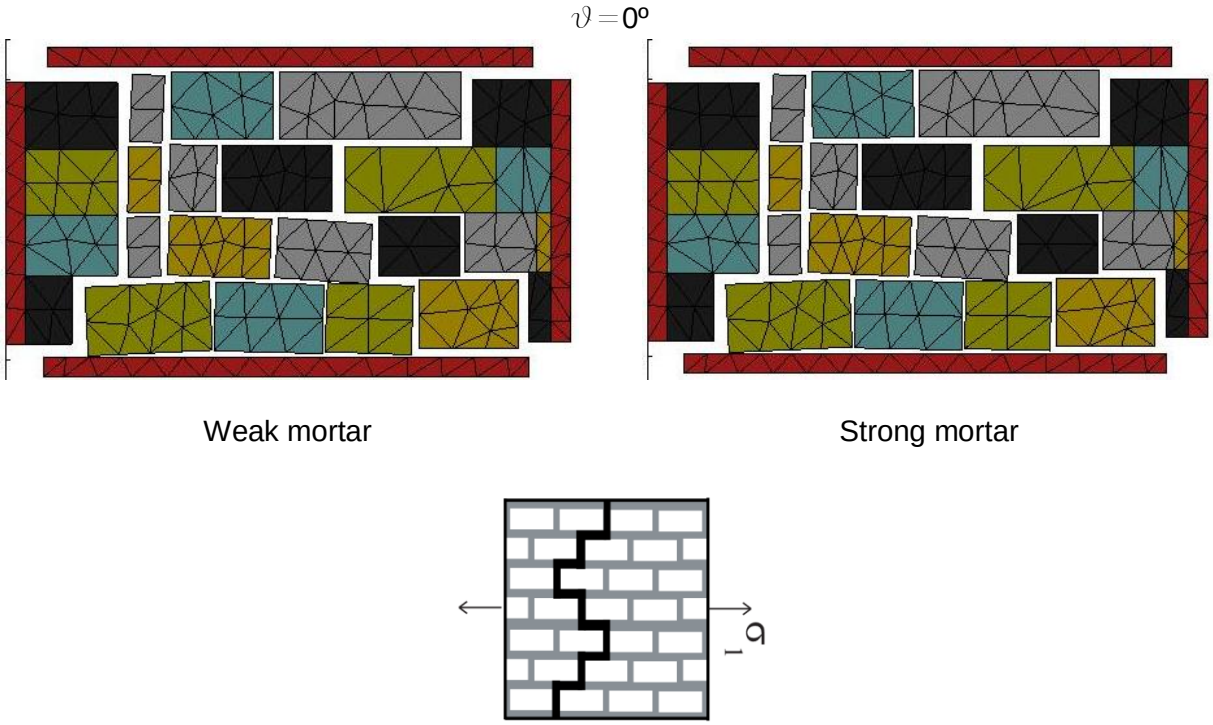

Figure 39. Qualitative comparison of failure mode between 4x4 RVE from masonry with strong mortar at orientations of the load equal to ϑ=0º and experimentally observed failure modes

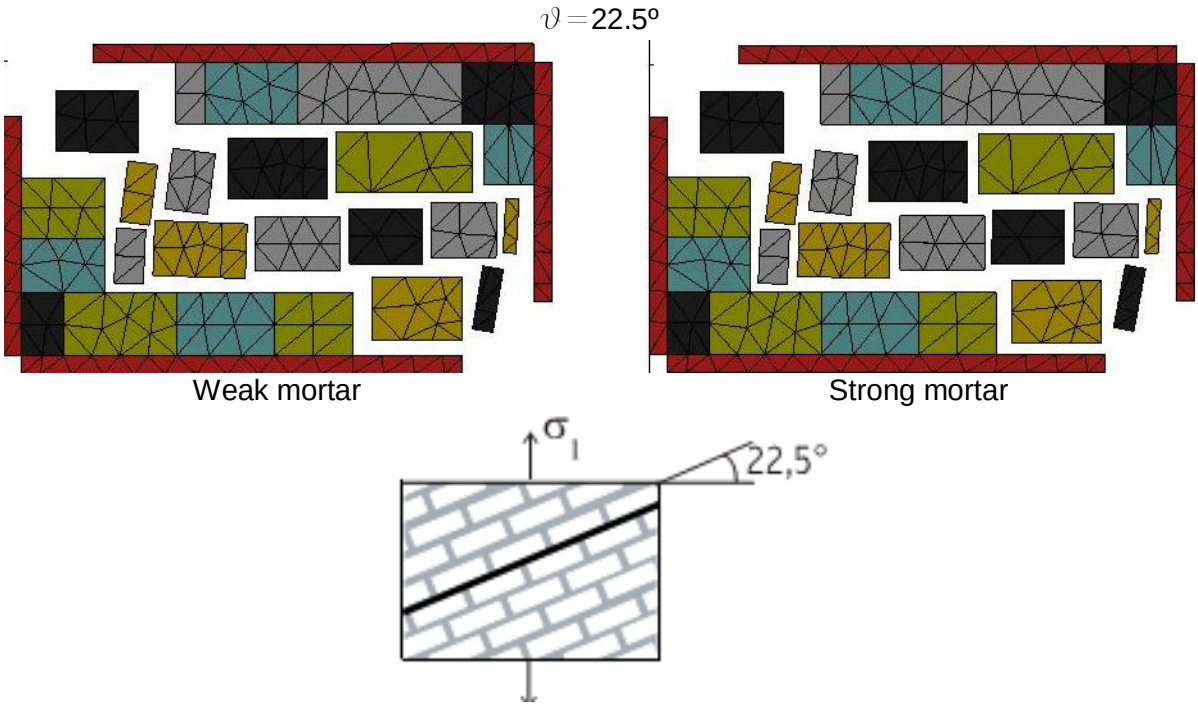

Figure 40. Qualitative comparison of mode failure between 4x4 RVE from masonry with strong mortar at orientations of the load equal to ϑ=22.5º and experimentally observed failure modes

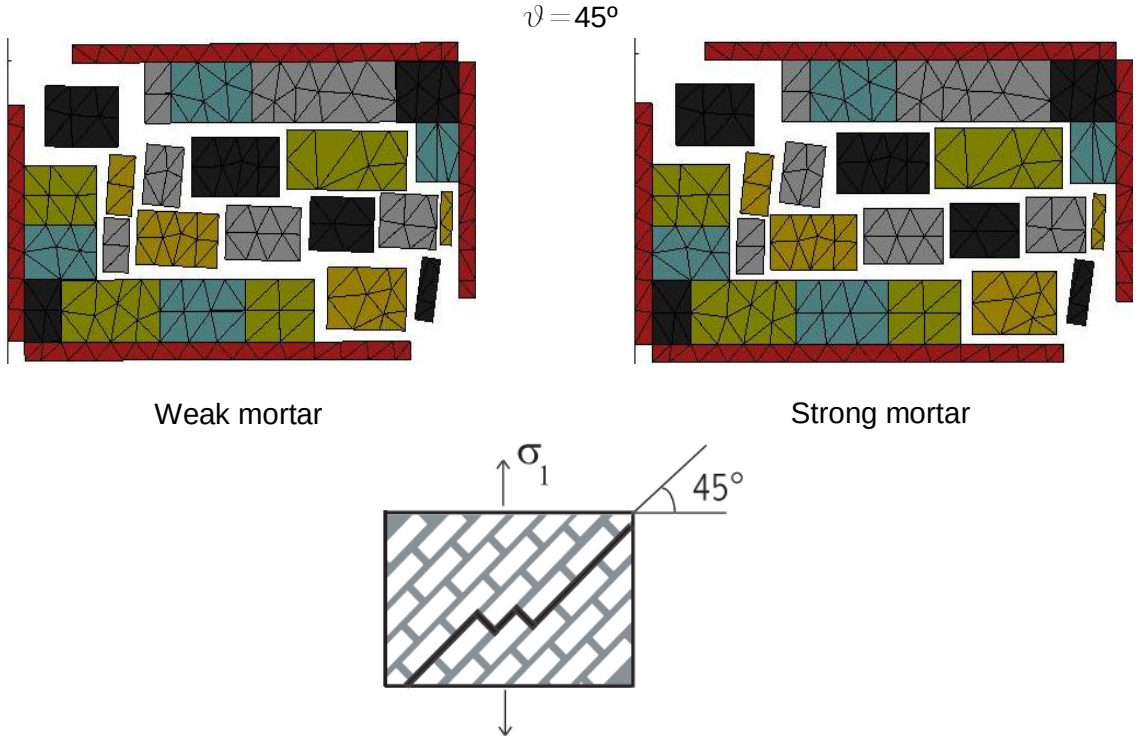

Figure 41 Qualitative comparison of mode failure between 4x4 RVE from masonry with strong mortar at orientations of the load equal to ϑ=45º and experimentally observed failure modes

4.4 Out-of-plane homogenized failure surfaces

4.4.1 Formulation for obtain out-of-plane homogenized failure surfaces

As post-earthquake surveys have shown out-of-plane loading causes the main failures and damages in masonry structures, and especially in historical buildings, whose façades are usually characterized by a relative small thickness in comparison with height and length [49].For this reason it is important to carry out a study about homogenized out-of-plane failure surfaces (M11-M22 and M11-M12) which are obtained from a combination of homogenization techniques and limit analysis. Again, plasticity and associated flow rule for the constituent materials are assumed [6]. The RVE is subdivided into 12 layers along the thickness (in the present case a conservative thickness is considered, assuming only the Alcaçova wall external leaf, with h=400 mm). For each layer, the out-of-plane components σ_{i3} (i=1, 2, 3) of the micro-stress tensor σ are set to zero, meaning that only the in-plane components σ_{ij} (i,j=1,2) are considered active and constant along the Δ_{il} thickness. This allows to handle the homogenized out-of-plane strength domain S^{hom} by means of a simple non-linear optimization problem (Equation 4.5) [50].

$$S^{\hom} \equiv \left\{ \begin{array}{l} \max\{\lambda\} \\ such\ that \left\{ \begin{array}{ll} \widetilde{\mathbf{N}} = \int_{k,i_L} \widetilde{\boldsymbol{\sigma}}^{(k,i_L)} dV & (a) \\ \widetilde{\mathbf{M}} = \int_{k,i_L} y_3 \widetilde{\boldsymbol{\sigma}}^{(k,i_L)} dV & (b) \\ \boldsymbol{\Sigma} = \left[\widetilde{\mathbf{N}} \quad \widetilde{\mathbf{M}}\right] = \lambda \mathbf{n}_{\Sigma} & (c) \\ \widetilde{\boldsymbol{\sigma}}^{(k,i_L)} = \widetilde{\mathbf{X}}^{(k,i_L)}(\mathbf{y})\widetilde{\mathbf{S}} & (d) \\ \widetilde{\boldsymbol{\sigma}}^{(k,i_L)} \in S^{(k,i_L)} & (e) \\ k = 1,\ldots,\ \text{number of } sub-domains & (f) \\ i_L = 1,\ldots,\text{number of } layers & (g) \end{array} \right. \end{array} \right. \quad 4.5$$

Here, λ is the load multiplier (ultimate moment, ultimate membrane action or a combination of moments and membrane actions) with fixed direction n_Σ in the six dimensional space of membrane actions Ñ= [N_{xx} N_{xy} N_{yy}] and bending torsion moments M=[M_{xx} M_{xy} M_{yy}]; $S^{(k,i_L)}$ denotes the non-linear strength domain of the constituent material (mortar or brick), corresponding to the k^{th} sub-domain and i^{th}_L layer see more details in Belytschko and Hodge [51] ; S collects all the unknown polynomial coefficients (of each sub-domain of each layer).

4.4.2 Algorithms for obtaining the out-of-plane homogenized failure surfaces

The out-of-plane homogenized failure surfaces in sections in the space of bending moment (M22) and horizontal bending moment (M11) are generated from the integration of in-plane homogenized stress for which the algorithm requires the following data: The thickness of the RVE, assumed as 0.40m; the number of layers in which the thickness of the RVE will be divided, selected as twelve layers; the compressive vertical load, which are considered at three different levels N22=0 (top), N22=self-weight/2 (mid-height), N22= self-weight (bottom) of the Alcaçova wall; and the values of the in-plane failure surfaces. On the other hand for obtaining the out-of-plane homogenized failure surfaces in sections in the space of torsion (M12) and horizontal bending moment (M11), the algorithm requests the geometry of the mesh, number of elements and the properties of the masonry, using a process similar to the case of in-plane loads. Again, there is a matrix A that stores all the information of the nodes, and a matrix B that stores the topology of elements in order to achieve the stress field σ12-σ11 and from them, it is possible to generate M12-M11.

4.4.3 Results of the analysis of the representative volume elements on out-of-plane loads

Figure 42, masonry with weak mortar, and Figure 43, masonry with strong mortar, show out-of-plane homogenized failure surfaces (M11-M22) for RVEs with increasing vertical compressive loads. As it can be seen, the vertical compression load applied increase not only the horizontal bending moment (M11) but also the vertical bending (M22) and torsion (M12).

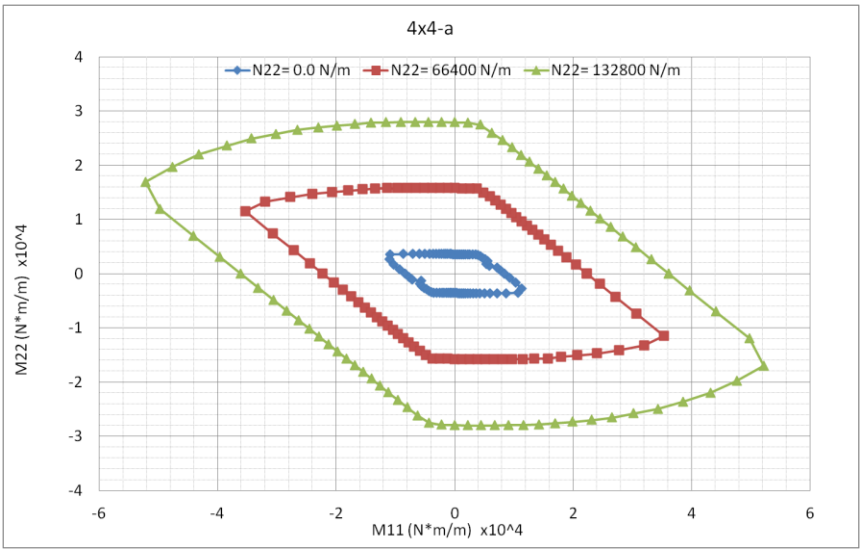

Figure 42. Out-of-plane homogenized failure surfaces (M11-M22) for 4x4 RVE of masonry with weak mortar at incremental vertical compressive loads

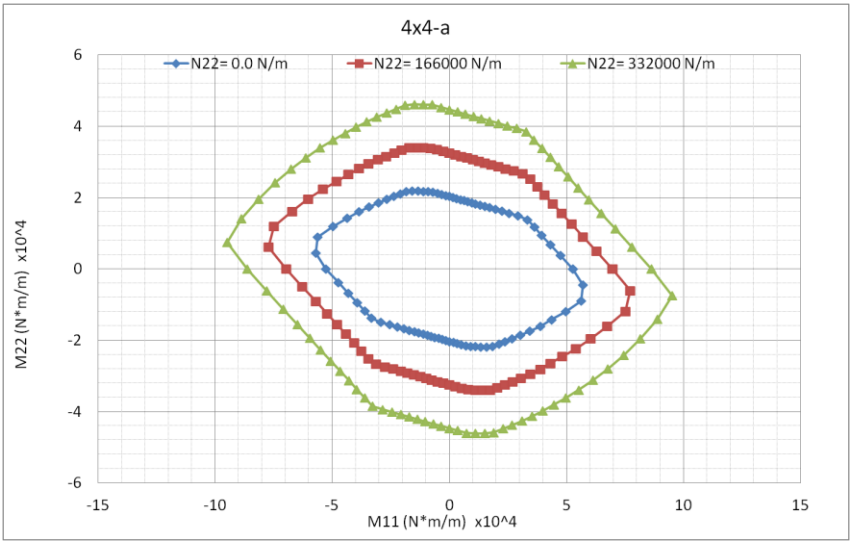

Figure 43. Out-of-plane homogenized failure surfaces (M11-M22) for 4x4 RVE of masonry with weak mortar at incremental vertical compressive loads

This result means that bed joints, in general, contribute to masonry vertical and torsion ultimate moment due to the friction effect of interlocking units. In some cases, due to insufficient staggering of the stones in the RVE with strong mortar (3x3b, 3x3c, 4x4c, 5x5b), M11 does not increase as a straight vertical crack is obtained. The failure surfaces of all the RVEs can be seen in the ANNEX Figure 77-Figure 82.

Figure 44, masonry with weak mortar, and Figure 45, masonry with strong mortar, show out-of-plane homogenized failure surfaces (M11-M12) for RVEs of masonry with increasing vertical compressive loads.

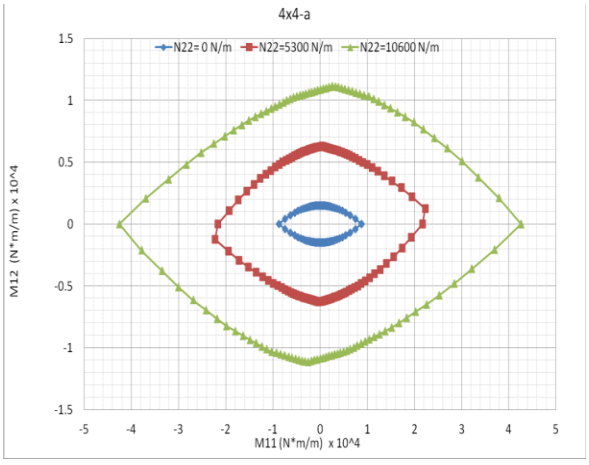

Figure 44. Out-of-plane homogenized failure surfaces (M11-M22) for 4x4 RVE of masonry with weak mortar at incremental vertical compressive loads

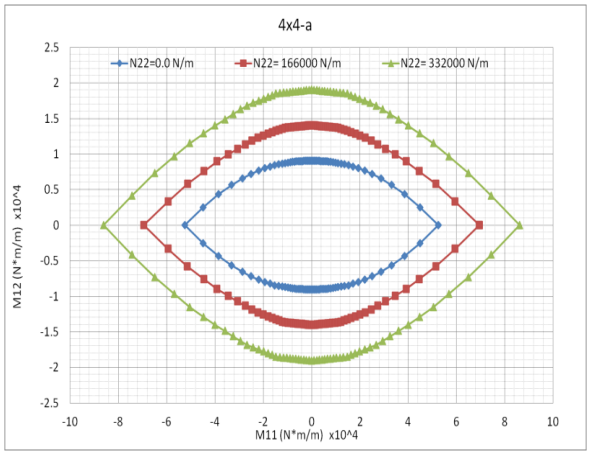

Figure 45. Out-of-plane homogenized failure surfaces (M11-M12) for 4x4 RVE of masonry with strong mortar at incremental vertical compressive loads

Again, the vertical compression load applied increases not only the horizontal bending moment but also the vertical bending moment (M11) and torsion (M12). In some RVEs with insufficient staggering of stones (4x4b, 4x4c, 5x5b), M11 does not increase with the vertical compression load. The failure surfaces of all the RVEs can be seen in the ANNEX Figure 83-Figure 88.

Figure 46a, masonry with weak mortar, and Figure 46b, with strong mortar, show a comparison between the mean values of out-of-plane homogenized failure surfaces of RVEs of the same size when the compressive load is maximum, N22=132,8 kN/m. As it can be observed, the vertical bending moment (M22) exhibits similar values for the different cell sizes (as well as the torsion M12, shown in the ANNEX). The horizontal bending moment (M11) exhibits some scatter for the different average results, as M11 is more sensitive to the compressive loads. Still, the scatter is moderate for engineering purposes.

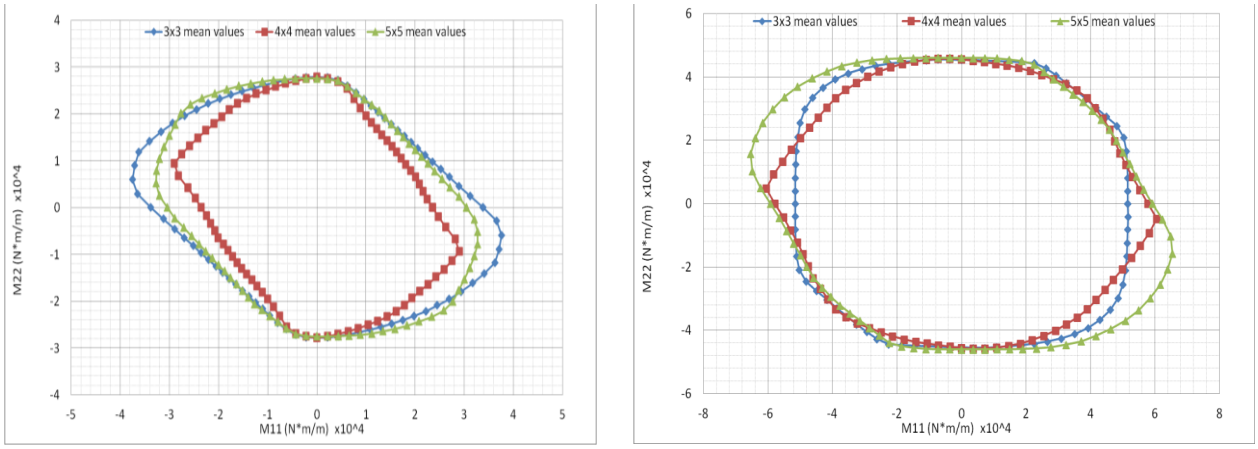

a) b)

Figure 46. Comparison between the mean values of out-of-plane homogenized failure surfaces for each RVE size: a) RVE with weak mortar b) RVE with strong mortar

A good benchmark to evaluate the reliability of results provided by the numerical models presented in this study is a comparison between ultimate vertical bending moments M22 provided by the present analysis and the following Equation 4.6 [52], which can be obtained by simple equilibrium considerations on the bed joint.

$$M_{22} = \frac{x(t-x)}{2}(f_c + f_t)$$
$$x = \frac{f_c t + N_{22}}{f_c + f_t} \qquad 4.6$$

Then, it is possible to draw a comparison graph (Figure 47), where it is seen that the correspondence is appropriated, meaning that reliable lower bound approximations might be achieved using the numerical models presented in this study. In the Figure 47a, the vertical bending moment of the 4x4-a RVE with weak mortar shows slightly higher values than vertical bending moment obtained by the equilibrated analytical formula (Equation 4.6), while in the Figure 47b, the vertical bending moment of the RVE with strong mortar shows slightly lower values than the vertical bending moment obtained by the equilibrated analytical formula.

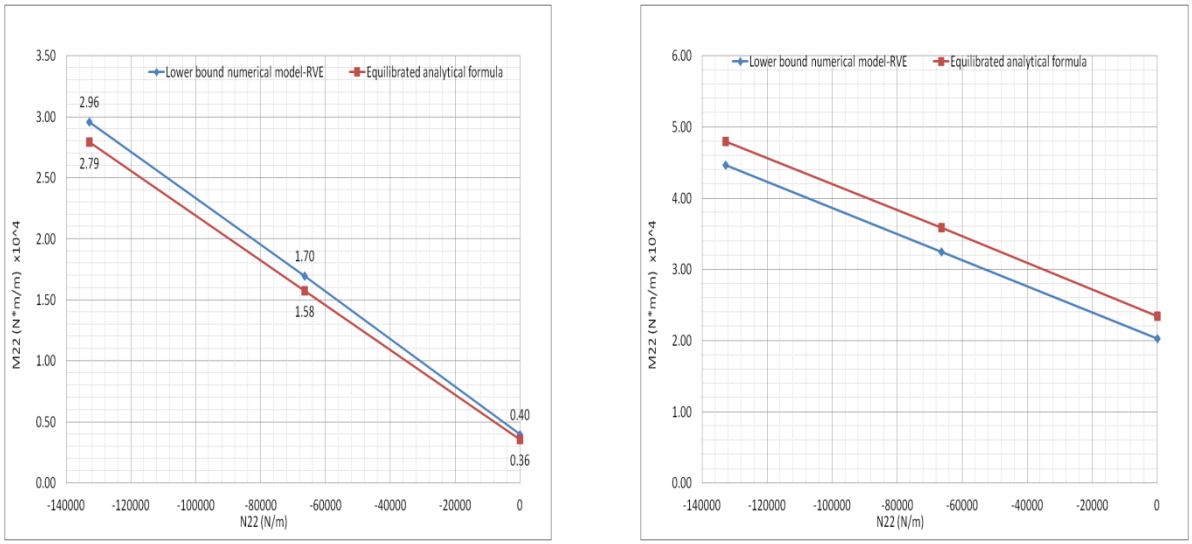

a) b(See Table 2))

Figure 47. Comparison between RVEs and a simplified analytical formula performed on bed joint to predict vertical ultimate bending moment with increasing vertical load: a) RVE with weak mortar; b) RVE with strong mortar

Given the moderate differences in the results using the three sizes for the RVE, from the nine representative volume elements, 4x4-a RVE was chosen for being used in the limit analysis of Alcaçova wall under out-of-plane load. The geometry of this RVE provides yield surfaces close to the average of the different cells shown.

5. CASE STUDY: LIMIT ANALYSIS OF THE ALCAÇOVA WALL OF GUIMARÃES CASTLE

Abstract

In this chapter, the limit analysis of the Alcaçova wall is carried out in a homogeneous model, built with a homogenized repetition of RVEs, and a heterogeneous model that represents the actual geometrical configuration of the wall, built with mortar joints reduced to interfaces. The aim of this study is to obtain the mechanism of failure and the limit load of the two models, with a subsequent comparison of the results, in order to show the reliability and efficiency of the homogeneous model.

5.1 Introduction

Non-linear analysis is one of the most popular tools for knowing the structural behavior of historical masonry buildings. The most used approach for carrying out non-linear analysis is through finite elements. Using non-linear finite elements analysis requires: An adequate knowledge of sophisticated non-linear processes and advanced solution techniques by the practitioner; comprehensive mechanical characterization of the materials, or an experienced analyst; and large time requirements for modeling, for performing the analyses themselves, often with a significant number of load combinations, and for reaching proper understanding of the results significance [53]. Limit analysis is a possible alternative, which provides collapse mechanisms, ultimate stress distributions (at least on critical sections) and load capacities, and has lower computational cost. But one of the attractive features of limit analysis is the low number of material parameters, given the difficulties in obtaining reliable data for historical masonry.

5.2 Alcaçova Wall Geometry

The Castle of Guimarães, located in the city of Guimarães, Portugal, was ordered to be built by Dona Mumadona Dias in the 10^{th} century, to defend her monastery from Muslim and Norman attacks. Count Dom Henrique (to whom the County of Portugal had been granted) chose Guimarães to establish his seat. The fortress, then over a century old, needed urgent renovation. The nobleman chose to destroy what remained from Mumadona's construction, while extending the area of the castle and adding two entrances. The castle became the official royal residence from 1139, when Portugal became independent from the Kingdom of León, until circa 1200.

The present study is focused in the part of the Alcaçova wall located above a much thicker wall part (Figure 48), composed by two external leaves of stone masonry and an infill material in the middle. This wall is supported on three edges, in the base of the wall, left side and right side. The dimensions of the wall are 14.25 m length, 6.85 m height and 0.40 m thickness for each leaf[29]. The wall has six openings which have the following dimensions: in the upper part of the wall, Opening O-1 is 1.57m x 2.40m, Opening O-2 is 1.59m x 2.40m, Opening is O-3 is 1.34m x 1.96m, and in the lower part of the wall Opening O-4 is 1.13m x 2.04m, Opening O-5 is 1.37m x 2.04m, Opening is O-6 is 1.56m x 2.04m and Opening O-7 is 0.79m x 0.80m. The openings represent approximately 20% of the area of the entire wall. Above each opening a lintel is present. In order to carry out the analysis of Alcaçova wall, two numerical models are developed, only for the (weaker and thinner) upper part of the wall.

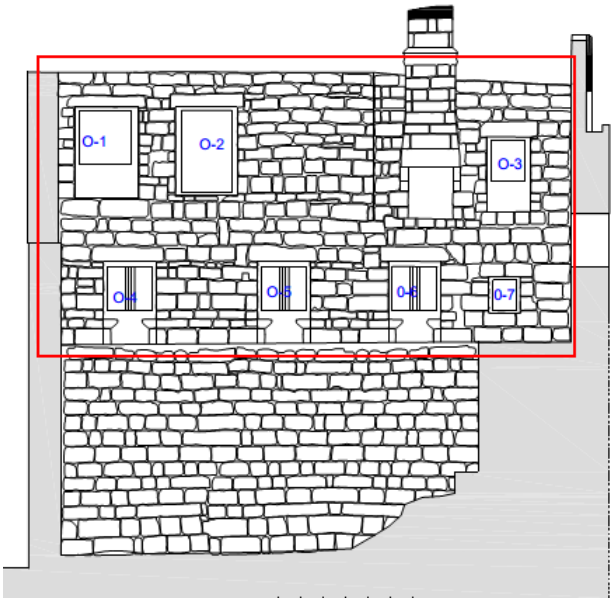

Figure 48. Alcaçova wall: Sector enclosed in the red box is considered in the numerical models.

5.3 Numerical Models: Model with homogenous material and model with heterogeneous material

The first model considered is a homogeneous numerical model built using 4x4-a RVE, composed by a mesh of 173 triangular elements and 127 nodes (Table 3 and Figure 49) whereas the second model is a heterogeneous model built considering the existing arrangement of stones, 308 unit stones in total, and mortar joints reduced to interfaces [34], as the thickness of the mortar joints is much smaller than the dimension of stones. This model is composed by a mesh of 1299 triangular elements and 740 nodes (Table 3 and Figure 50). The geometry of the models was prepared using commercial finite element software, building each triangular element manually, and then exported the mesh to the algorithm that runs the limit analysis.

Model	Elements	Nodes	Features
Heterogeneous	1299	740	Built in RVE
Homogenous	173	127	Micro-modeling

Table 3. Main features of the numerical models

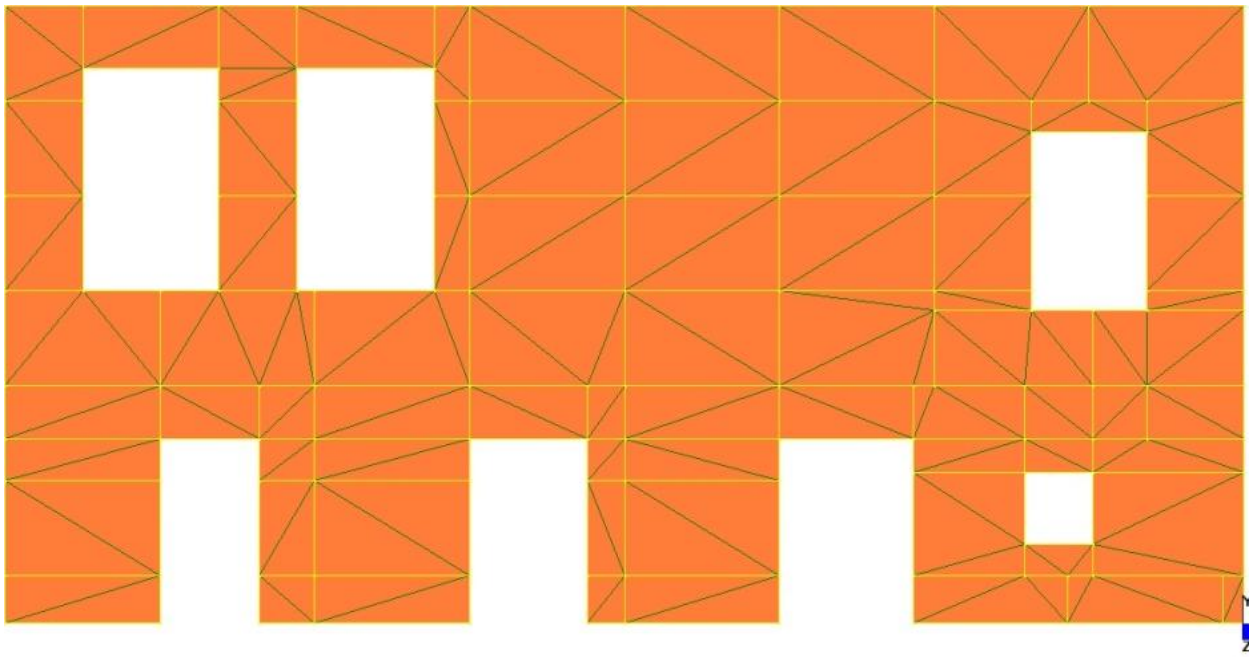

Figure 49. Numerical homogenous model of Alcaçova wall (173 triangular elements)

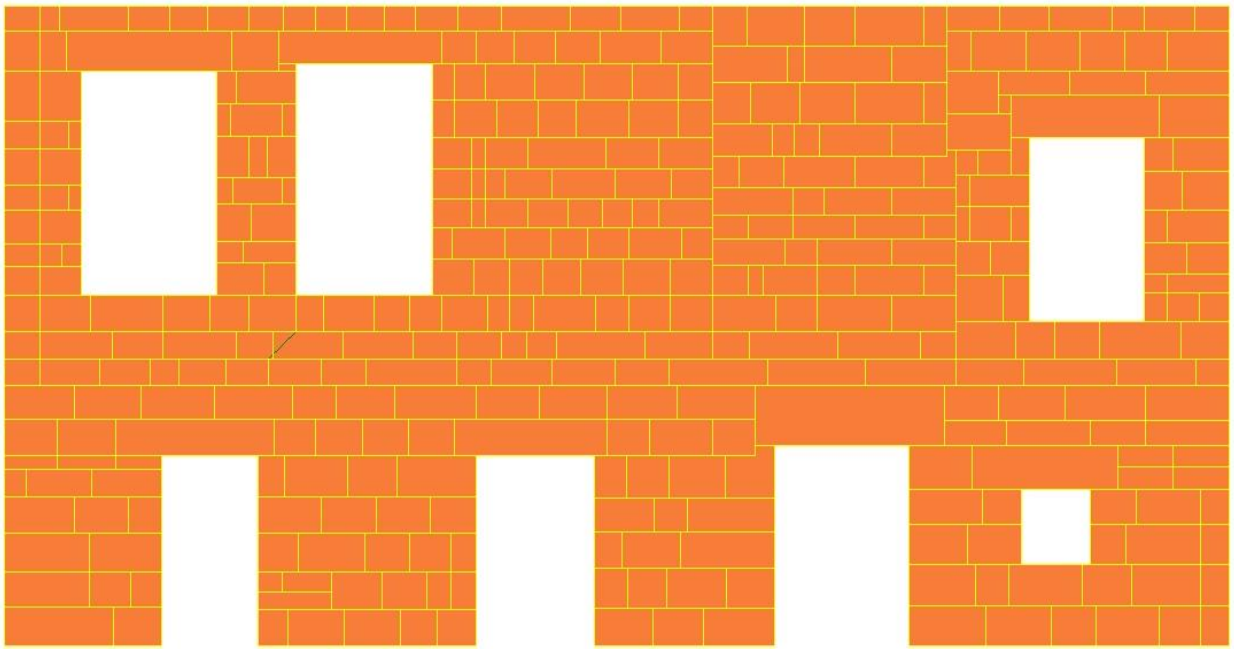

Figure 50. Numerical heterogeneous model of Alcaçova wall (1299 triangular elements)

5.4 Algorithms for obtaining the limit load and the pattern failure of the Alcaçova wall under out-plane loads

5.4.1 Input data for the homogeneous numerical model

As it was done for the cases of out-plane loads, the geometry of the numerical model is input to algorithm through to matrix A (Figure 51) and matrix B (Figure 52) which stores the information of all the nodes and elements respectively, having both matrix the same structure of the matrix A and matrix B of the in-plane case.

```
A=[ Node      1     4.0719159494495E-1     6.8359677109180E+0     0.0000000000000E+0
    Node      2     6.3973160385171E-1     6.8359677109180E+0     0.0000000000000E+0
    Node      3     1.4474705313430E+0     6.8359677109180E+0     0.0000000000000E+0
                    .
                    .
                    .
    Node    738     4.7628567756419E-14    4.0581782028106E+0     0.0000000000000E+0
    Node    739     4.7628567756419E-14    5.3175285369938E+0     0.0000000000000E+0
    Node    740     4.7628567756419E-14    4.2959887375904E+0     0.0000000000000E+0];
```

Figure 51. Matrix A stores the location of the nodes for numerical model of Alcaçova wall

```
B=[ Tri3      1      1      2     228     656      2
    Tri3      2      1      2     656     657      3
    Tri3      3      1      2     656       3      2
     .
     .
     .
    Tri3   1297      1      4     737     564    738
    Tri3   1298      1      4     733     226    227
    Tri3   1299      1      4     733     227    734 ];
```

Figure 52. Matrix B stores the location of elements for numerical model of Alcaçova wall

The next step is to impose a distributed out-of-plane load in each element of the numerical model using a vector called “t” (Figure 53) in which the number “4” into parenthesis represents the location of the element in matrix B and the number “1” into parenthesis represents the number of element in which the load will be imposed and the number “1” outside the parenthesis represents the value of the distributed out-of-plane load. It is necessary to write the vector 1299 times to the heterogeneous model and 173 times for the homogeneous model, which are the number of elements in each case.

```
t   (   4   ,   1   )   =   1   ;
```

Figure 53. Vector “t” used to impose the distributed out-of-plane load in Alcaçova wall

Then, the boundary conditions of rotation and displacement are setup by the matrix bc that stores the boundary condition of rotation (Figure 54a) and bc_U that stores the boundary condition of displacement (Figure 54b), where [L_min H_min L_max H_min] represent the horizontal edge of the Alcaçova wall in which the out of plane displacement and rotations are fixed, [L_min H_min L_min H_max] represent the vertical left side edge, in which only the out of plane displacement is fixed, and [L_max H_min L_max H_max] represent the vertical right side edge in which only the out of plane displacement is fixed.

```
bc=[L_min H_min  L_max  H_min  0     0     1];
```

a)

```
bc_U=[ L_min H_min  L_max  H_min  0     0     1
       L_min H_min  L_min  H_max  0     0     1
       L_max H_min  L_max  H_max  0     0     1 ];
```

b)

Figure 54 a) Boundary conditions of rotation. b) Boundary conditions of displacements

The last step before running the algorithm is to input the characteristic of the materials with the following values: For masonry with weak mortar, the tensile strength of stones is equal to 0.93N/mm^2, the tensile strength and cohesion of mortar joints reduced to interfaces are 0.05 N/mm^2 and 0.05 N/mm^2, respectively; for masonry with strong mortar, the tensile strength of stones is equal to 0.93N/mm^2, the tensile strength and cohesion of mortar joints reduced to interfaces are 0.3 N/mm^2 and 0.45 N/mm^2, respectively

5.4.2 Input data for the heterogeneous numerical model

The process to input the data of geometrical characteristics and boundary conditions for the homogeneous models is the same as it was done for the heterogeneous model, while the input of material properties is different. The input of material data are the out-of-plane failure surfaces obtained from the analysis of the 4x4-a representative volume element which are assigned according the different values of the vertical load along the height of the Alcaçova wall as follows: from the lower part to upper part of the wall, the out-of-plane failures surfaces M11-M22 and M11-M2 obtained for N22=0, N22=self-weight/2, N22= self-weight of Alcaçova wall respectively (Figure 55). After completing all the previous requirements, the algorithm can be run and will show the failure mechanism and limit load for the collapse.

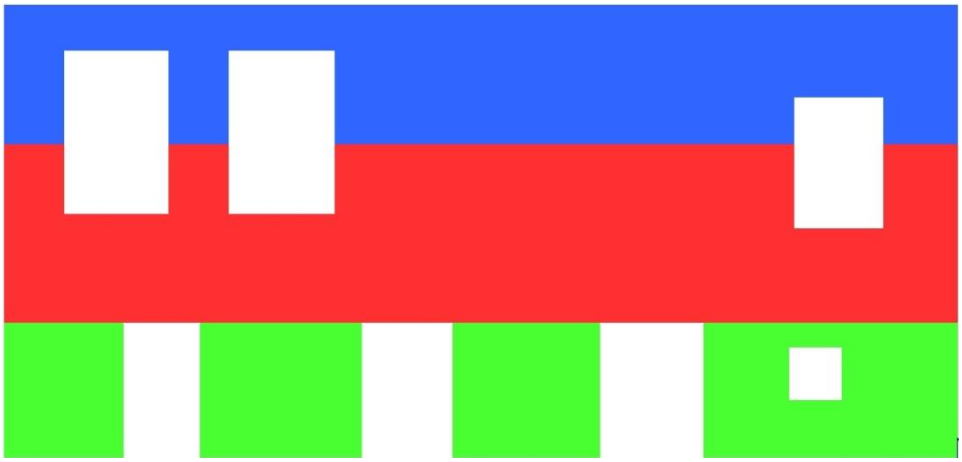

M11-M22 and M11-M12 for N22= 0

M11-M22 and M11-M12 for N22= Wself/2 of Alcaçova wall.

M11-M22 and M11-M12 for N22= Wself of Alcaçova wall.

Figure 55. Input of the homogenized properties in the model

5.5 Results

5.5.1 Comparison between heterogeneous and homogeneous model with weak mortar: Crack pattern and limit load

The results of non-linear limit analysis show the limit load and the possible collapse mechanisms of Alcaçova wall under out-of-plane loads, which can be caused by a seismic action. It is worth to remind that limit analysis does not provide information related with displacements. The possible mechanisms are identified taking into account the cracks patterns. The results, obtained from the numerical homogenous model and numerical heterogeneous model are compared in order to know how accurate and reliable the homogeneous model is.

First of all, the results obtained from the heterogeneous model are described regarding to numeration of the cracks that were drawn in Figure 56. Cracks a4, a5, a13, a14, a17 show two types of vertical cracks located in the middle third of the wall. These cracks are caused by vertical bending moment and according to the quality of arrangement of the stones can be a line (a4) due to the aligned head joints in eleven masonry courses, which makes inexistent any interlocking between stones and, as a consequence, the contribution of friction of the bed joint is lower. The main feature of crack a13 is its propagation following head and bed joints. Cracks a8 and a18 (see Figure 56) show horizontal patterns which mean that the flexural tensile strength of bed joints is exceeded by horizontal bending moment.

Cracks a1, a2, a3, a6, a7, a9, a10, a11, a12, a15, a16 (see Figure 56) appear on corners and surrounding parts of the openings, and are mostly diagonal cracks with slipping over the horizontal joints due to a combined effect of horizontal bending moment and vertical bending moment. This combination of effects is caused by the restraint in the connections of Alcaçova wall and the orthogonal walls, and in the horizontal base. It is important to remark that these types of cracks are in areas of the wall close to the lateral edges. Finally, the failure mechanism obtained is well-known as a local overturning in historical masonry buildings, which, as it can be seen, are affecting lintels of openings.

When comparing the results obtained from the homogenous model with the heterogeneous model, it should be taken in to account that homogenous mode was built using 4x4 RVE and cracks can only follow the mesh lines. Figure 57 shows that, in term of cracks, the homogenous model is in agreement with the heterogeneous model as follows: b1 with a1, b2 with a2, b3 with a3, in the case of b4 is shown slightly to the right side but keeping the same pattern (vertical crack), b5 with a5, a6 with b6, b7 with b7 with a9, b8 with a11, b14 with a19, b15 with a14, b16 with b15, b17 with a16, b18 with a18, b19 with a17. Cracks b10, b11, b12 and b20 are not in full agreement. The agreement seems adequate as two tests in masonry walls often also provide slightly different failure modes, due to the scatter in material properties.

Finally, the limit analysis reported the limit load of the heterogeneous model equal to 8.90% of the self-weight and the limit load of homogeneous model is equal to 6.89% of the self-weight, both results seem in reasonable agreement (20% difference, see Table 4).

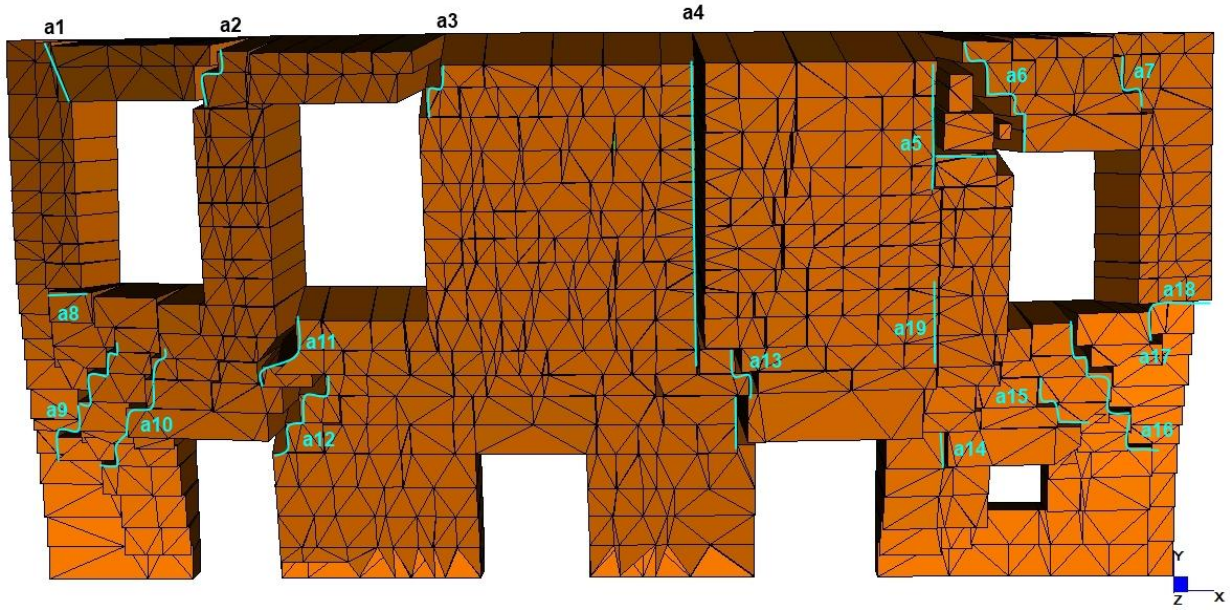

Figure 56. Collapse mechanism of heterogeneous model with weak mortar

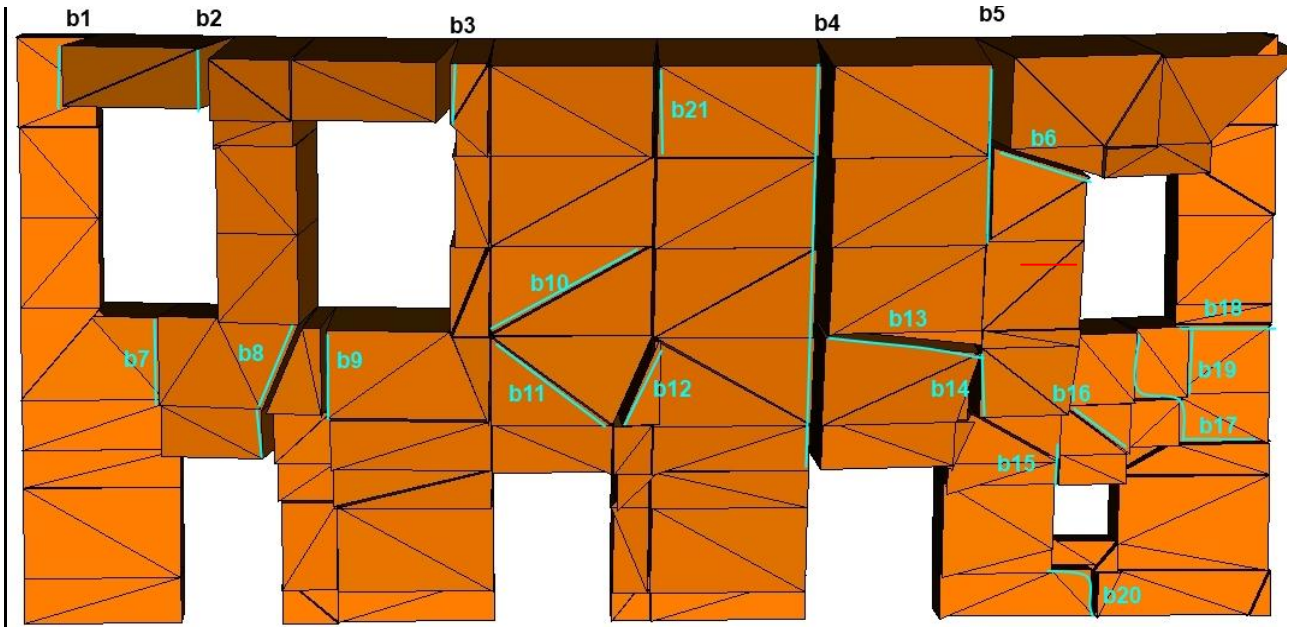

Figure 57. Collapse mechanism of homogenous model with weak mortar

5.5.2 Comparison between heterogeneous and homogeneous model with strong mortar: Crack pattern and limit load

Figure 58 and Figure 59 for the heterogeneous and homogeneous model with strong mortar are also characterized by meaningful vertical cracks pattern even if the quality of the mortar is better: Again, the vertical alignment of the eleven head joints has a important influence on the formation of crack patterns and the vertical bending moment partly controls the stability of the Alcaçova wall. Furthermore, horizontal cracks are still present in the corners of the openings as the compressive vertical load generated by the self-weight in that zone of the wall is not enough to control the effect of the horizontal bending moment on the bed joint. Diagonal cracking produced by combination of vertical and horizontal bending moment is still presented surrounding of the edges of the wall and also in the corners of openings. As it can be seen in Figure 58 and Figure 59, the cracks pattern in the heterogeneous and homogeneous model seem in very good agreement In particular, the following considerations may be done:c1 is comparable with d1, c2 with d2, c3 with d3, c4 with d6, c21 with d7, c6 with d8, c20 with d18, c8 with d10, c9 with d19, c10 with d20, c11 with d11, c12 with d12, c18 with d13, c16 with d14, c15 with d15, c14 with d21, c17 with d16.

It is worth pointing out that the crack patterns present in heterogeneous and homogeneous models with strong mortar keep a certain similarity to the ones present in the models with weak mortar. The main

reason is that the failure mode is heavily controlled by the geometrical restraints. The purpose of using a strong mortar (i.e. a lime grout based injection) is also not to change the structural behavior of the wall but is improve its behavior as a more homogeneous material and to increase its capacity.

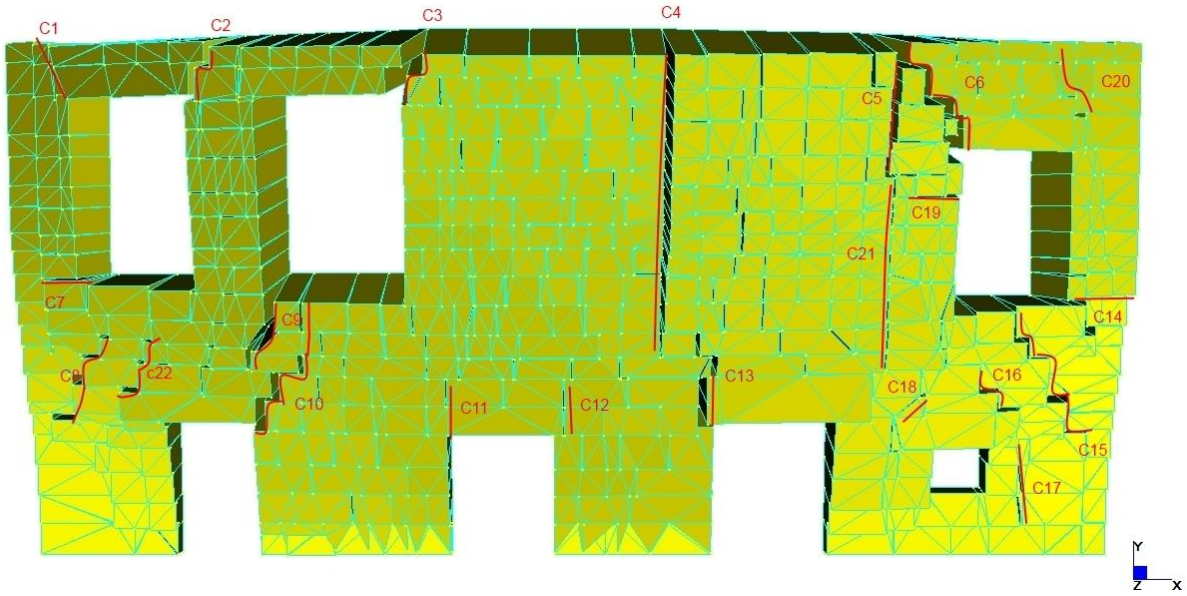

Figure 58. Collapse mechanism of heterogeneous model with strong mortar

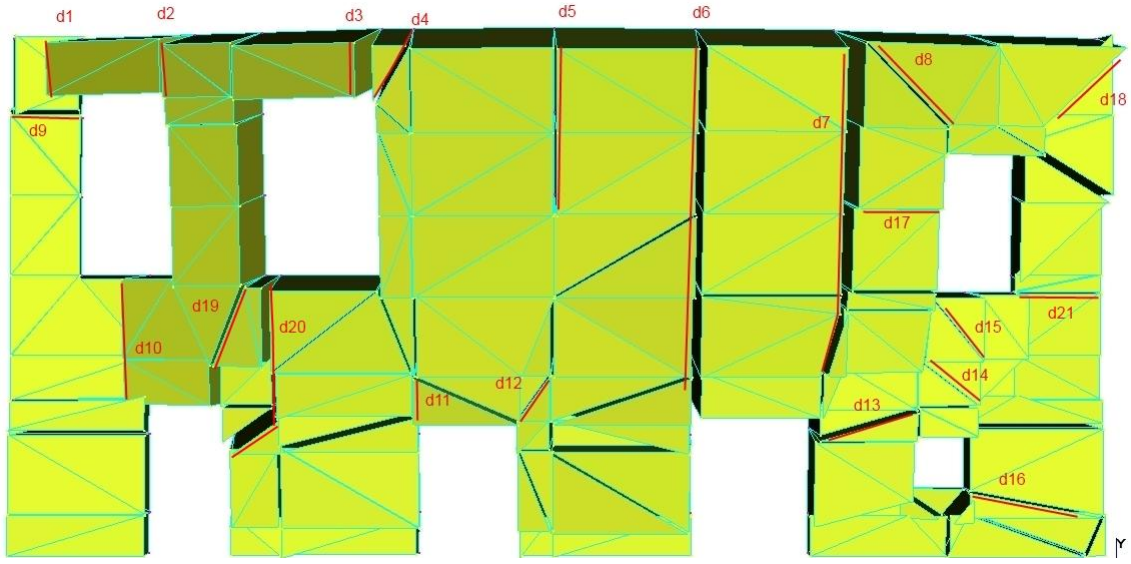

Figure 59. Collapse mechanism of homogeneous model with strong mortar

Finally, it has to be underlined that the limit load associated to the heterogeneous model is equal to 34.4% of the self-weight, whereas the limit load of the homogeneous model is equal to 31.6% of the self-weight.

The results seem in reasonable agreement (less than 10% difference, see Table 4), with closer match between the original and the strengthened wall. It is also interesting to observe that the introduction of strong mortar significantly increases the limit load of the Alcaçova wall (almost four times).

Joints	Heterogeneous model (% of self-weight)	Homogenous model (% of self-weight)	Accuracy of homogeneous model (%)
Weak mortar	8.9	6.9	80
Strong mortar	34.4	31.6	90

Table 4. Comparison of limit loads from the heterogeneous model and homogeneous model.

5.5.3 Qualitative comparison between the failure mechanism of the numerical models and typical mechanism on historical masonry buildings

In this section, a qualitative comparison between the failure mechanism obtained by means of the limit analysis and typical failures mechanisms in historical masonry buildings is made, in order to increase the confidence in the numerical model and discuss the behavior of masonry walls.

Figure 60 shows a collapse mechanism known as vertical strip overturning which is produced due to a regular position of the two openings in vertical arrays and poor connection of the horizontal spandrels across the openings. This kind of sub-mechanism of failure is found in the left part of the wall.
Figure 61 shows the wall overturning as a rigid block, which is found in the central part of the Alcaçova wall, a long wall about 14m without any bracing and high percentage of openings. Finally, Figure 62, shows that the type of failure has been well identified in post-earthquake surveys, as an out of plane failure mechanism.

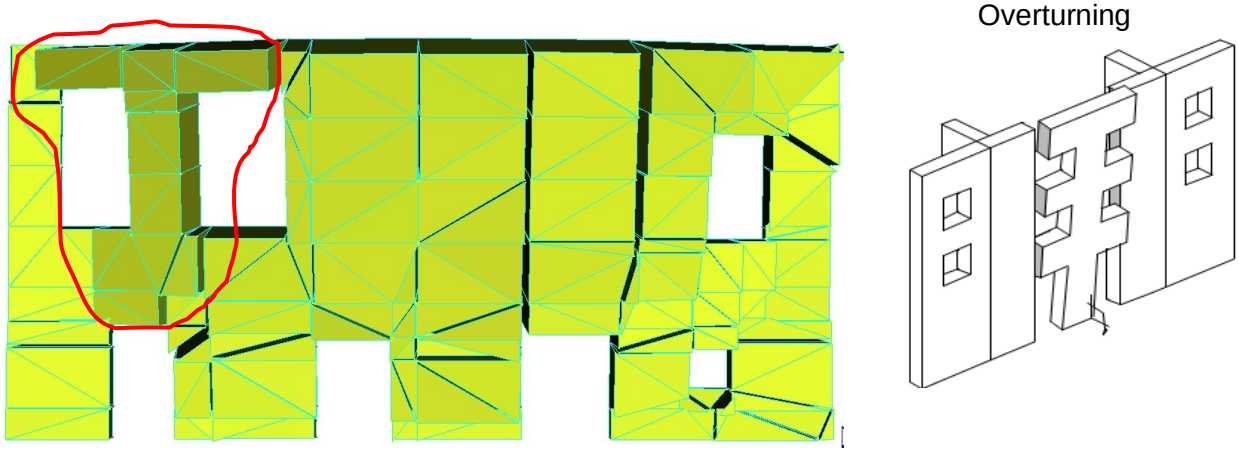

Figure 60. Local mechanism #1 for Alcaçova wall

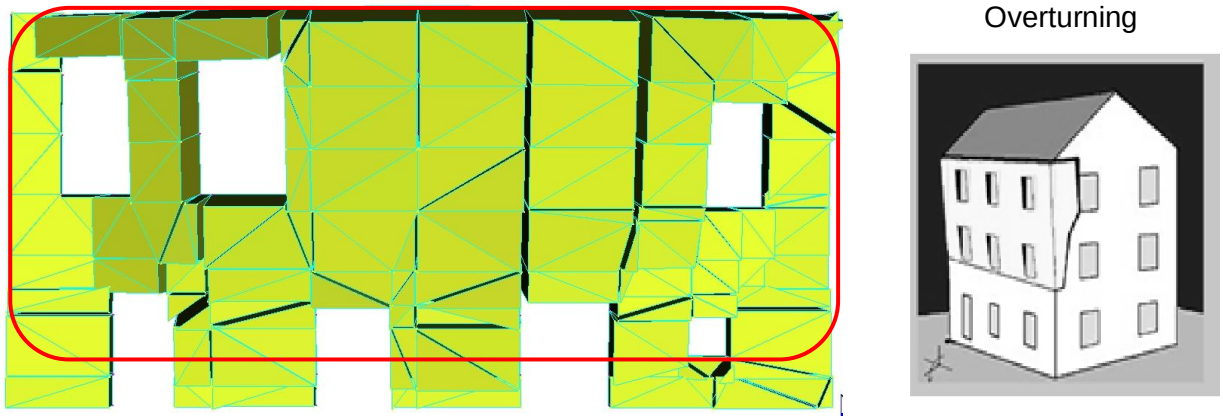

Figure 61. Local mechanism #2 for Alcaçova wall

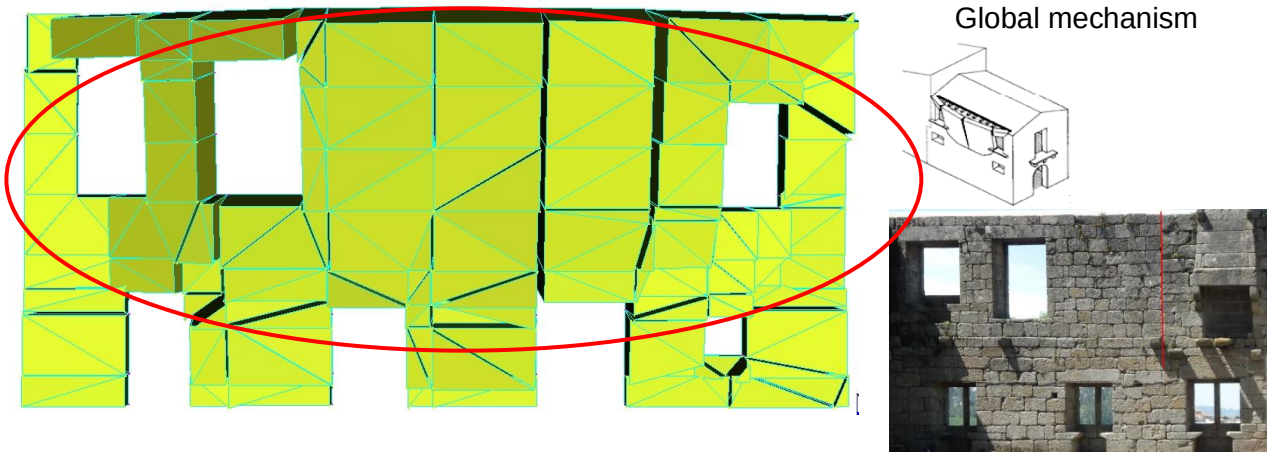

Figure 62. Global mechanism of Alcaçova wall

5.5.4 Comparison of computing time

The heterogeneous and homogeneous models have been used to obtain the failure mechanism and limit load of collapse under out-of-plane loads (seismic action). The analysis was performed on a standard PC Intel Pentium Dual 2.12 GHz equipped with 3Gb RAM, and it was found that far less time was spent using the homogeneous model, in comparison with heterogeneous model. A comparison in terms of processing time, only for computing, indicates that the homogeneous model is more efficient than the heterogeneous model, saving about 95% calculation time (30 second vs. 600 second). Moreover, the mesh preparation times is heavily reduced in the homogenous model, with an estimate of 3 hours to prepare the heterogeneous model and 16 hours to prepare the homogenous model.

6. CONCLUSIONS

6.1 Conclusions

It is clear, that non-linear approaches are a possible choice in the engineering assessment of historical structures and they require practical computational tools. These tools often imply expensive computational costs, a good knowledge about non-linear processes and, especially, a larger time to build the model and perform the analysis. This problem is addressed in the present thesis by means of a geometrical investigation and homogenization of masonry. The conclusions of the thesis can be summarized as given next.

The geometrical investigation and statistical analysis of the stone units from four sample walls of Guimarães castle provide much relevant information about the stone geometrical ratio, which is rather important for the quality of the masonry bond. The value found of the height to length ratio (h/l) for the average geometrical dimensions is about 56% (1:1.8). Only in Wall 2 has a slightly different h/l ratio, equal to 63% (1:1.6).. The mean value of the height of the stones is 38.4 cm with a coefficient of variation (CoV) about 19%, with a variation of height lower than 1% in case of stones from the same row. The mean value of the length of stones is 68.6 cm, with a CoV about 36%. The scatter found in the length is always much larger than the scatter found in the height, being the scatter in the full sample not so much different from the scatter in the individual samples. The data is consistent with a lognormal distribution, which is skewed for the length and relatively symmetric for the height. These results confirm the quasi periodic arrangement of the stones that was envisaged visually.

The homogenized limit analysis of representative volume elements shows the following results: In-plane failure surfaces with the usual anisotropic behavior of masonry and different shape for each orientation of the load; failure modes well captured, even if the similarity with experimental tests from biaxial testing of masonry is not perfect. For the case of out-of-plane failure surfaces, the vertical compression load applied increases the horizontal bending moment (M22), the vertical bending moment (M11) and torsion (M12), in general. It was also observed that this increase does not occur in some RVEs due to insufficient staggering of stones, verifying this way that the staggering of stones has a significant influence in failure surfaces, as expected.

The limit analysis of the Alcaçova wall of Guimarães castle is carried out by means of two models, the first one with a heterogeneous material and the second one with an homogenized material, obtained from limit analysis of representative volume elements. The limit load of the homogeneous model seems in reasonable agreement with the heterogeneous model. In the qualitative comparison of the failure mechanisms, a good agreement was found between the homogeneous model and the heterogeneous

model. In terms of computational time, the homogeneous model is more efficient than the heterogeneous model. Finally, given the results, the homogeneous model can be used for preliminary studies of the Alcaçóva wall.

REFERENCES

[1] ICOMOS, The Venice Charter, 1964, p. 1.

[2] J. Rots, Numerical simulation of cracking in structural masonry, 1991, pp. 49-63.

[3] P. Suquet, Local and Global Aspects in the Mathematical Theory of Plasticity, Plasticity Today: Modelling, Methods and Applications, pp. 279 - 310 .

[4] P. Lourenço, G. Milani, A. Tralli and A. Zucchini, Analysis of masonsry structures: review of and recent trends in homogeniztion techniques, Canada, 2007.

[5] P. Pegon and A. Anthoine, Numerical strategies for solving continuum damage problems with softening: application to the homogenisation of masonry. Computers & Structures, 1997, p. 64: 623– 642.

[6] P. Suquet, Analyse limite et et homogeneisation. Comptes Rendus de l'Academie des Sciences - Series IIB – Mechanics, 1983, pp. 296: 1355-1358.

[7] G. Milani, P. Lourenço and A. Tralli, Homogenised limit analysis of masonry walls, Part I: failure surfaces. Computers& Structures, 2006, p. 84: 166–180..

[8] P. Suquet, Analyse limite et et homogeneisation, Comptes Rendus de l'Academie des Sciences-Series II-Mechanics, 1983, pp. 296: 1355-1358.

[9] A. Taliercio and P. Sagramoso, Uniaxial strength of polymeric-matrix fibrous composites predicted through a homogenization approach. International Journal of Solids and Structures, 1995, pp. 32 (14): 2095-2123.

[10] P. de Buhan and G. de Felice, A homogenisation approach to the ultimate strength of brick masonry. Journal of the Mechanics and Physics of Solids, 1997, pp. 45 (7): 1085-1104.

[11] G. Pande, J. Liang and J. Middleton, Equivalent elastic moduli for brick masonry, Computer A Geotechnics, 1989, pp. 243-265.

[12] Felice, Metodi di omogeneizzazione per sistemi rego-lari di corpi rigidi. In Proceedings of the XII AIMETA Con-gress, Naples, Italy: University of Naples, 1995, p. 453–479.

[13] A. Cecchi and K. Sab, A multi-parameter homogenization study for modelling elastic masonry, European Journal of Mech-anics A-Solids, 2002, p. 249–268.

[14] A. Cecchi, G. Milani and A. Tralli, Validation of analytical multiparameter homogenization models for out-of-plane loaded masonry walls by means of the finite element method, Journal of Engineering Mechanics, 2005, p. 185–198.

[15] J. Lopez, S. Oller, E. Oñate and J. Lubliner, A homogeneous constitutive model for masonry, International Journal for Numerical Methods in Engineering, 1999, p. 1651–1671.

[16] A. Zucchini and P. Lourenço, A micro-mechanical model for the homogenization of masonry, International Journal of Solids and Structures, 2002, p. 39: 3233–3255.

[17] P. Lourenço, A matrix formulation for the elastoplastic homogenisation of layered materials. Mechanics of Cohesive-Frictional Materials, 1996b, p. 273–294.

[18] G. Maier, E. Papa and A. Nappi, On damage and failure of unit masonry. In Proceedings of the Experimental and Numerical Methods in Earthquake Engineering, Brussels and Luxembourg: Balkema Editions, 1991, p. 223–245.

[19] J. Lee, G. Pande, J. Middleton and B. Kralj, Numerical modelling of brick masonry panels subject to lateral load-ings. Computers & Structures, 1996, p. 61: 735–745.

[20] R. Van der Pluijm, Out of plane bending of masonry: behaviour and strength. Ph.D.

dissertation, The Netherlands: Eindhoven University of Technology, 1999.

[21] R. Luciano and E. Sacco, Homogenisation technique and damage model for old masonry material, International Journal of Solids and Structures, 1997, p. 34: 3191–3208.

[22] L. Gambarotta and S. Lagomarsino, Damage models for the seismic response of brick masonry shear walls. Part I: the mortar joint model and its applications. Earthquake Engineering & Structural Dynamics, 1997, p. 26(4): 423–439.

[23] C. Calderini and S. Lagomarsino, A micromechanical inelastic model for historical masonry, Journal of Earthquake Engineering, 2006, p. 10(4): 453–479.

[24] P. de Buhan and G. Felice, A homogenisation approach to the ultimate strength of brick masonry, Journal of the Mech-anics and Physics of Solids, 1997, p. 45: 1085–1104.

[25] T. Massart, R. Peerlings and M. Geers, Mesoscopic modeling of failure and damage induced anisotropy in brick masonry, European Journal of Mechanics A-Solids, 2004, p. 23: 719–735.

[26] T. Massart, Multi-scale modeling of damage in masonry structures. Ph.D. thesis, Belgium: University of Bruxelles, 2003.

[27] DGEMN, O Castelo de Guimarães, Porto, 1937.

[28] F. Teixeira, O castelo e as muralhas de Guimarães: apontamentos para a sua história, Guimarães : Cidade Berço, 2001.

[29] R. da Silva Azevedo, Evolução dos Sistemas Fortificados: O Castelo e as Muralhas de Guimarães, Guimarães: Universidade do Minho Escola de Engenharia, 2011.

[30] B. Fonte, O Castelo de Guimarães, Braga: Correio do Minho, 1995.

[31] I. Sereno and P. Dordio, Castelo de Guimarães, http://www.monumentos.pt/Site/APP_PagesUser/SIPA.aspx?id=1060, 1994.

[32] J. Gonçalves, Castelo de Guimarães, http://www.monumentos.pt/Site/APP_PagesUser/SIPA.aspx?id=1060, 2003.

[33] S. Moreira, Relatório ensaios não-destrutivos no castelo de Guimarães - Tecminho, Guimarães: Universidade do Minho, 2010, p. 79.

[34] P. Lourenço and J. Rots, A multi-surface interface model for the analysis of masonry structures, 1997: Journal of Engineering Mechanics ASCE, pp. 123(7), 660-668.

[35] D. Sutcliffe, H. Yu y A. Page, Lower bound limit analysis of unreinforced masonry shear walls, Comput Struct, 2001, p. 79:1295–312.

[36] G. Milani and P. Lourenço, Monte Carlo homogenized limit analysis model for randomly assembled blocks in-plane loaded, Springer-Verlag, 2010.

[37] Page, A biaxial failure criterion for brick masonry in the tension-tension range, Int J Masonry, 1987, p. 1:26–30.

[38] P. Lourenço, P. Roca and C. Modena, Homogenisation Approaches for Structural Analysis of Masonry Buildings, New Delhi: MacMillan, 2006, pp. 20060745-20060745.

[39] A. Lyamin y S. Sloan, Lower bound limit analysis using nonlinear programming, International Journal for Numerical Methods in Engineering, 2002, p. 55(5):573–611.

[40] E. Anderheggen y H. Knopfel, Finite element limit analysis using linear programming, International Journal of Solids and Structures, 1972, p. 8:1413–31.

[41] G. Maier, Mathematical programming methods for deformation analysis at plastic collapse, Computers and Structures, 1977, p. 7:599–612.

[42] S. Sloan and P. Kleeman, Upper bound limit analysis using discontinuous velocity fields, Computer Methods in Applied Mechanics and Engineering, 1995, p. 127(1–4):293–314.

[43] A. Cannarozzi, P. Sacchi y A. Tralli, On the limit analysis of steel structures in presence of shear, Journal de Mecanique Theorique et Appliquee, 1982, p. 1(3):379–401.

[44] G. Milani, A homogenization approach for the limit analysis of out-of-plane loaded masonry walls, Journal of Structural Engineering, 2012.

[45] G. Milani, P. Lourenço and A. Tralli, Homogenised limit analysis of masonry walls, Part I: Failure surfaces, Computers and Structures, 2005, p. 172.

[46] G. de Vasconcelos, Thesis-Experimental investigations on the mechanics of stone masonry: Characterization of granites and behavior of ancient masonry shear walls, Guimaraes: University of Minho, 2005, p. 77.

[47] M. Dhanasekar, A. Page and P. Kleeman, The failure of brick masonry under biaxial stresses, Proc. Instn Civ. Engrs, 1985, p. 295–313.

[48] P. Lourenço, L. Ramos and G. Vasconcelos, The cyclic behaviour of stone dry masonry joints, Amsterdam: 13th International Brick and Block Masonry Conference, 2004.

[49] R. Spence and A. Coburn, Strengthening building of stone masonry to resist earthquakes, Meccanica, 1992, pp. 27, 213-221.

[50] G. Milani, P. Lourenço and A. Tralli, 3D Homogenized limit analysis of masonry buildings subjected to horizontal loads, Lisbon, Portugal: European Conference on Computational Mechanics Solids, Structures and Coupled Problems in Engineering, 2006.

[51] T. Belytschko and P. Hodge, Plane stress limit analysis by finite elements, ASCE Journal of Engineering Mechanics, 1970, pp. 931-943.

[52] G. Milani, Simple lower bound limit analysis homogenization model for in- and out-of-plane loaded masonry walls, Construction and Building Materials, 2011.

[53] A. Orduña and P. Lourenço, Limit analysis as a tool for the simplified assessment of ancient masonry structure, Third International Conference on Structural Analysis of Historic Constructions, 2001.

[54] E. Bultote, L. Van Parys and S. Datoussaid, Out-of-plane Behaviour of URM Walls: Experimental studies, Belgium: 9th National Congress on Theoretical and Applied Mechanics, 2012.

[55] S. Pietruszczak y R. Ushaksarei, Description of inelastic behaviour of structural masonry, Int J Solids Struct, p. 40:4003–19.

ANNEX

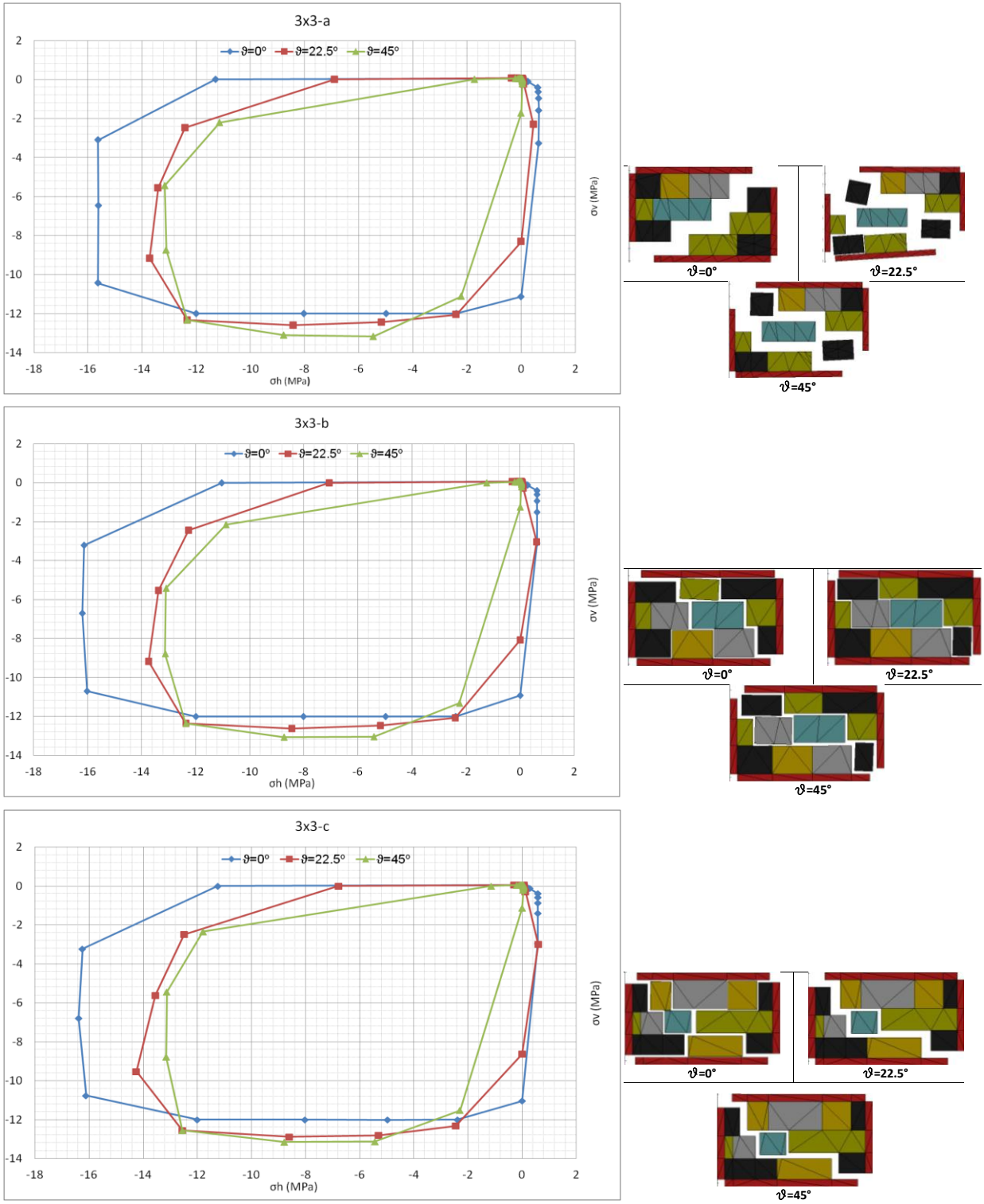

Figure 63 . In-plane homogenized failure surfaces for 3x3 RVE for masonry with weak mortar at different orientations of the load with respect to the bed joint

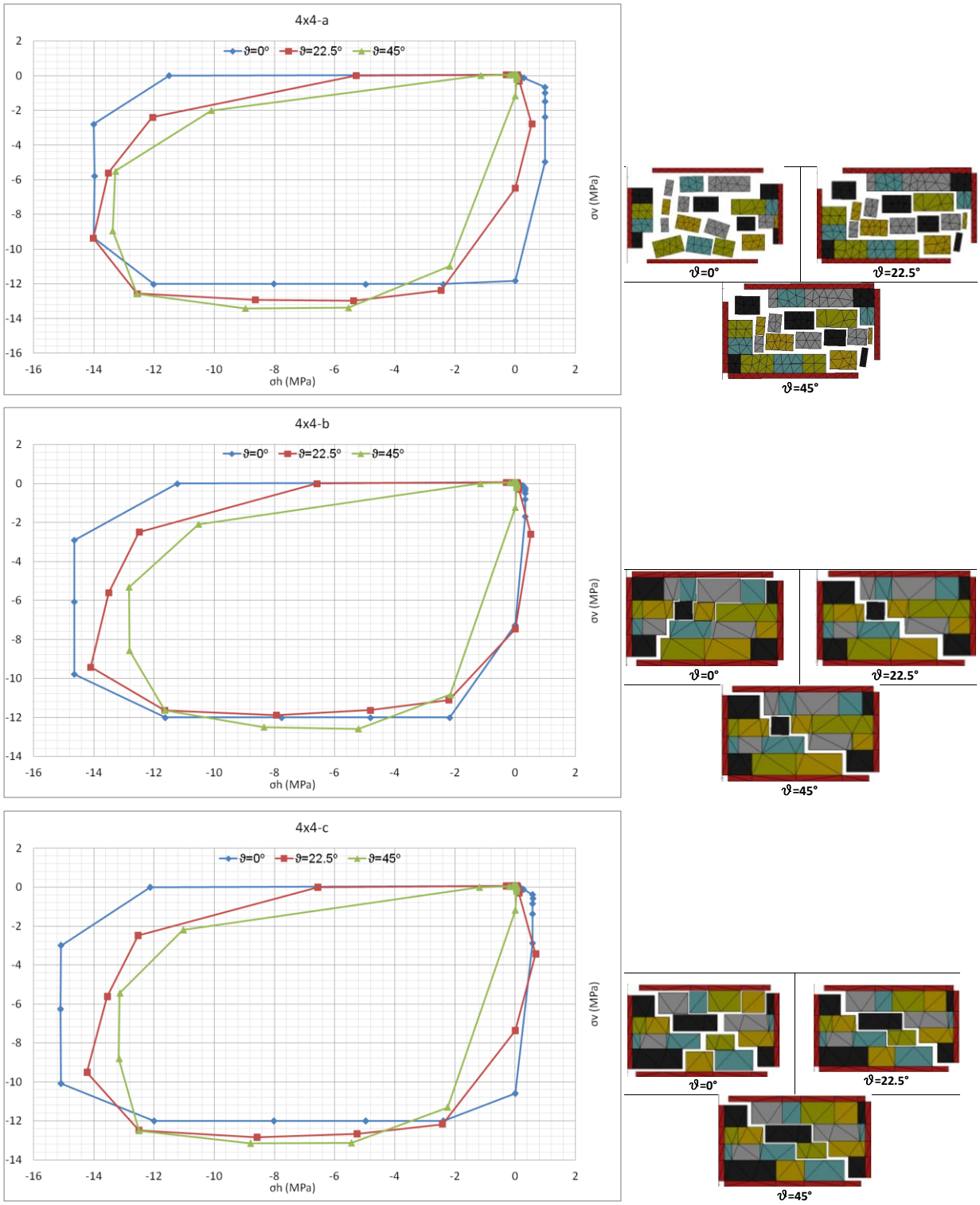

Figure 64 In-plane homogenized failure surfaces for 4x4 RVE for masonry with weak mortar at different orientations of the load with respect to the bed joint

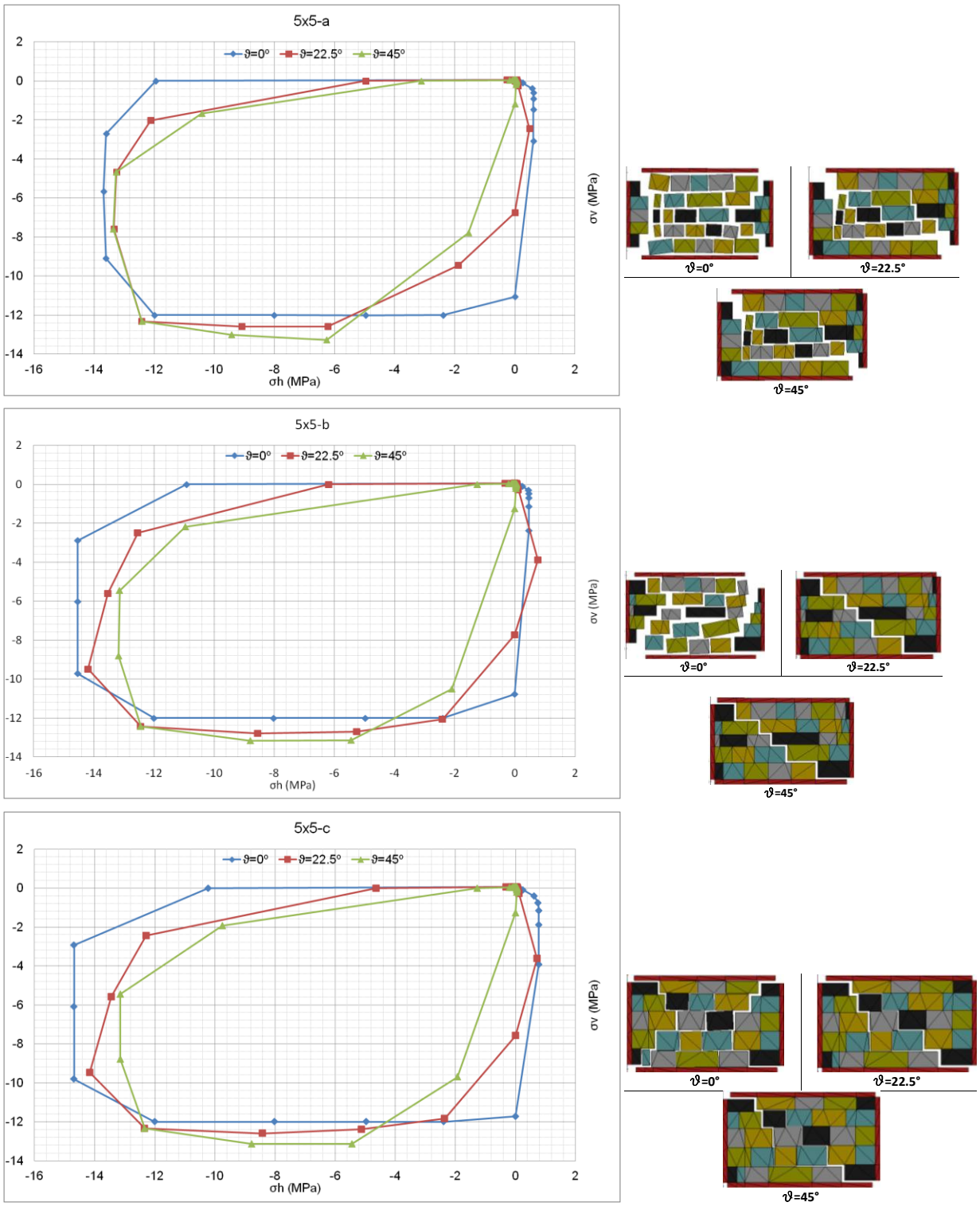

Figure 65 . In-plane homogenized failure surfaces for 5x5 RVE for masonry with weak mortar at different orientations of the load with respect to the bed joint

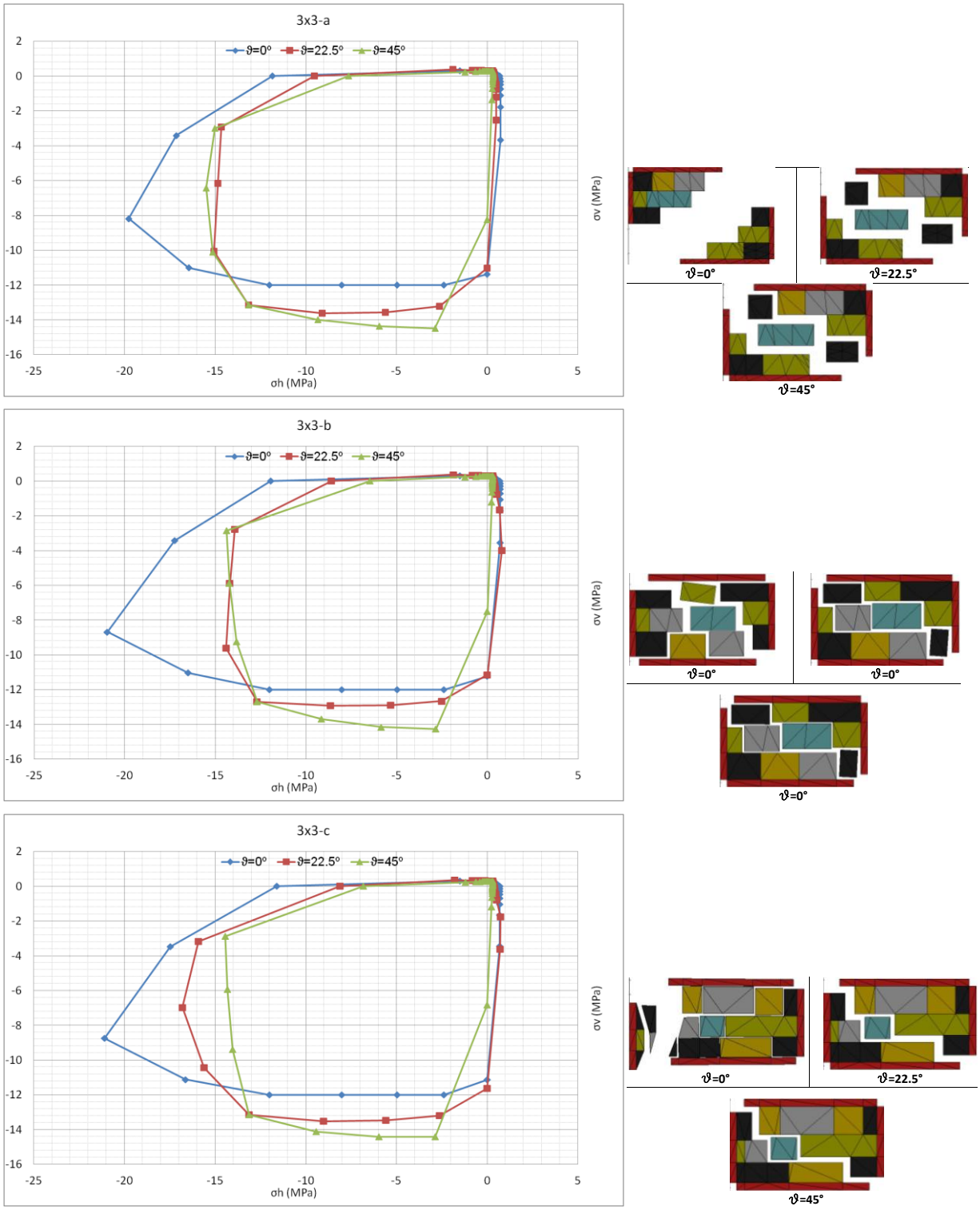

Figure 66. In-plane homogenized failure surfaces for 3x3 RVE for masonry with strong mortar at different orientations of the load with respect to the bed joint

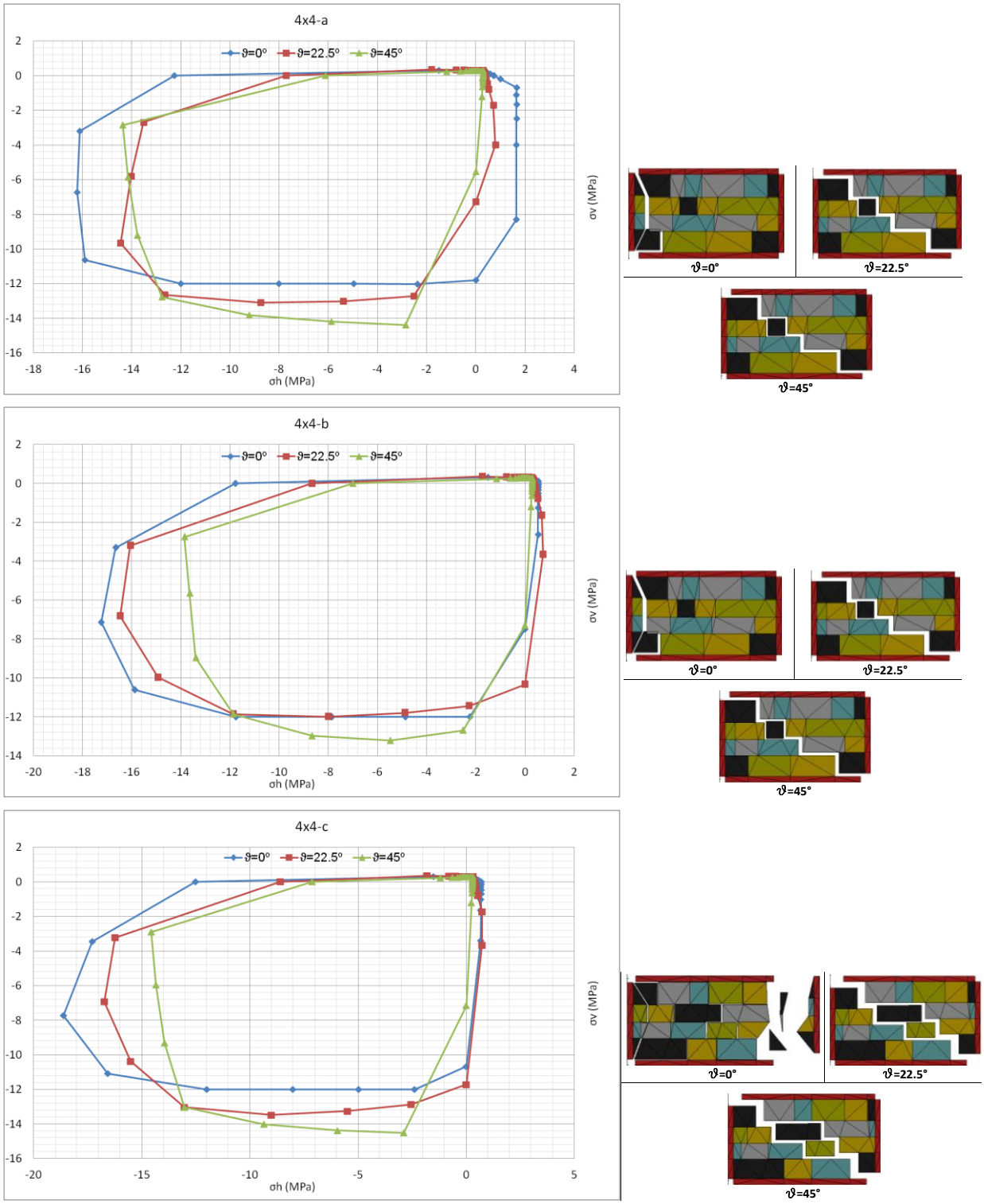

Figure 67. In-plane homogenized failure surfaces for 4x4 RVE for masonry with strong mortar at different orientations of the load with respect to the bed joint

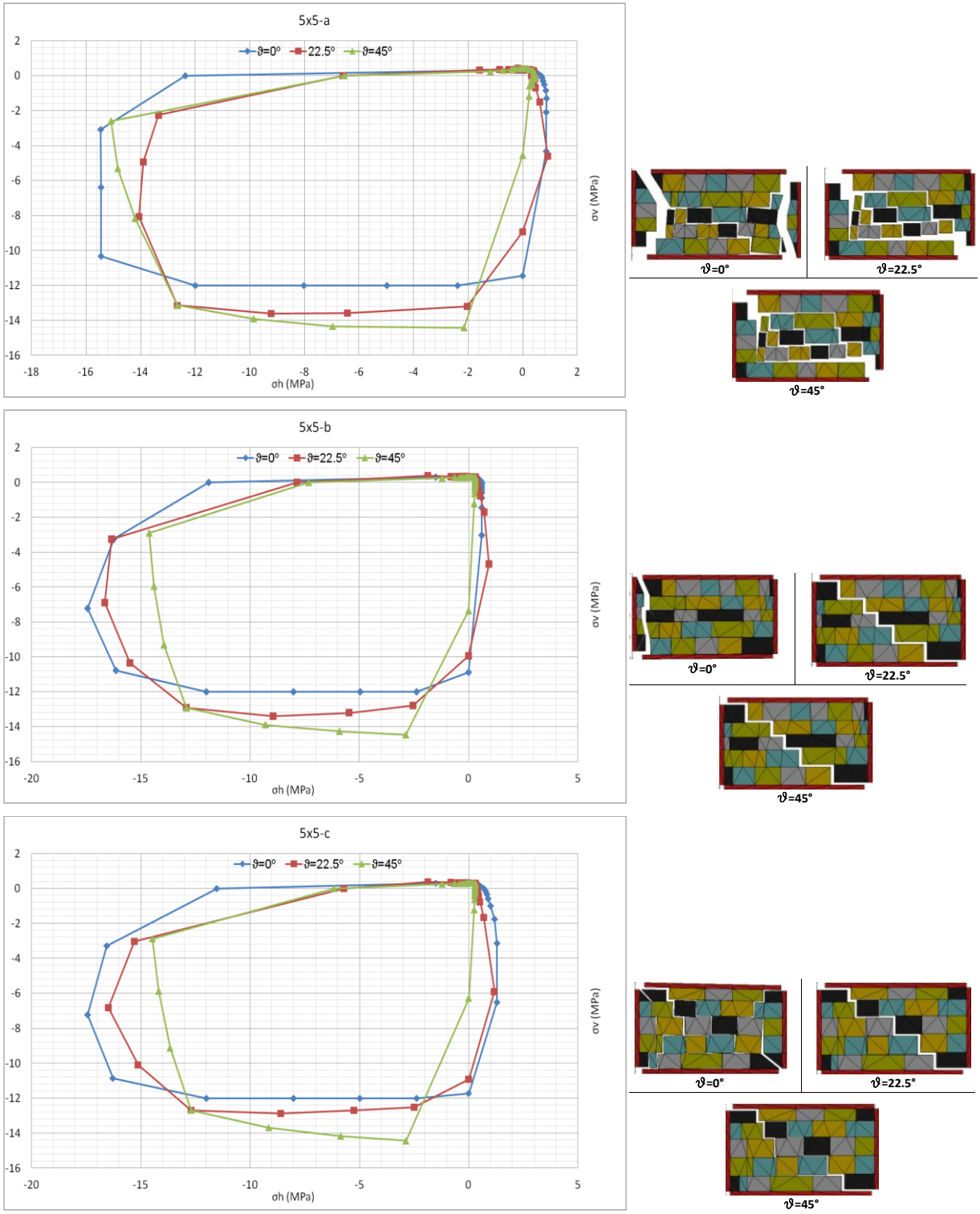

Figure 68. In-plane homogenized failure surfaces for 5x5 RVE for masonry with strong mortar at different orientations of the load with respect to the bed joint

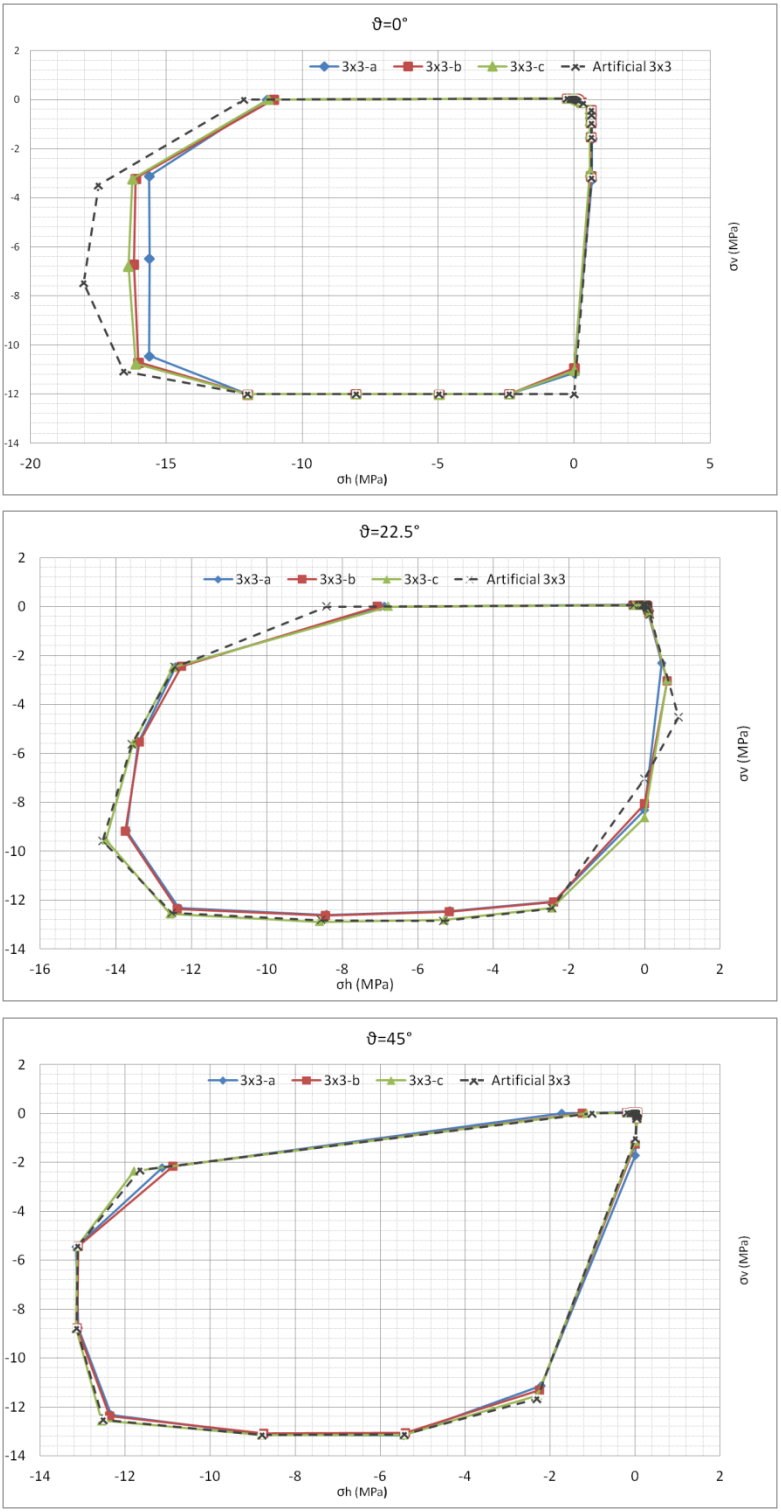

Figure 69. Comparison between in-plane homogenized failure surfaces obtained from 3x3 RVEs and artificial 3x3 RVE for masonry with weak mortar at different orientations of the load with respect to the bed joint

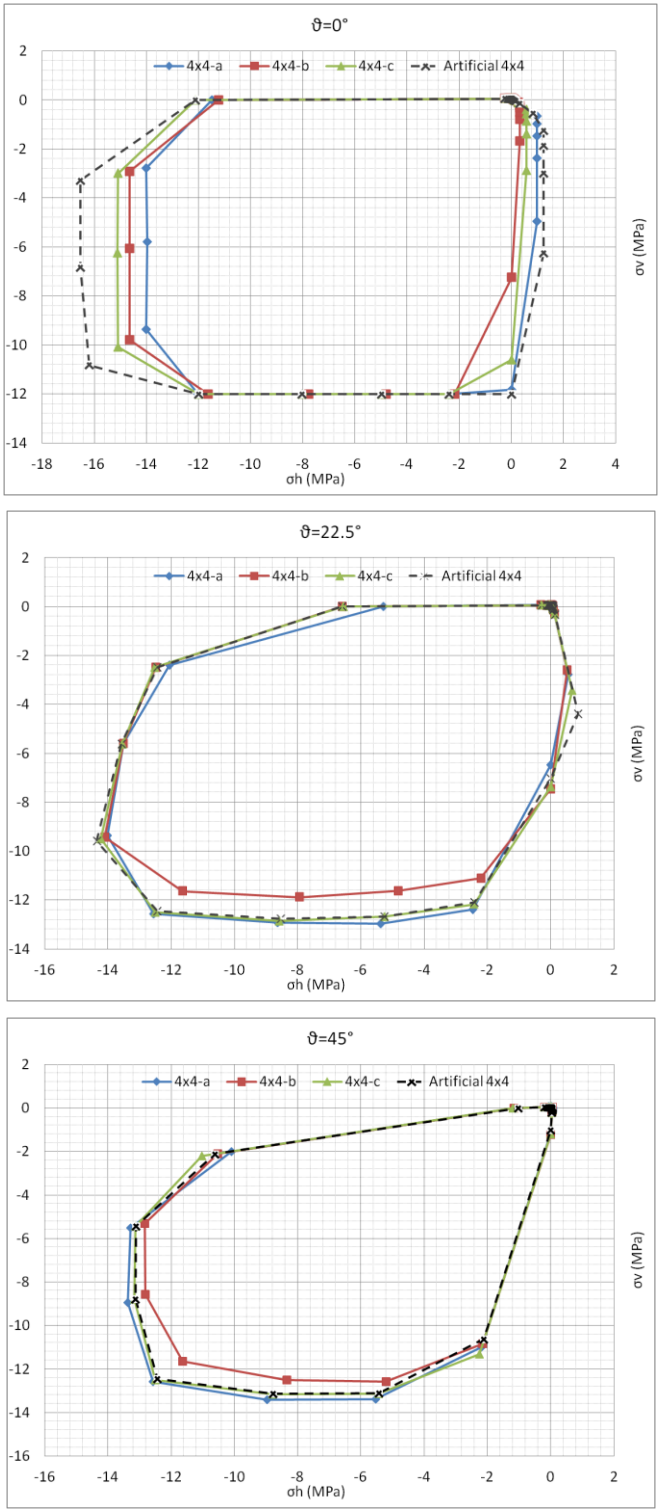

Figure 70. Comparison between in-plane homogenized failure surfaces obtained from 4x4 RVEs and artificial 4x4 RVE for masonry with weak mortar at different orientations of the load with respect to the bed joint

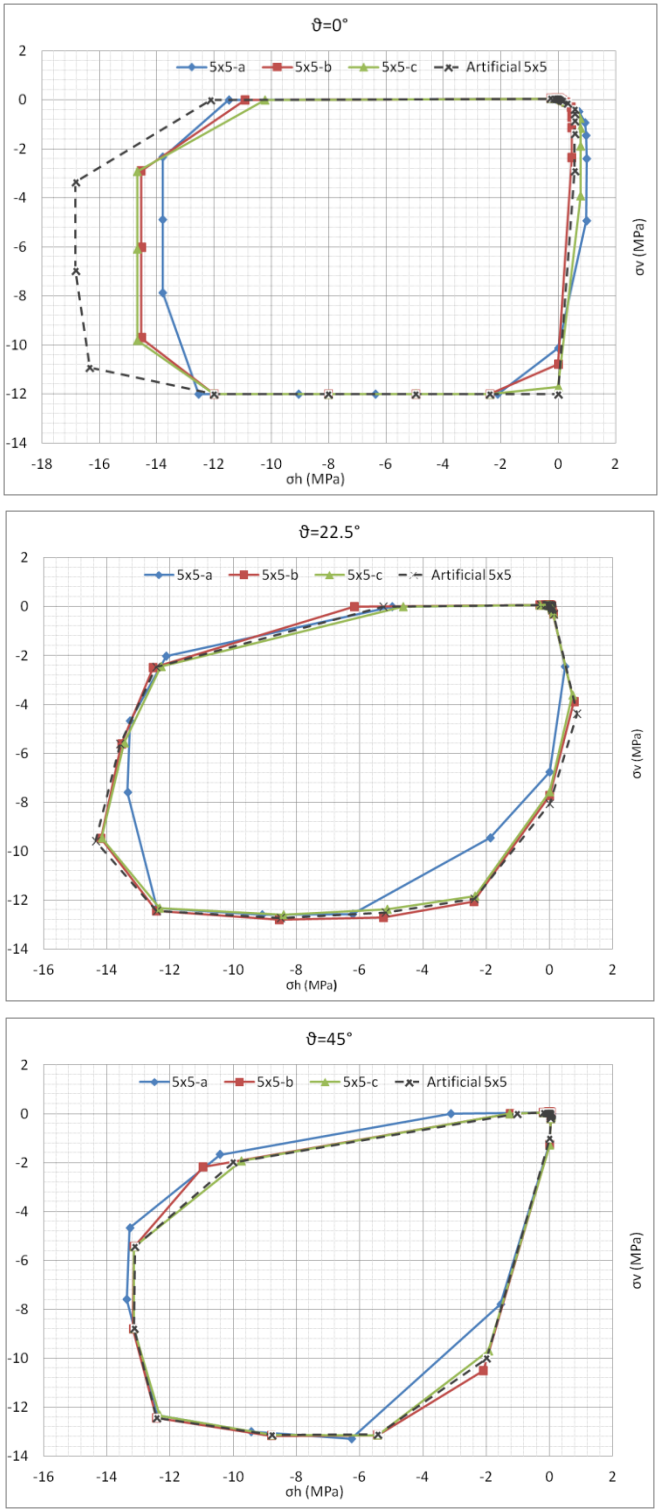

Figure 71. Comparison between in-plane homogenized failure surfaces obtained from 5x5 RVEs and artificial 5x5 RVE for masonry with weak mortar at different orientations of the load with respect to the bed joint

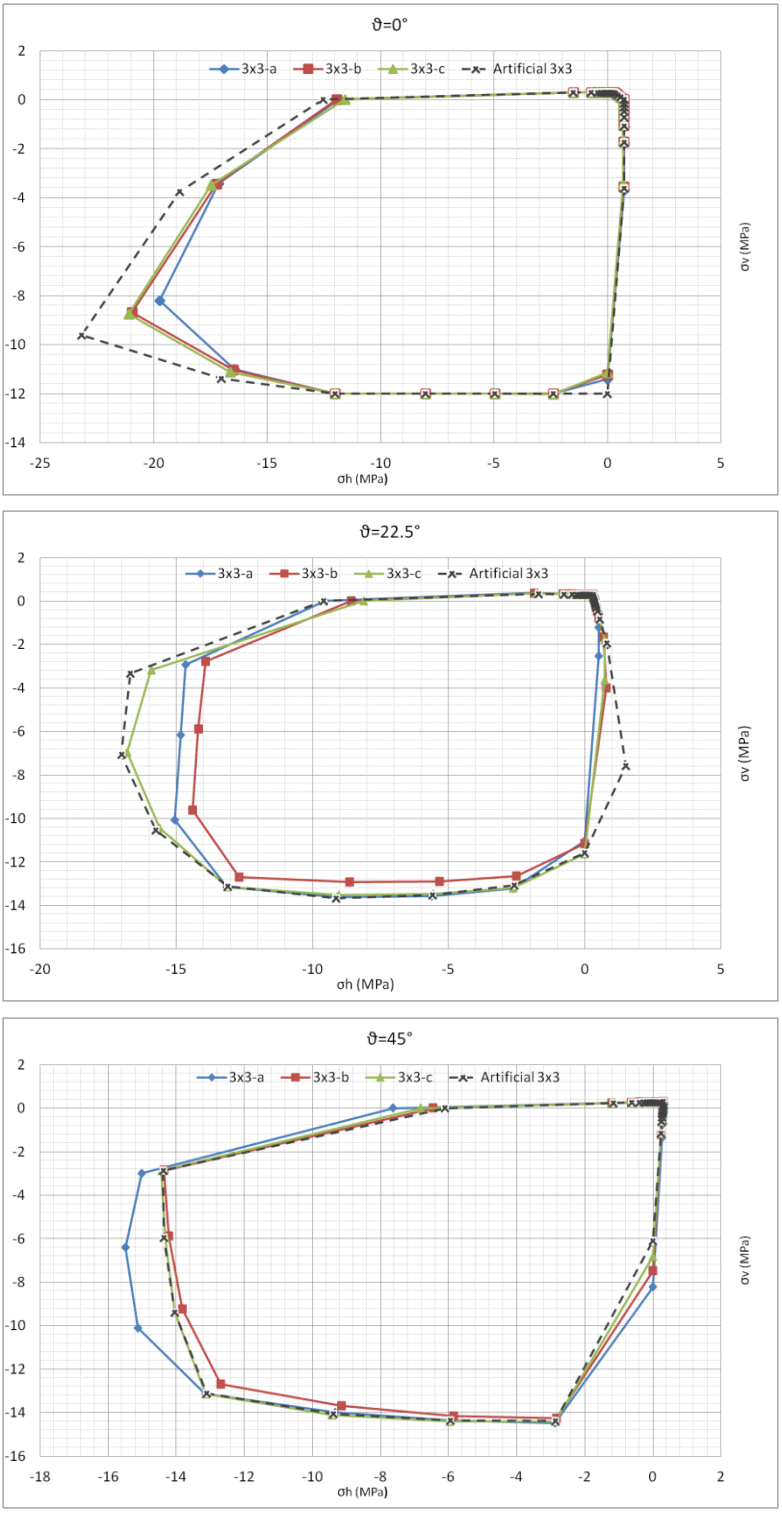

Figure 72. Comparison between in-plane homogenized failure surfaces obtained from 3x3 RVEs and artificial 3x3 RVE for masonry with strong mortar at different orientations of the load with respect to the bed joint

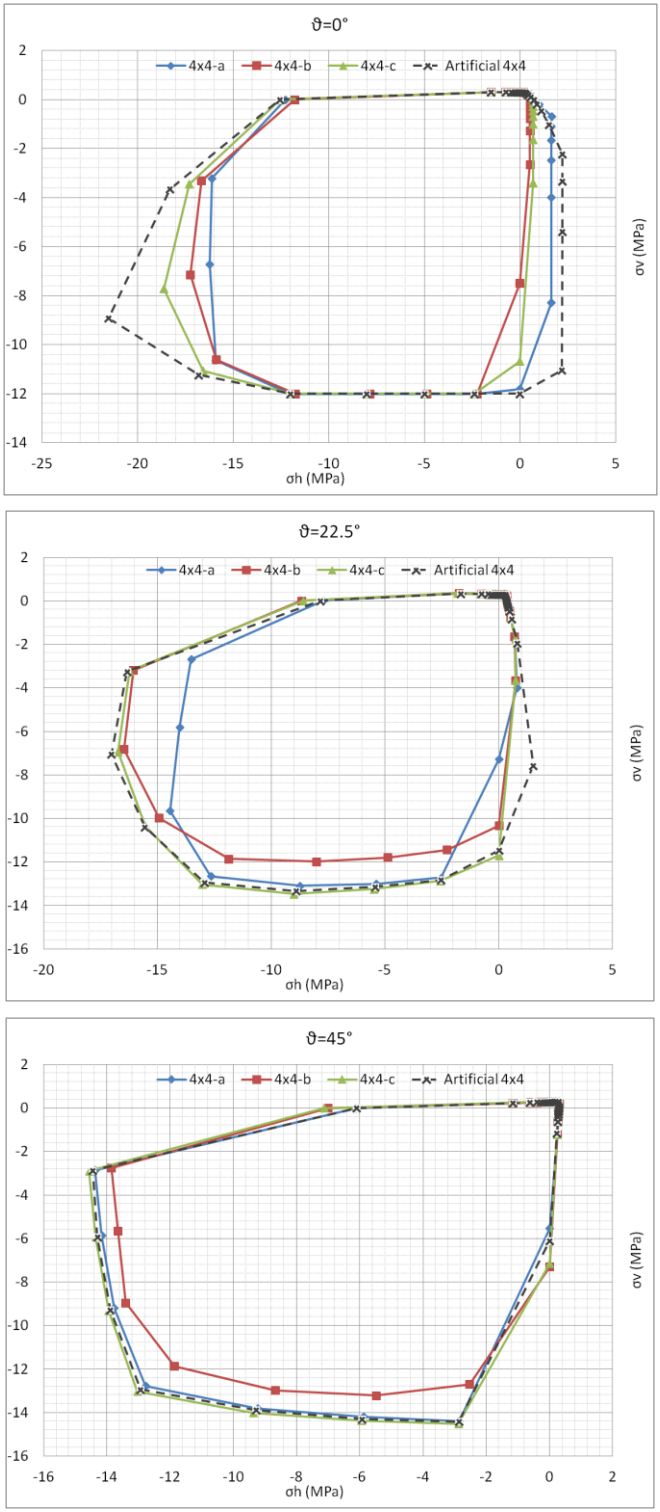

Figure 73. Comparison between in-of-plane homogenized failure surfaces obtained from 4x4 RVEs and artificial 4x4 RVE for masonry with strong mortar at different orientations of the load with respect to the bed joint

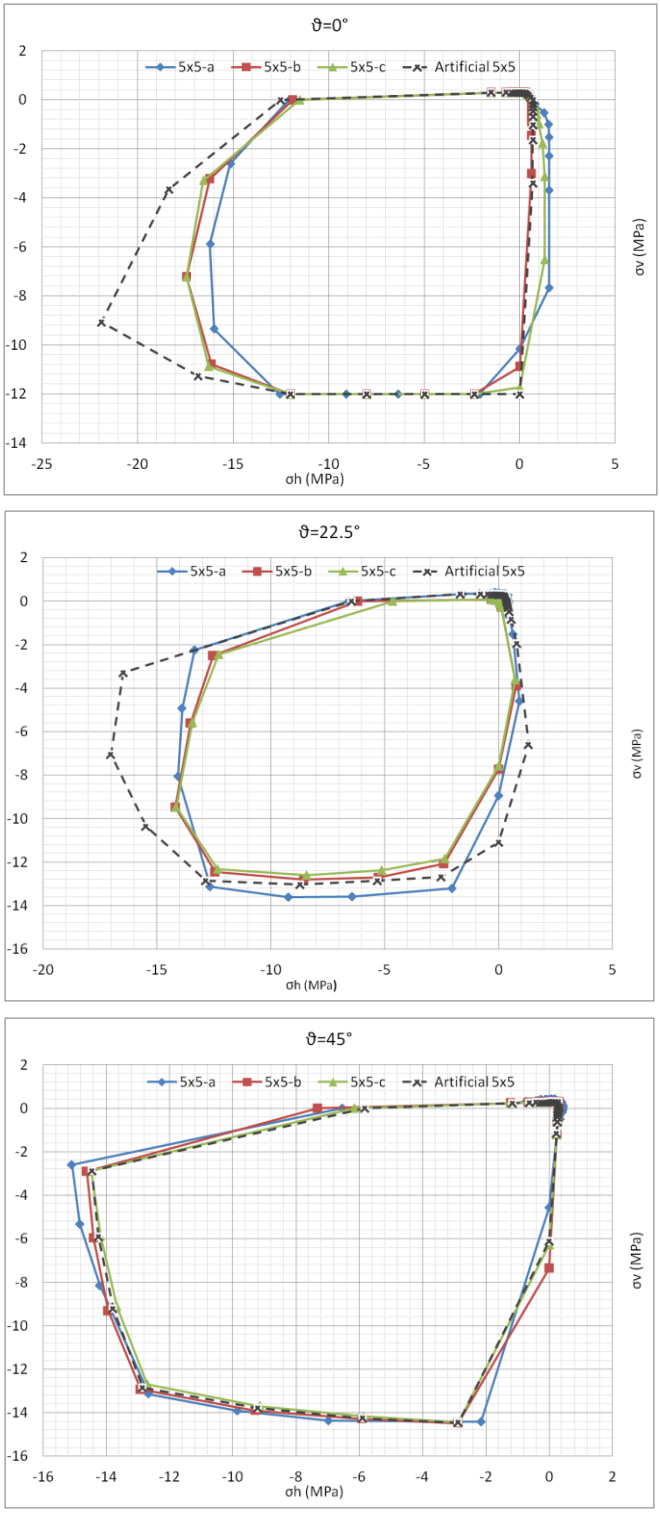

Figure 74. Comparison between in-plane homogenized failure surfaces obtained from 5x5 RVEs and artificial 5x5 RVE for masonry with strong mortar masonry at different orientations of the load with respect to the bed joint

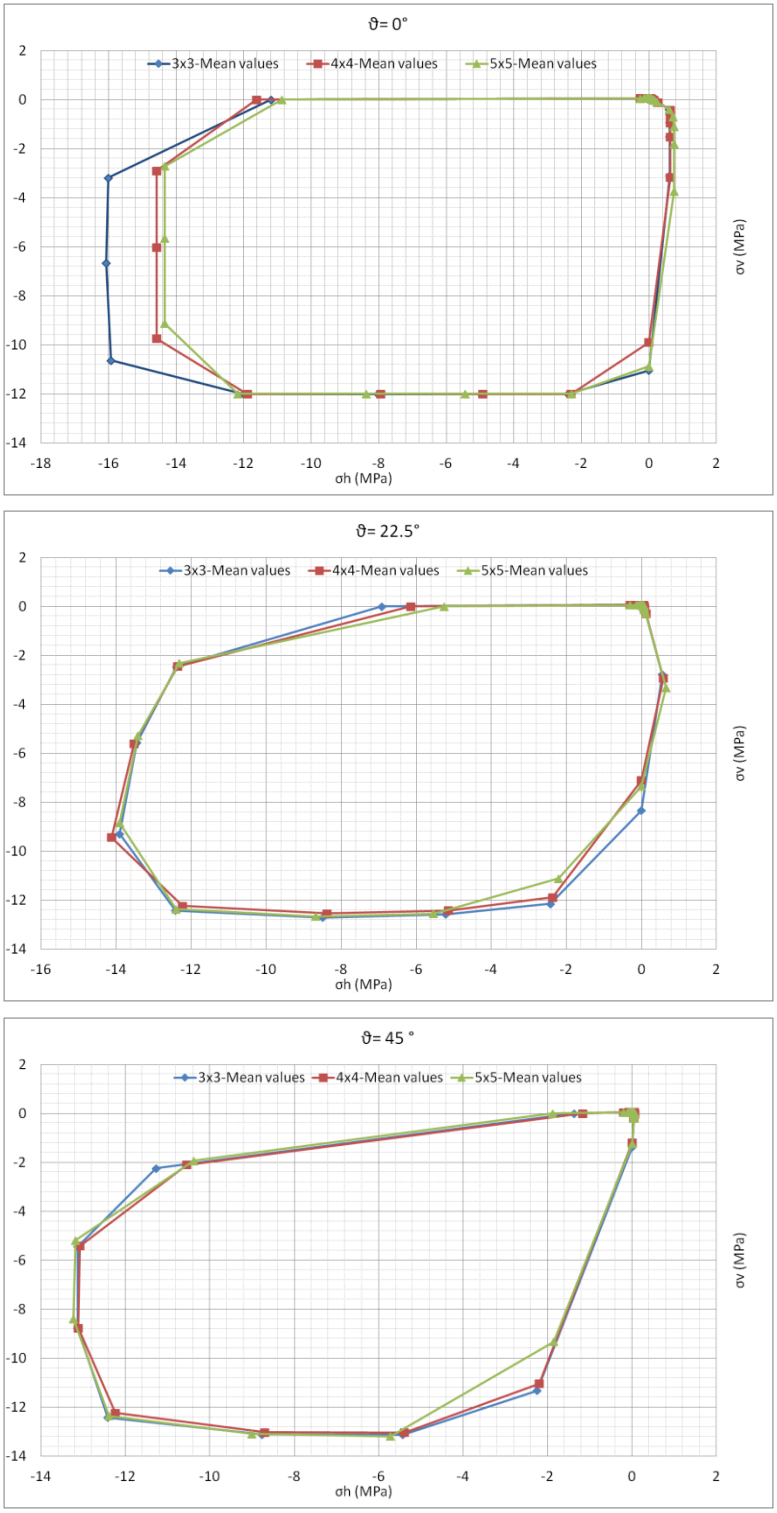

Figure 75. Comparison between in-plane homogenized failure surfaces obtained from mean values of RVEs for masonry with weak mortar at different orientations of the load with respect to the bed joint

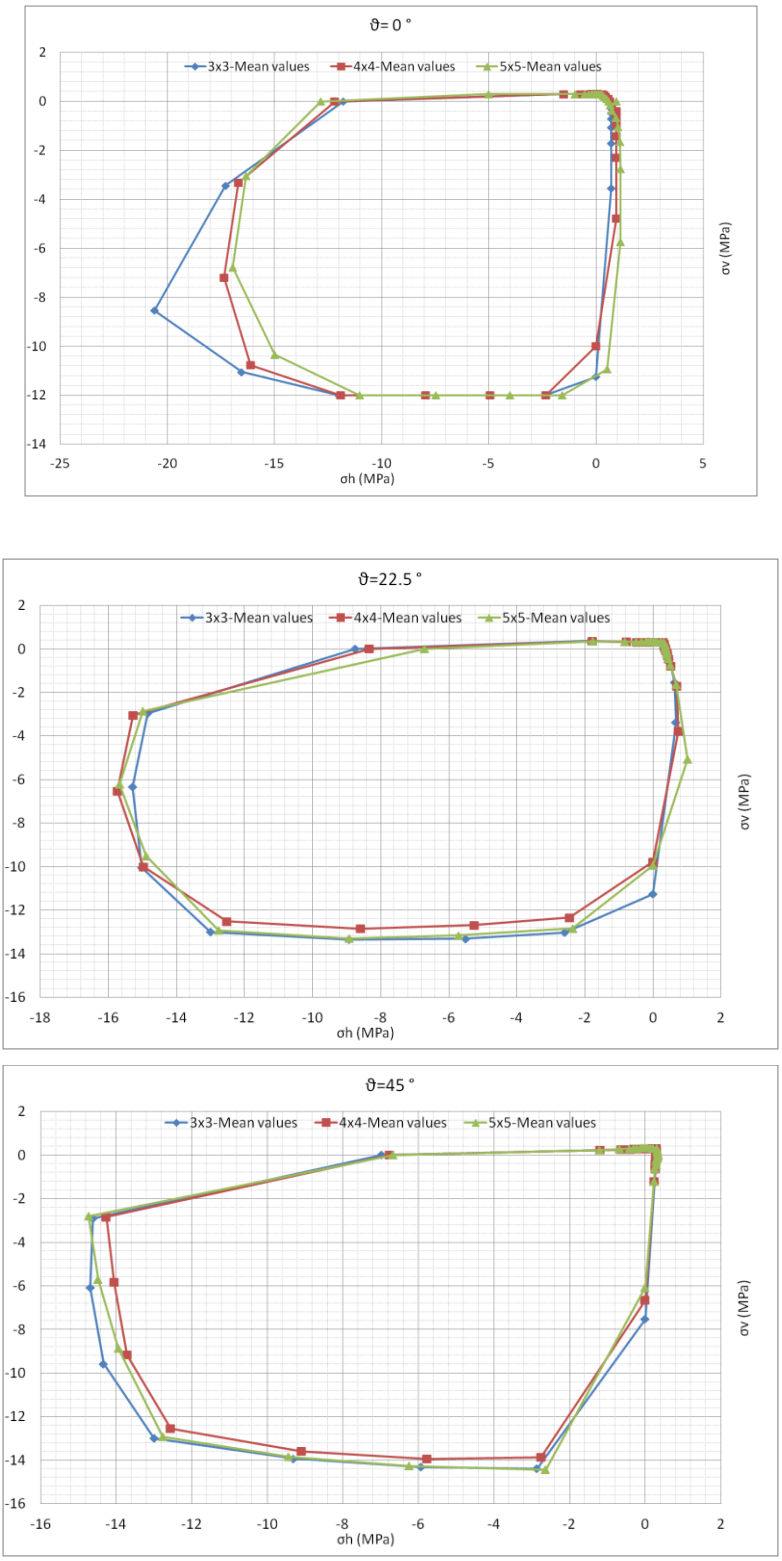

Figure 76. Comparison between in-plane homogenized failure surfaces obtained from mean values of RVEs for masonry with strong mortar at different orientations of the load with respect to the bed joint

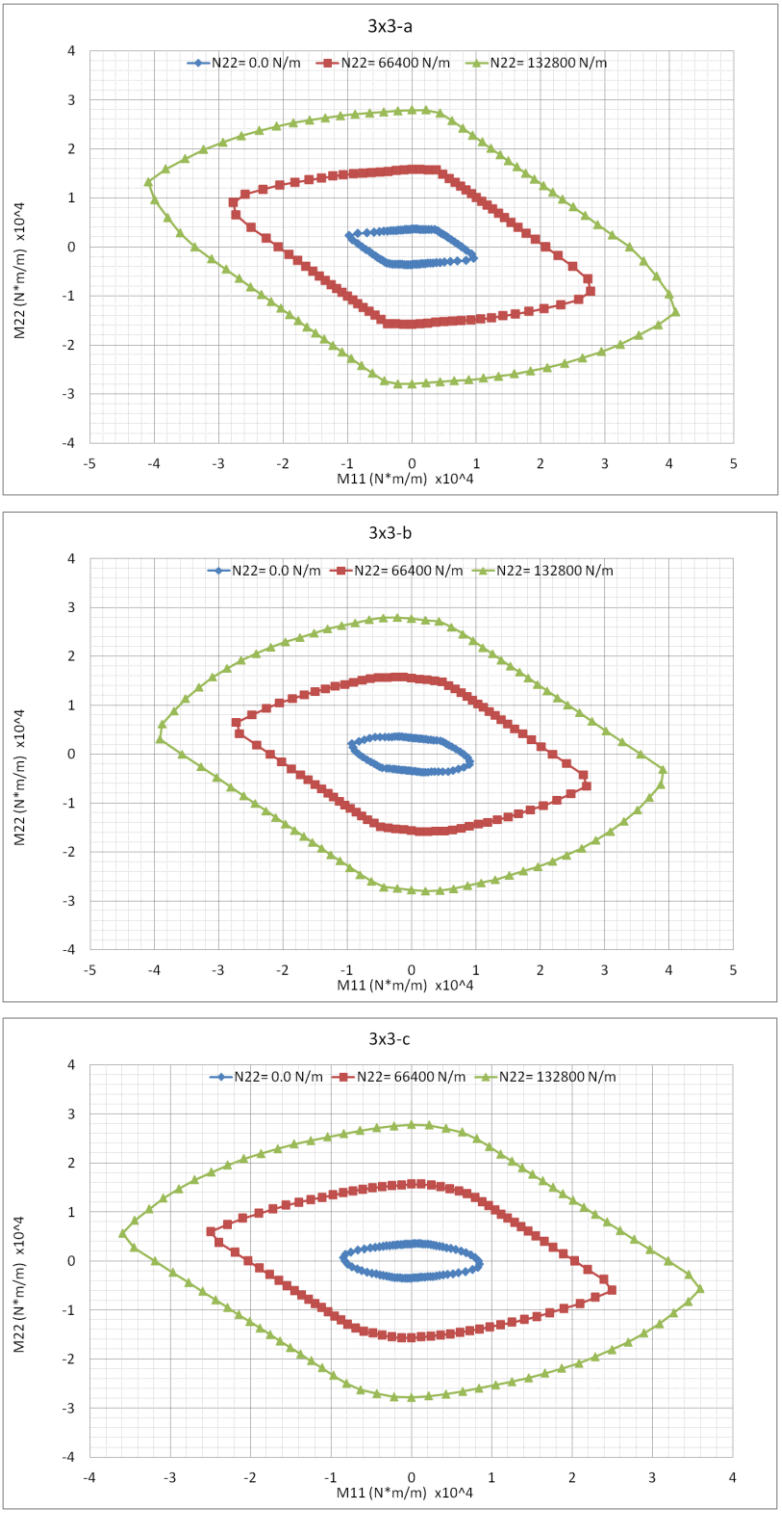

Figure 77. Out-of-plane homogenized failure surfaces (M11-M22) obtained from 3x3 RVE for masonry with weak mortar at incremental vertical compressive loads

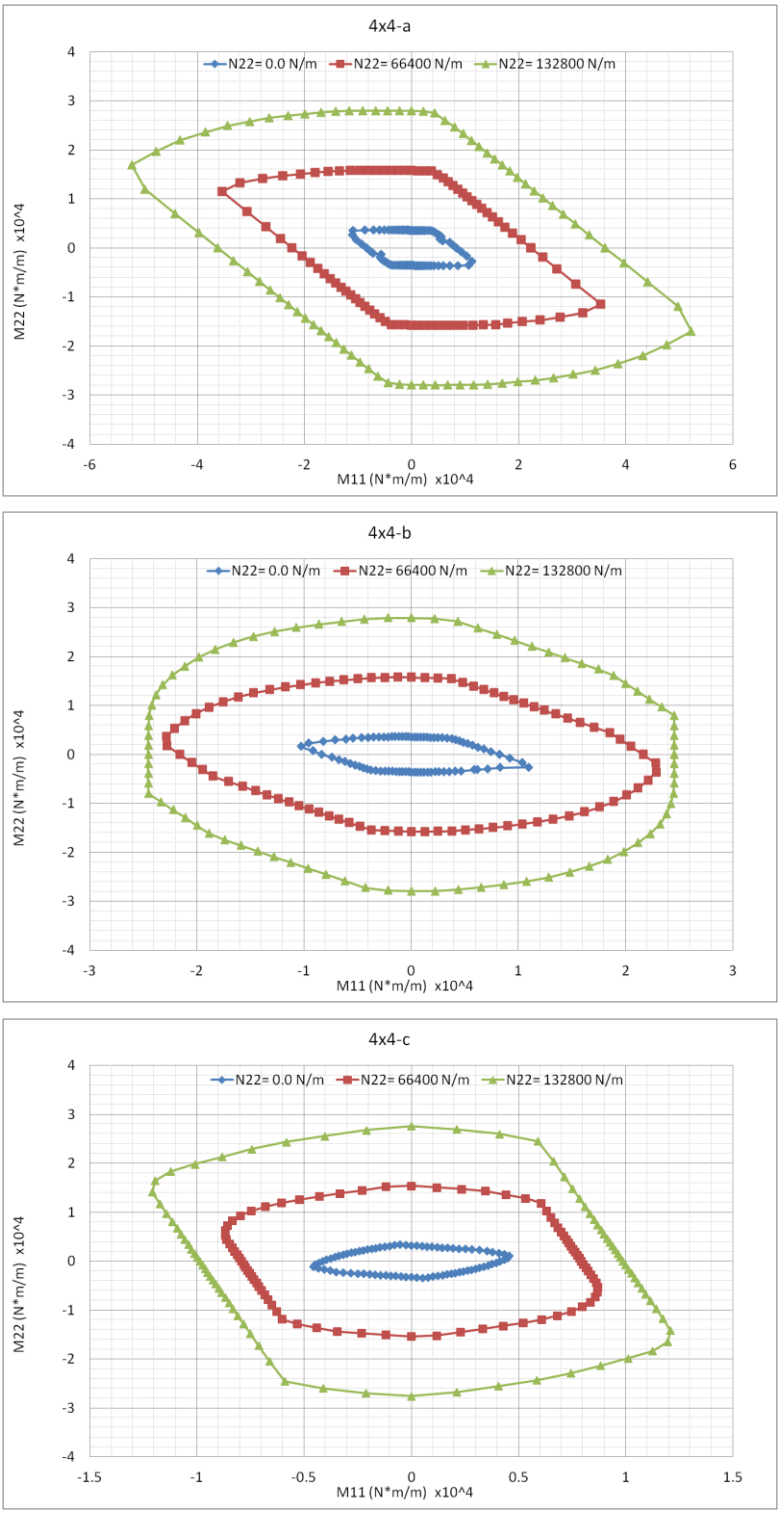

Figure 78. Out-of-plane homogenized failure surfaces (M11-M22) obtained from 4x4 RVE for masonry with weak mortar at incremental vertical compressive loads

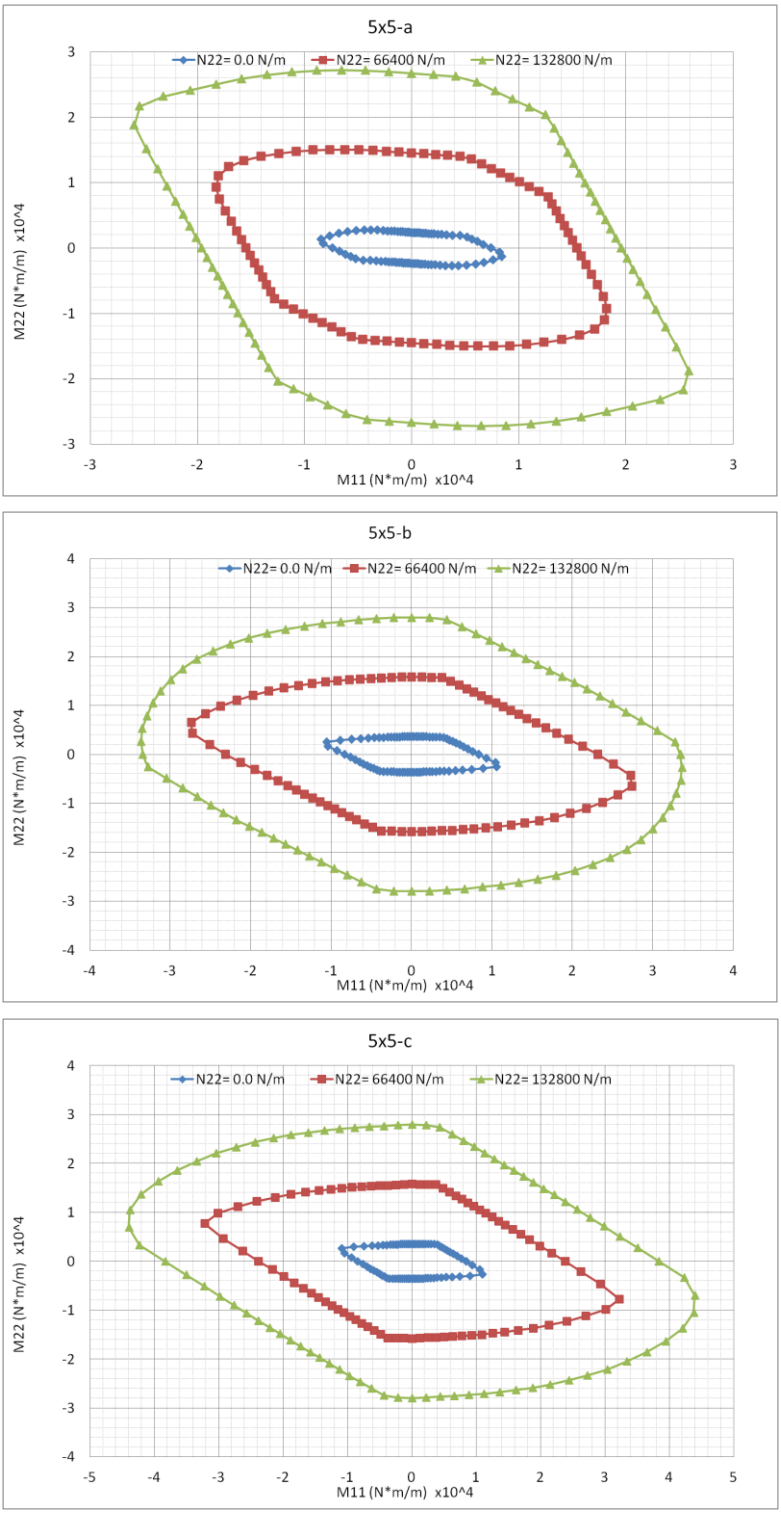

Figure 79. Out-of-plane homogenized failure surfaces (M11-M22) obtained from 5x5 RVE for masonry with weak mortar at incremental vertical compressive loads

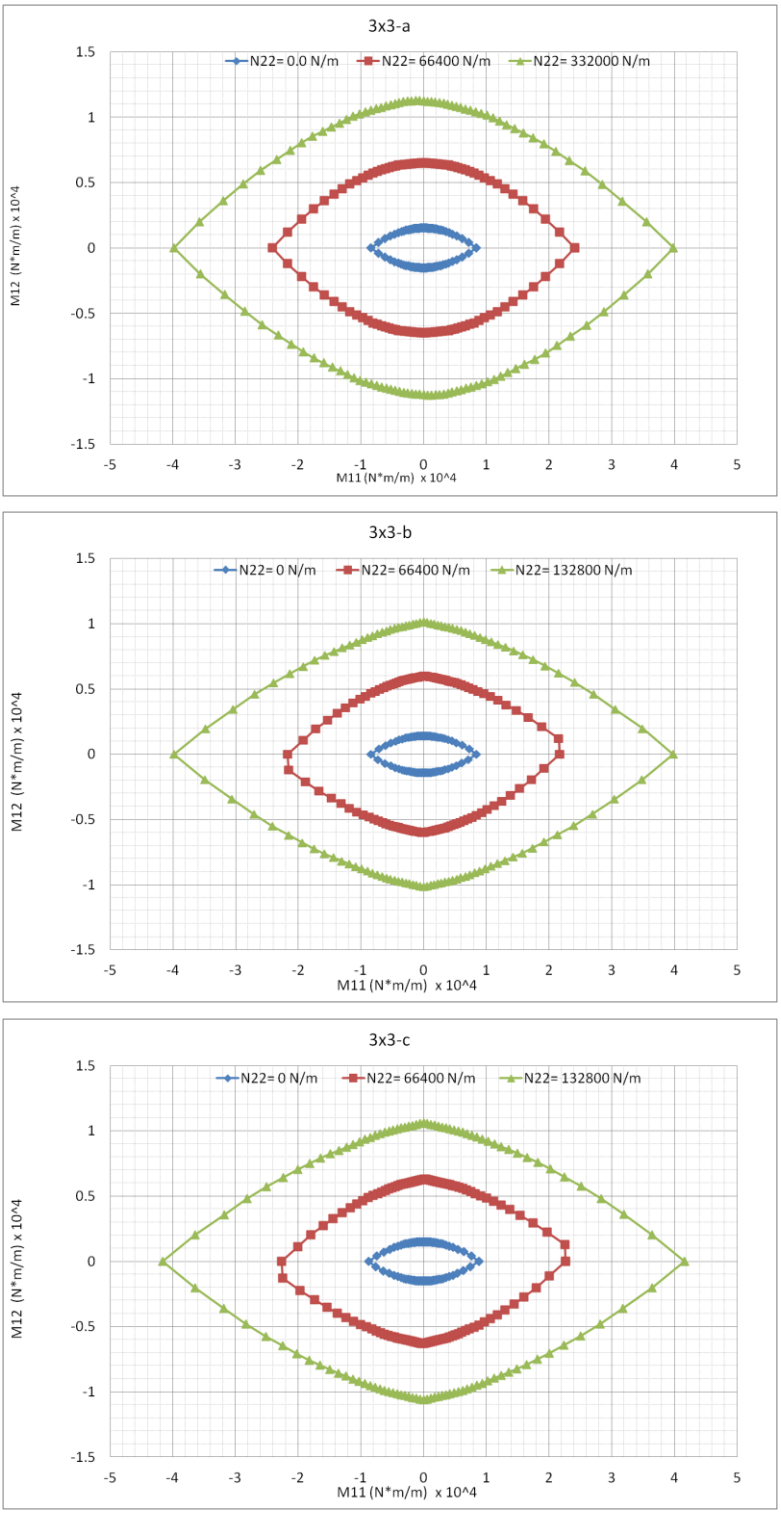

Figure 80. Out-of-plane homogenized failure surfaces (M11-M12) obtained from 3x3 RVE for masonry with weak mortar at incremental vertical compressive loads

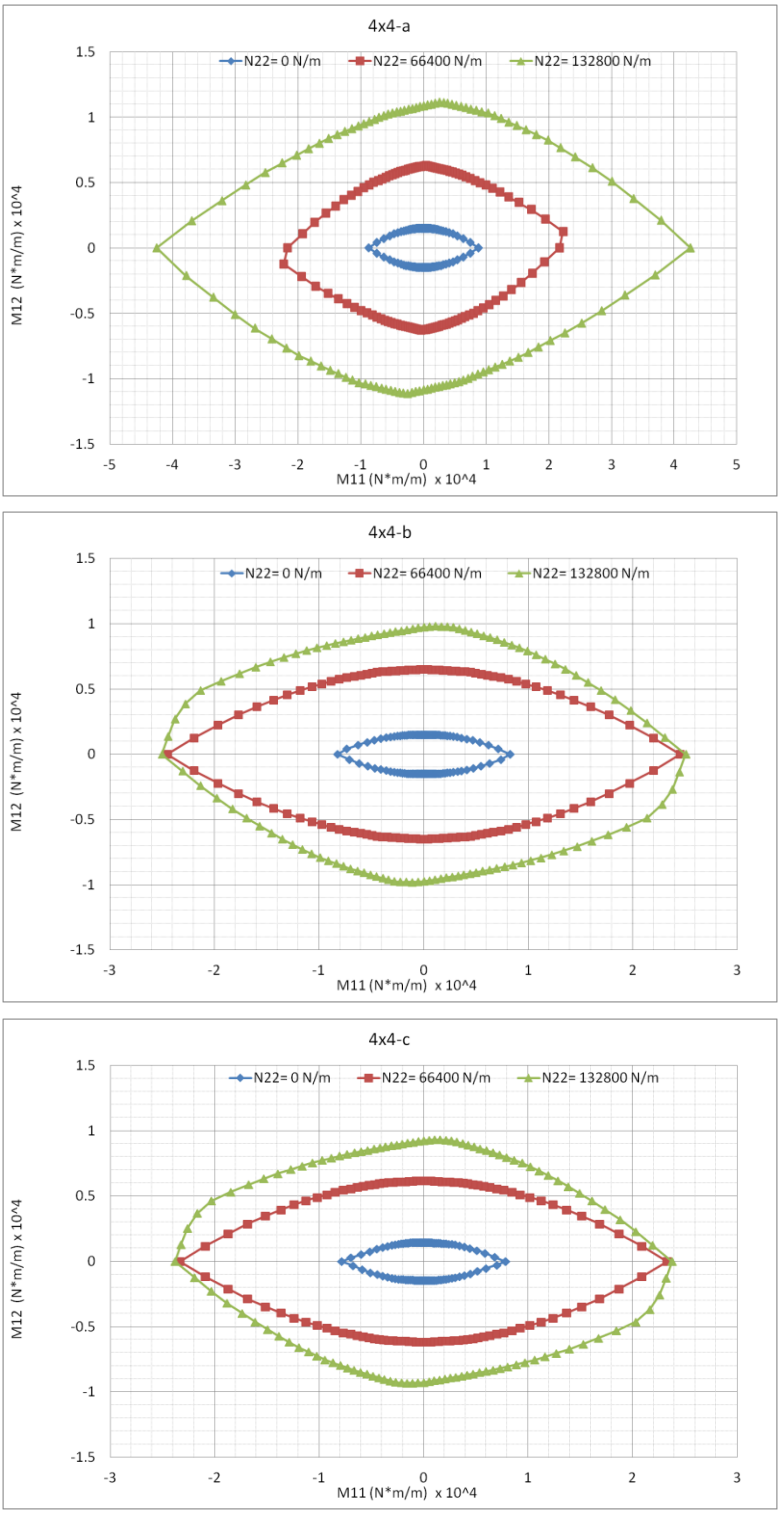

Figure 81. Out-of-plane homogenized failure surfaces (M11-M12) obtained from 4x4 RVE for masonry with weak mortar at incremental vertical compressive loads

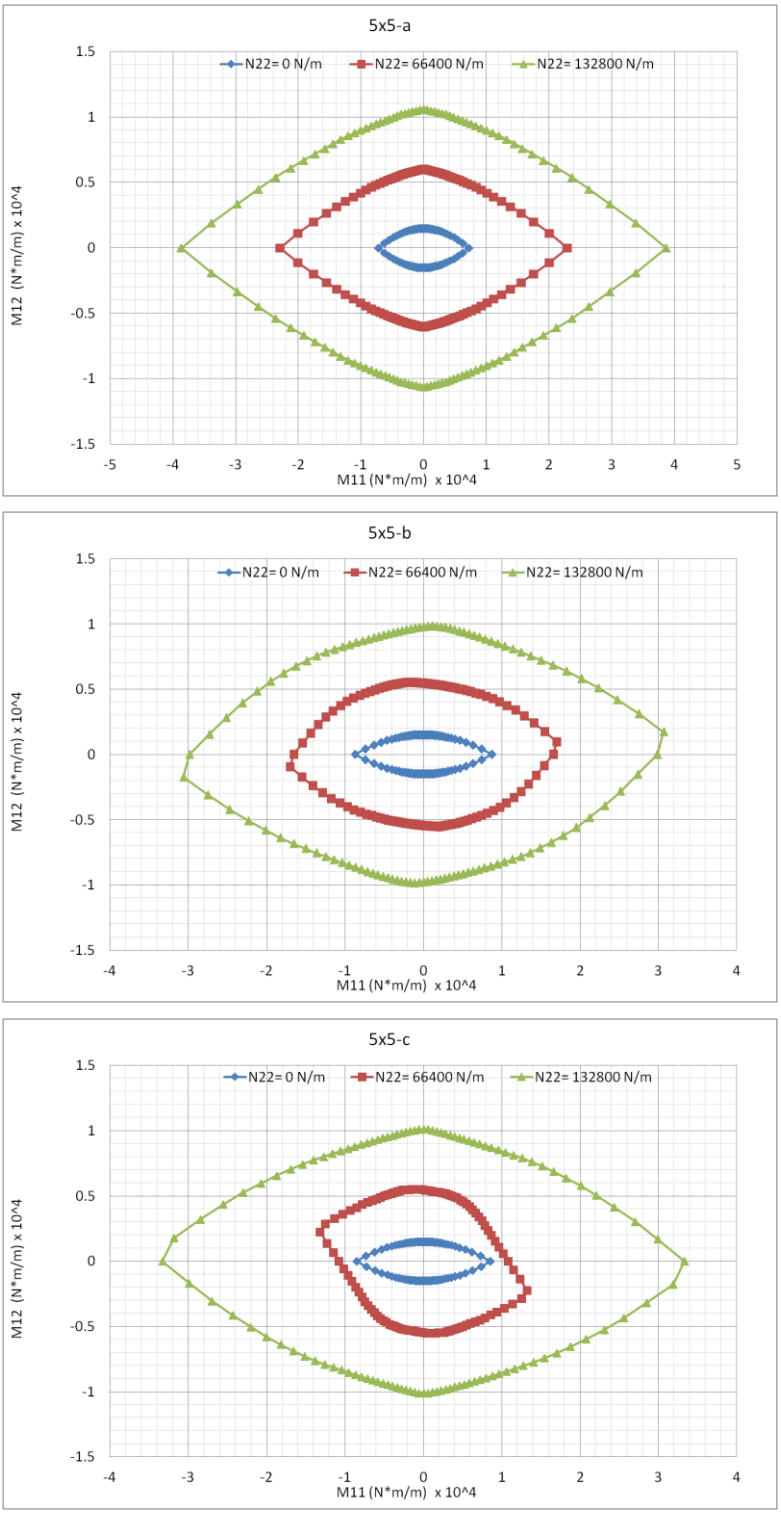

Figure 82. Out-of-plane homogenized failure surfaces (M11-M12) obtained from 5x5 RVE for masonry with weak mortar at incremental vertical compressive loads

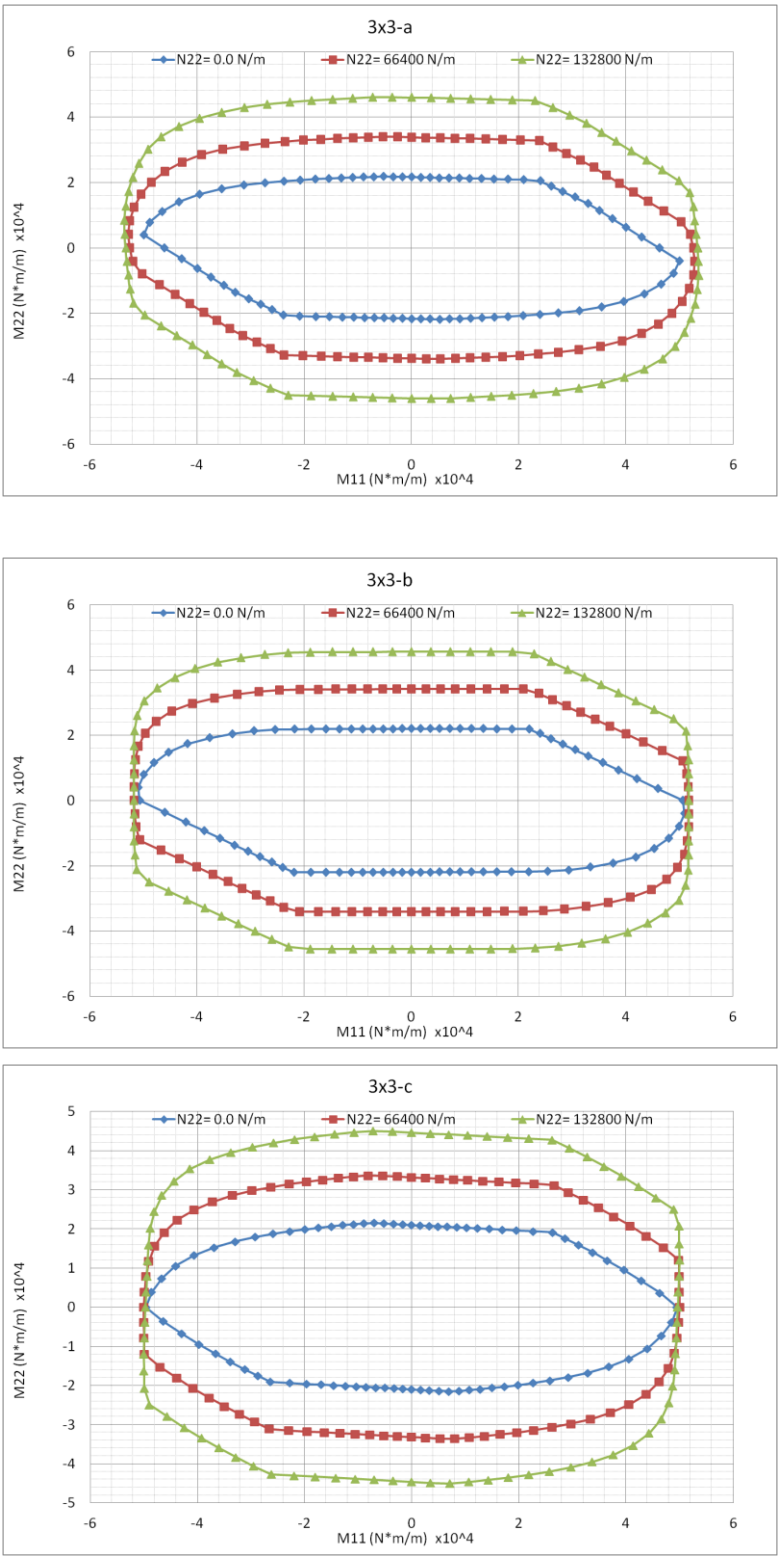

Figure 83. Out-of-plane homogenized failure surfaces (M11-M22) obtained from 3x3 RVE for masonry with strong mortar at incremental vertical compressive loads

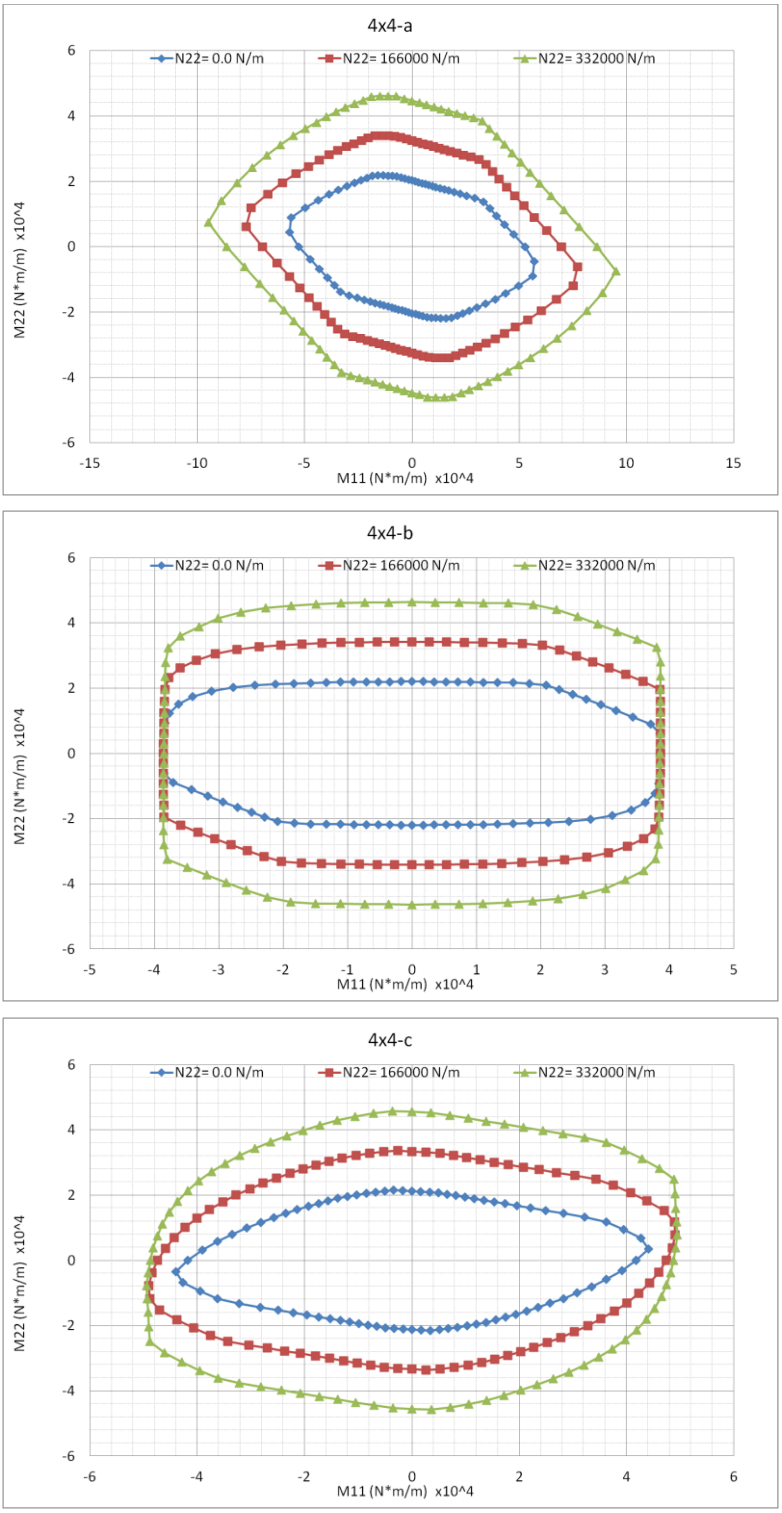

Figure 84. Out-of-plane homogenized failure surfaces (M11-M22) obtained from 4x4 RVE for masonry with strong mortar at incremental vertical compressive loads

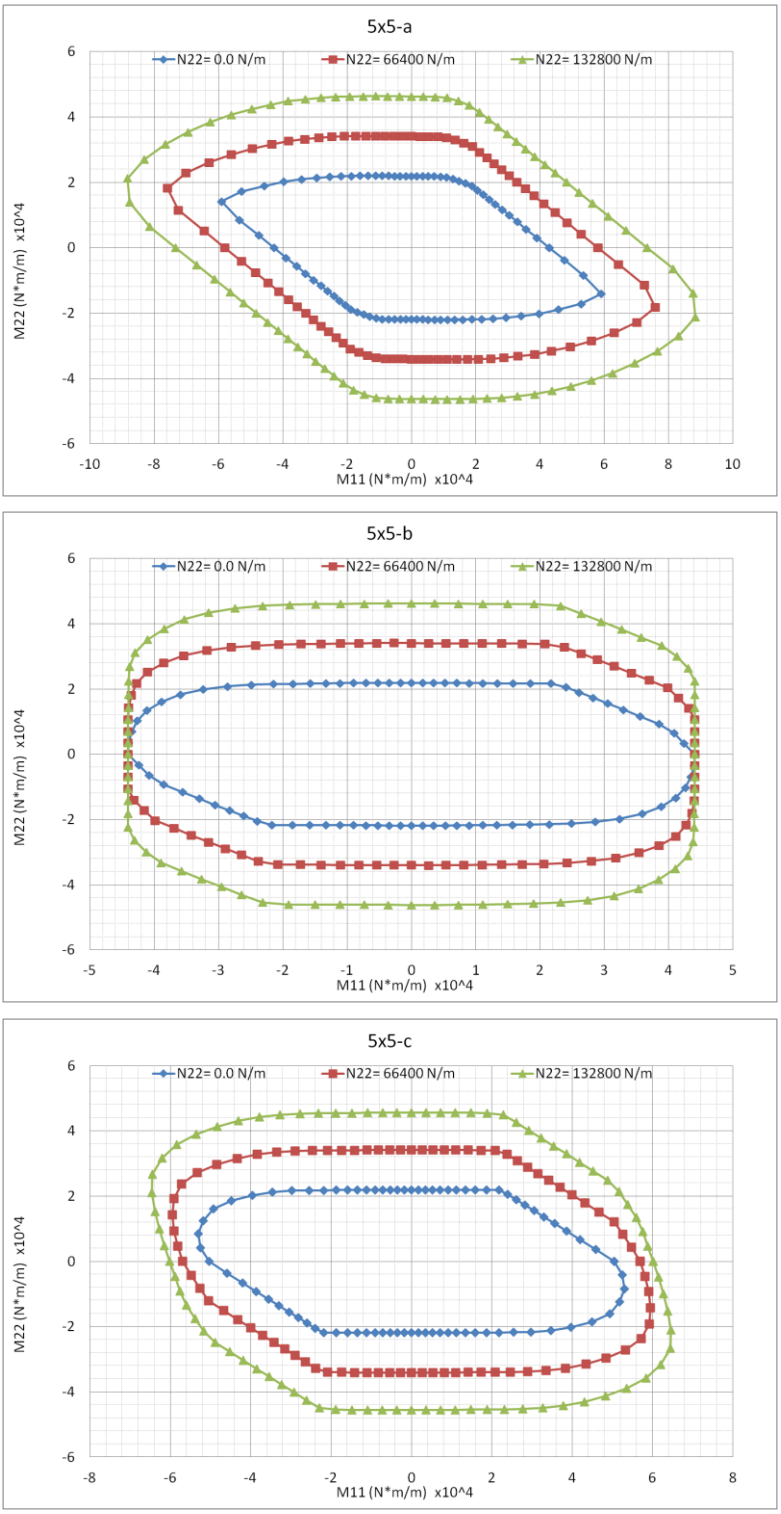

Figure 85. Out-of-plane homogenized failure surfaces (M11-M22) obtained from 5x5 RVE for masonry with strong mortar at incremental vertical compressive loads

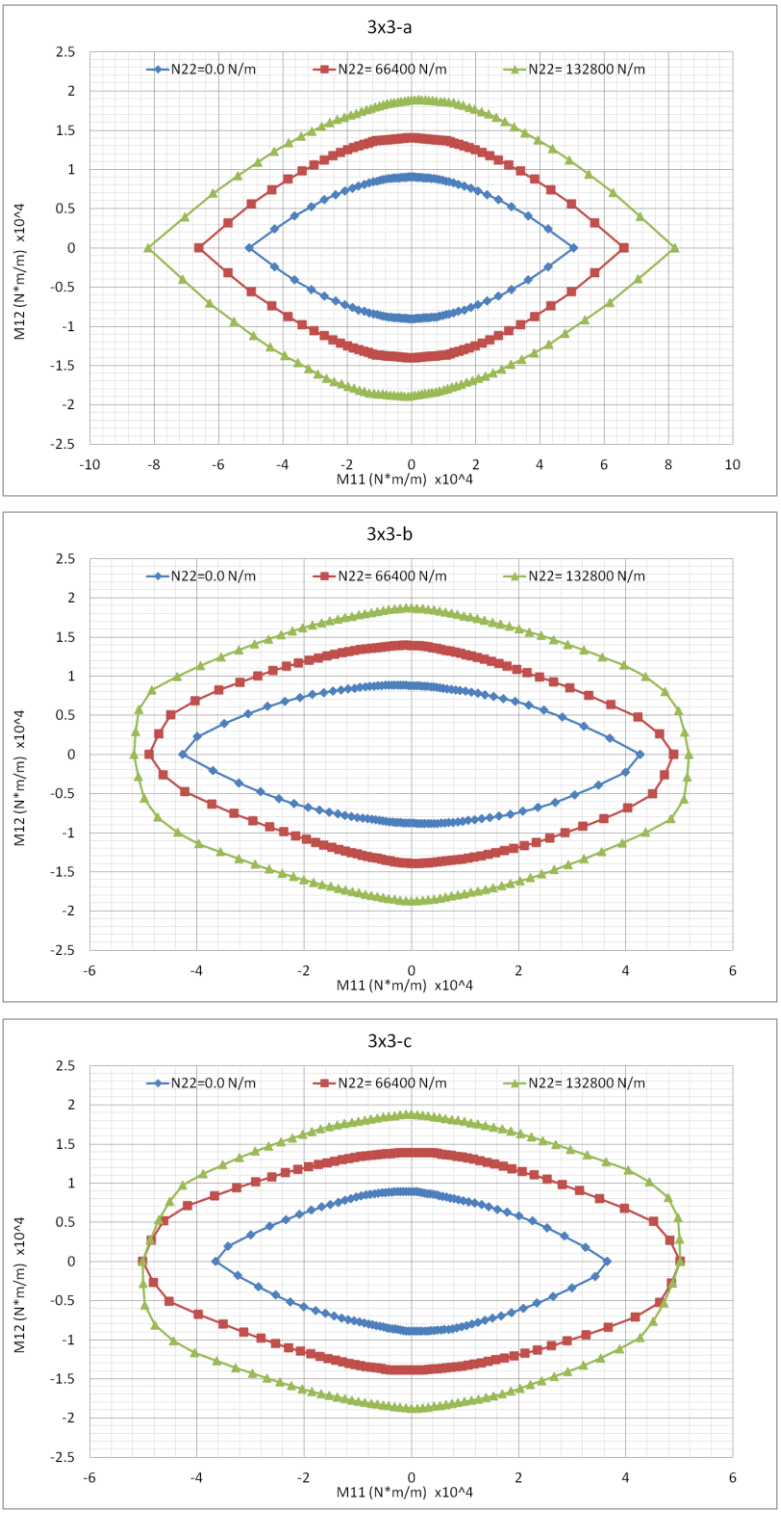

Figure 86. Out-of-plane homogenized failure surfaces (M11-M12) obtained from 3x3 RVE for masonry with strong mortar at incremental vertical compressive loads

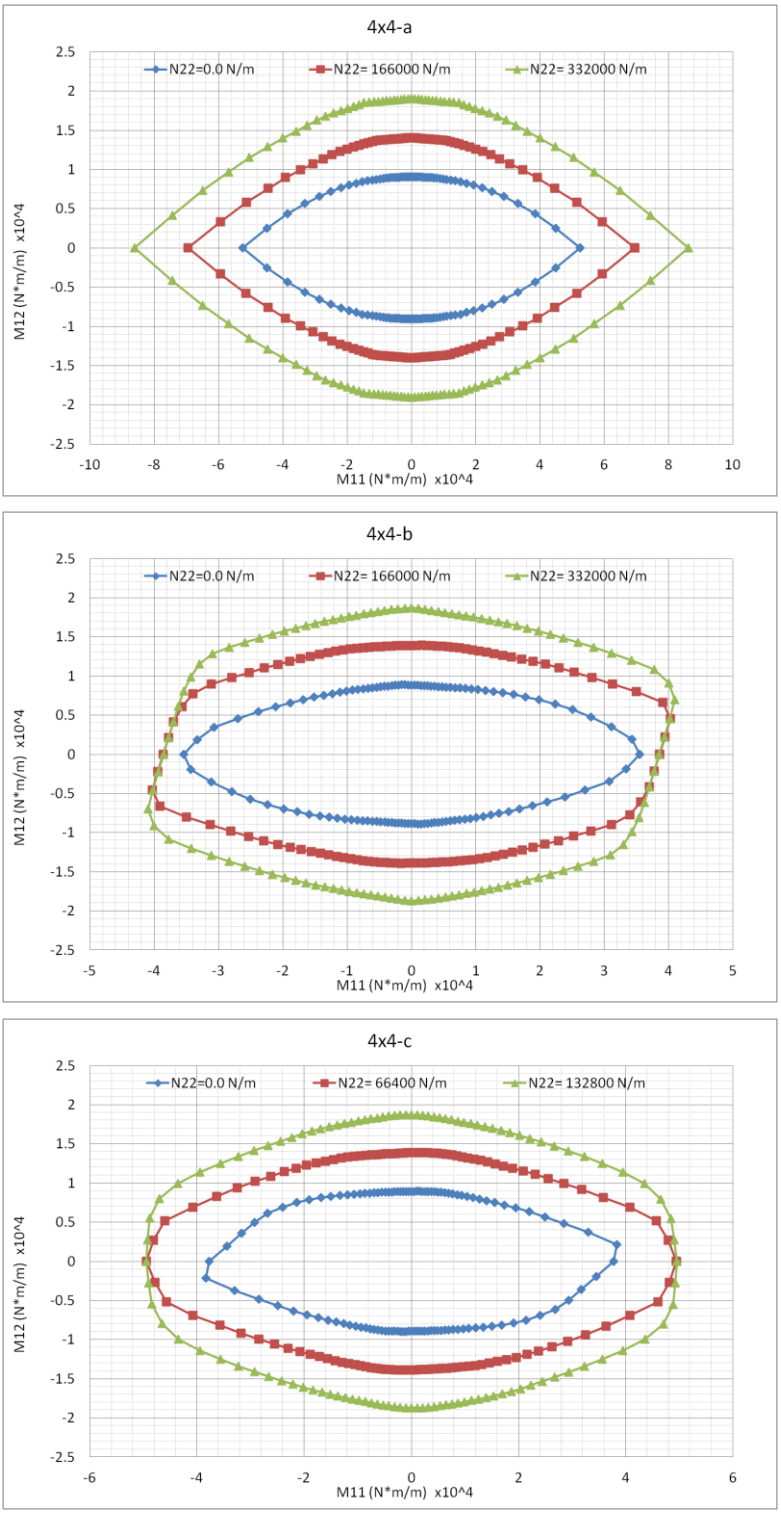

Figure 87. Out-of-plane homogenized failure surfaces (M11-M12) obtained from 4x4 RVE for masonry with strong mortar at incremental vertical compressive loads

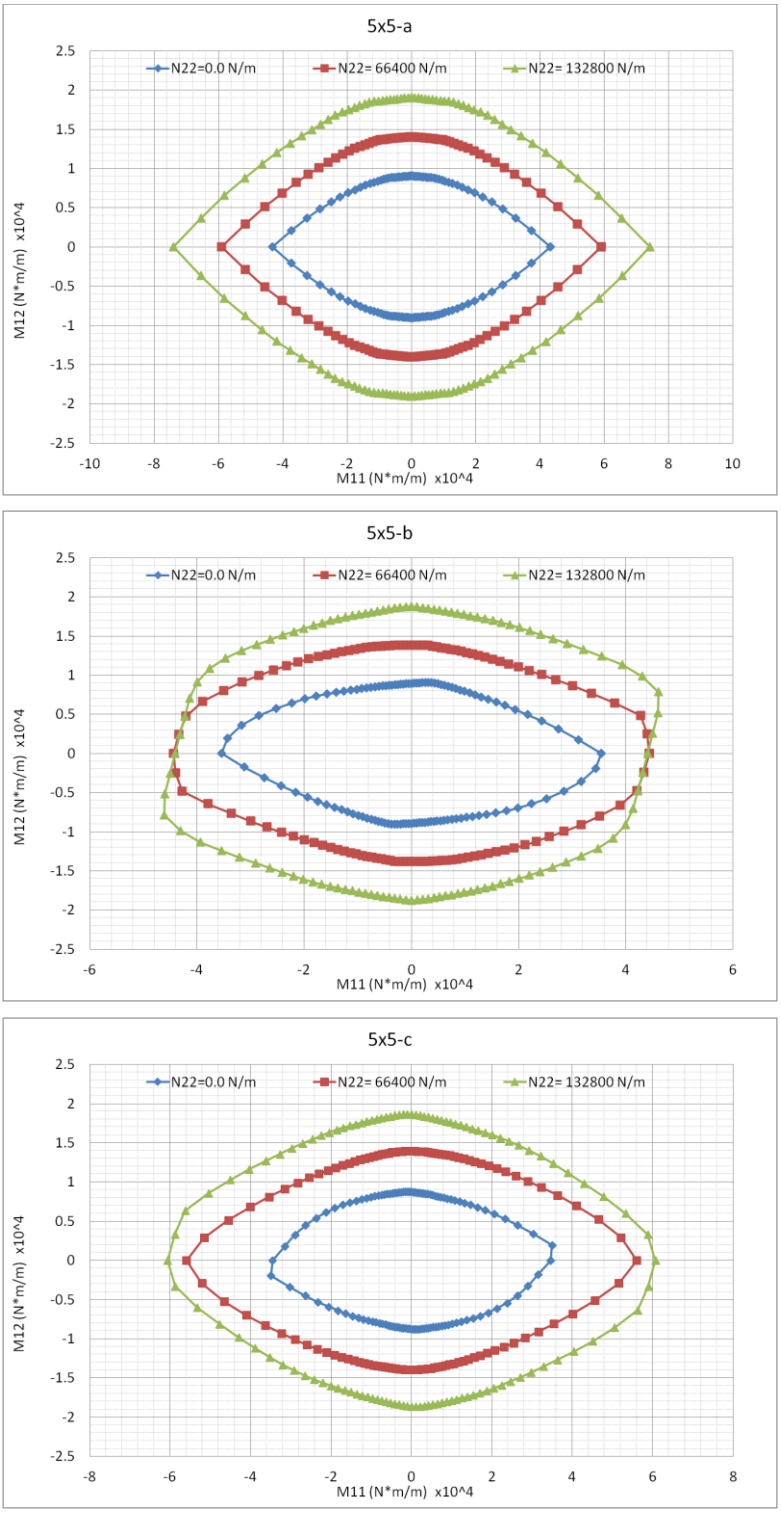

Figure 88. Out-of-plane homogenized failure surfaces (M11-M12) obtained from 5x5 RVE for masonry with strong mortar at incremental vertical compressive loads

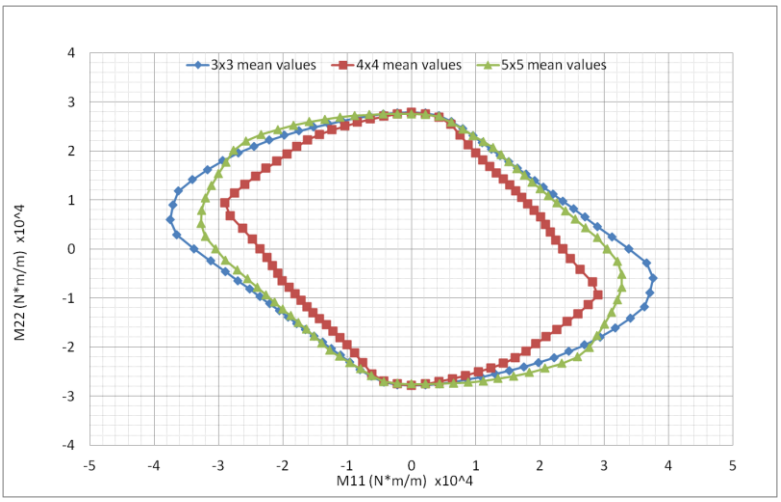

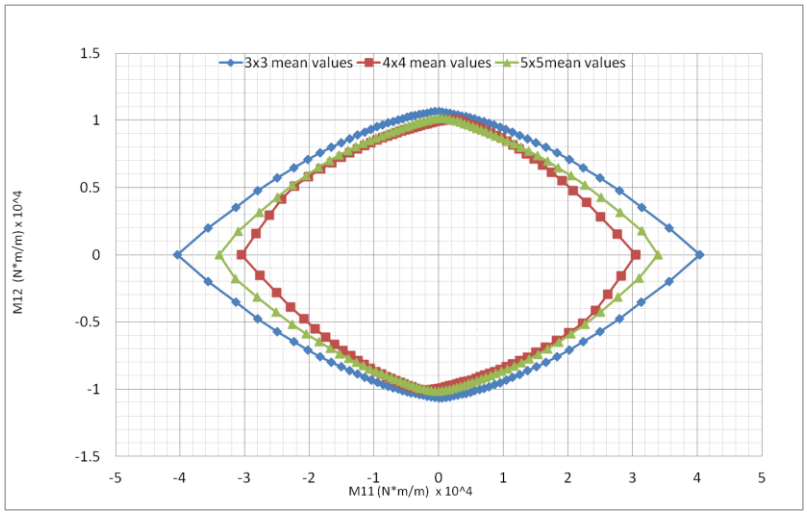

Figure 89 Comparison between out-of-plane homogenized failure surfaces obtained from mean values of the three different RVEs for masonry with weak mortar

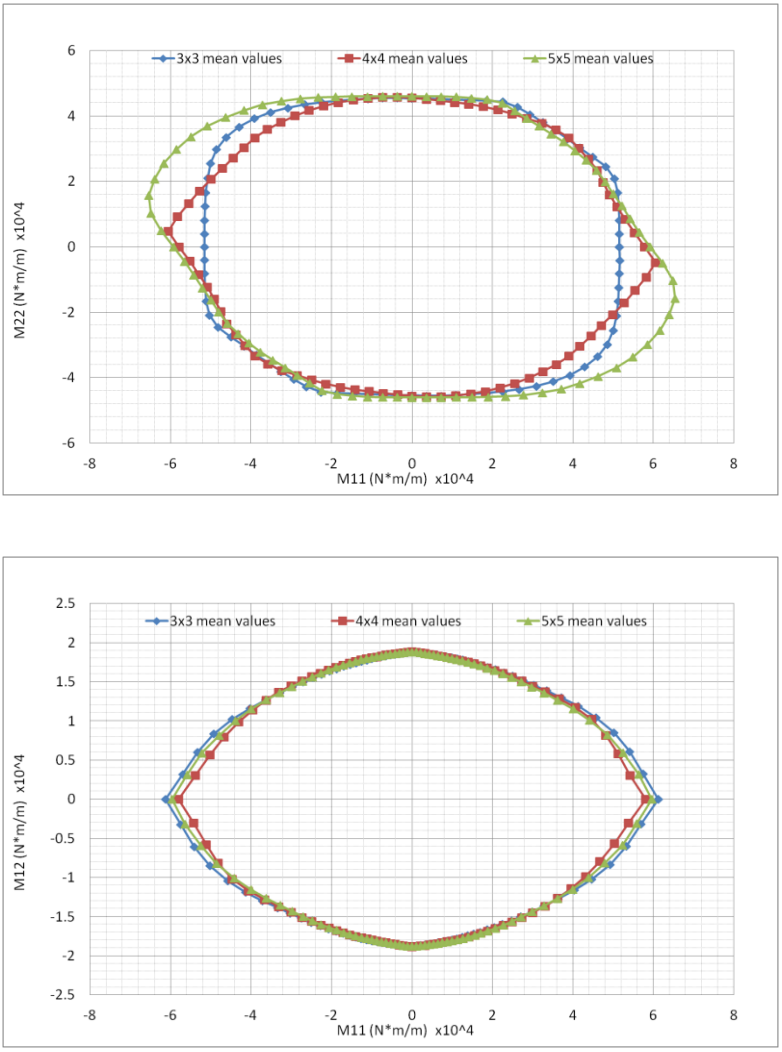

Figure 90. Comparison between out-of-plane homogenized failure surfaces obtained from mean values of the three different RVEs for masonry with strong mortar